UNIVERSITY OF OKLAHOMA

GRADUATE COLLEGE

A HIGH RESOLUTION DISTRIBUTED HYDROLOGIC MODEL CLIMATOLOGY OVER THE CONTERMINOUS UNITED STATES FOCUSED ON FLASH FLOODING

A DISSERTATION

SUBMITTED TO THE GRADUATE FACULTY

in partial fulfillment of the requirements for the

Degree of

DOCTOR OF PHILOSOPHY

By

ZACHARY LOLOS FLAMIG
Norman, Oklahoma
2016

A HIGH RESOLUTION DISTRIBUTED HYDROLOGIC MODEL CLIMATOLOGY OVER THE CONTERMINOUS UNITED STATES FOCUSED ON FLASH FLOODING

A DISSERTATION APPROVED FOR THE SCHOOL OF METEOROLOGY

BY

Dr. Robert Palmer, Chair

Dr. Jonathan Gourley, Co-Chair

Dr. Randall Kolar

Dr. Phillip Chilson

Dr. Jeffrey Basara

Dr. Yang Hong

Acknowledgments

I would like to offer a sincere thank you to Dr. JJ Gourley, my advisor, for taking a chance on a freshman back in 2007 that lead us to this day, and for the countless opportunities to explore new and exciting areas of research over the last decade. I could not have picked a better person to have as a mentor during this time.

I must also thank Dr. Yang Hong, my co-advisor, for always dreaming big, and pushing us into new opportunities.

I give a special thank you to Dr. Pierre Kirstetter for his encouragement, kind words, and willingness to put up with my crazy ideas.

Last I would like to thank all the members of the HyDROS Lab over the years that have been some of the best colleagues for work, COFFEE and BEER.

Contents

List Of Tables

List Of Figures

Abstract

This study will describe the MRMS reanalysis precipitation dataset created for the time period from 2001 to 2011. This high resolution 1-km^2 5-minute dataset is ideal for simulating flash floods with a distributed hydrologic model. The Ensemble Framework For Flash Flood Forecasting (EF5) is created for the purpose of exploiting this high resolution precipitation information by conducting simulations with multi water balance models. The Coupled Routing and Excess Storage distributed hydrologic model and the Sacramento Soil Moisture Accounting are both adapted for use in EF5.

EF5 is then used to simulate all time series gauged basins in the CONUS with basin areas less than 1,000 km^2. The water balance models are then evaluated in terms of bias, correlation coefficient and Nash Sutcliffe Efficiency. The results show that the water balance models have skill over most of the CONUS with the exception for the mountain west where low quality precipitation estimates may be to blame.

Finally, a climatology of simulated flash floods is produced over the CONUS by running EF5 to produce gridded daily maximum discharge, time of maximum discharge, and minimum soil moisture outputs. Thresholds are then developed to relate minor flood conditions to basin area and mean annual precipitation so that flooding conditions can be defined even for ungauged watersheds. Maps of the mean annual number of flash flood days are created which show an enhanced region over the central plains particularly Texas and Missouri.

Chapter 1

Introduction

Flash floods are defined by the U.S. National Weather Service (NWS) as "a rapid and extreme flow of high water into a normally dry area, or a rapid water level rise in a stream or creek above a predetermined flood level, beginning within six hours of the causative event (e.g., intense rainfall, dam failure, ice jam). However, the actual time threshold may vary in different parts of the country" (NWS 2016a). This definition is matched by definitions from the World Meteorological Organization (WMO) which puts the time scale as between four to six hours (WMO 1988) and the American Meteorological Society (AMS) policy statement on flash floods which establishes an upper bound for affected basin size at 1,000 km^2 (AMS 2000). A WMO survey on disaster risk reduction found that 105 out of 139 responding countries identified flash floods as a hazard, second to strong winds as the most common hazard. Further of the 99 countries that responded as issuing flash flood warnings, 91 said improvements to the warnings are necessary (WMO 2008).

Floods are second to heat in terms of number of fatalities in the U.S. (Ashley and Ashley 2008). Kunkel et al. (1999) found that flash floods account for 80–90% of all flood fatalities and that there is a steady upward trend in flood damages (constant dollars) over the past century. The increasing trend may be do to climate change with several studies finding a link between warming and extreme rainfall events (Kharin et al. 2007; Hirabayashi et al. 2013). Mallakpour and Villarini (2015) along with Hirsch and Archfield (2015) argue that the magnitude of floods may not be increasing but the frequency with which floods occur is increasing. In either scenario an appropriate historical database of flash flood events, one which can easily be adapted

to include new flood events, is necessary for monitoring of these events. Figure 1.1 shows the fatalities due to weather hazards recorded by the NWS for 2015 and the 10- and 30-year average fatalities per year. 2015 had a well above average number of flood fatalities. Only heat has a higher 30-year average number of fatalities than flooding.

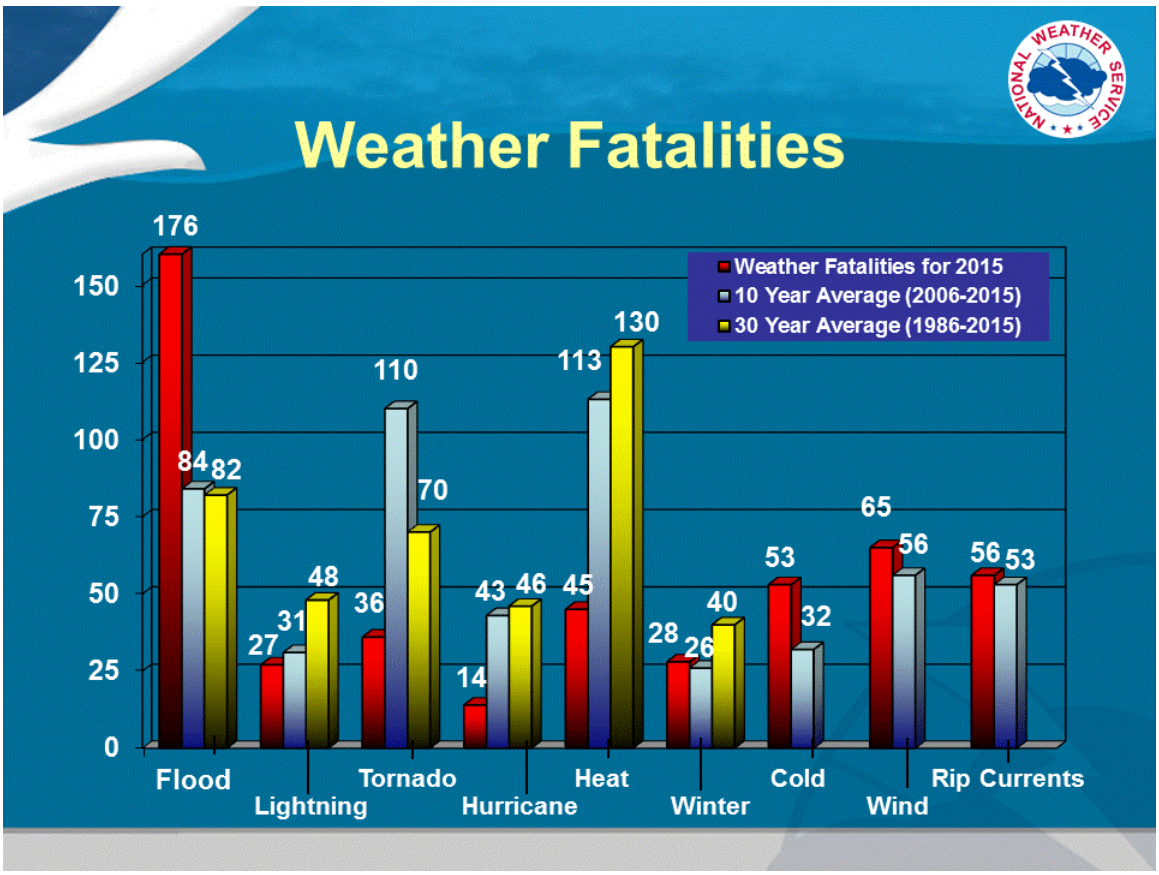

Figure 1.1: Fatalities due to weather hazards for 2015 with 10- and 30-year averages. Figure adapted from NWS (2016b).

A few examples of recent fatal flash floods in the U.S. include June 11th, 2010 in Arkansas where 20 campers lost their lives. May 31st, 2013 in Oklahoma City, Oklahoma had significant flash flooding that killed 13 people, the most in the Norman WFO area since 1934. The event is documented in a NWS service assessment (NWS 2014) and several papers have covered the environmental setup leading to over 150 mm of rainfall (Yussouf et al. 2016; Bluestein et al. 2015). Figure 1.2 shows the recorded damage locations across Oklahoma City, Oklahoma for this event. Private

property as well as public property such as schools, hospitals and roads were damaged by this high impact event. September 14th, 2015 in Hildale, Utah, 19 people were killed in a flash flood event; this event is the most deadly weather disaster in Utah history.

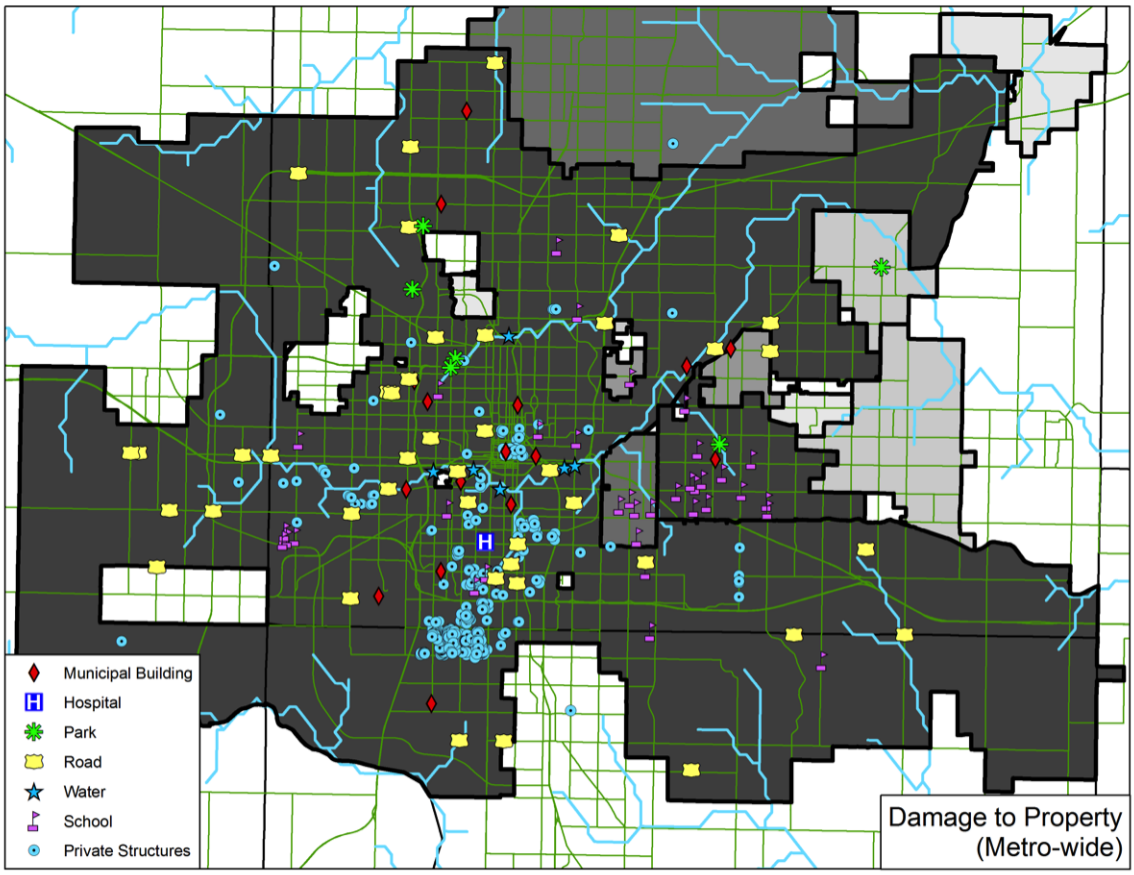

Figure 1.2: Damage location and types of damage for the May 31st, 2013 flash flood across the Oklahoma City, Oklahoma region. Figure adapted from Clark (2016).

Flash flood events are poorly understood and poorly documented when compared to their cost in terms of dollars and human impact. The AMS policy statement on the prediction and mitigation of flash floods states, "Still further, the databases created by the new observing capabilities facilitate better studies of the physical character of such rainfall events. This is especially true for understanding flash flood dynamics and microphysical processes, knowledge that is vital for the development of improved radar rainfall estimates" (AMS 2000). This study will develop the first continental

scale flash flood climatology from a distributed hydrologic model at 1 km^2 and five minute spatiotemporal resolution.

In doing so this study proposes two hypotheses. The first is if the hydrological processes governing the generation of flash floods are explained by the distributed hydrologic model forced by radar quantitative precipitation estimate (QPE), then time series of discharge for flash flood events can be produced. If the first hypothesis is true and if the discharge threshold for flooding can be modeled using a statistical relationship with basin area and mean annual precipitation then spatial climatologies of flash flooding can be produced.

This study works to better document flash flood events in the U.S. during the 2002–2011 time period by providing supplemental information from hydrologic simulations forced by the improved radar rainfall estimates from the Multi-Radar Multi-Sensor (MRMS) system. This information will include peak discharge, time of day of peak discharge and antecedent soil saturation. To do this a hydrologic modeling framework will be developed where multiple water balance and routing models can be easily combined to produce simulation results from a single set of input data.

This study is part of the much larger Flooded Locations And Simulated Hydrographs (FLASH) project, which aims to provide NWS forecasters with better warning decision support tools for issuing flash flood warnings (Hong and Gourley 2014; Gourley et al. 2016; NSSL 2016). Specifically the goal of the project is to improve the spatial specificity, timing, and accuracy of flash flood warnings by leveraging MRMS rainfall products for high resolution forward simulation. This study documents the hydrologic models used for FLASH, their setup, and their performance over the current period of record for the precipitation forcing. These hydrologic models have already been used for experimental evaluations with NWS forecasters in the Hydrometeorology Testbed (HMT) Hydro experiment (Martinaitis et al. 2016) and the Flash Flood And Intense Rainfall (FFAIR) experiment (Barthold et al. 2015). In

both places the hydrologic products presented here received favorable reviews. These hydrologic products have been used for experiments with automation in the warning decision process by recommending locations for possible flash flood warnings (Argyle et al. 2016).

This study is organized into five chapters which document the hydrologic model, setup, and the simulation results. A description of each chapter follows, with the first chapter being this introduction.

Chapter 2 describes existing observations of flash floods, the MRMS radar precipitation dataset that will be utilized in this study, and how future flash flood databases may be crowd sourced using tools like meteorological Phenomena Identification Near the Ground (mPING). This chapter provides literature review on existing climatologies and that databases used to create them. This includes many databases in both the U.S. and worldwide.

Chapter 3 is a description of Ensemble Framework For Flash Flood Forecasting (EF5). The chapter will discuss design decisions behind EF5, the water balance options, and routing options available for use. A case study of simulations in Arkansas is presented, followed by bulk analysis of the time series over the conterminous United States (CONUS) for basins with United States Geologic Survey (USGS) discharge gauges and basin areas less than 1,000 km^2. Finally, discussions of training are capacity building activities with EF5 are presented. This includes how EF5 is being used for work with NASA SERVIR in Africa.

Chapter 4 details a flash flood climatology created over the CONUS using EF5 forced with MRMS precipitation rates for the period from 2002 through 2011. The chapter will show the climatology as a function of season, and detail the hour of the day that flooding is most experienced. This dataset has the potential to be a database of flash flood events from the 2002–2011 time period and could be further exploited in future research as well.

Last, chapter 5 presents a brief review of the work conducted, and conclusions drawn from the work. Possible future work will also be presented that details how improvements can be made to the MRMS QPE, better collection of observations for model verification, and how better models can be developed.

Chapter 2

Datasets

2.1 Flash Flood Databases

Despite the impact of flash floods, recorded information in the National Center for Environmental Information (NCEI) *Storm Data*, the official record of storm occurrence in the United States contains sparse information on the hydrologic response from heavy rainfall. For a flash flood event the free style narrative may contain information on how much rain fell and if there was a stream gauge impacted, the associated stage height change. However, this information is not standardized or always included. An example *Storm Data* narrative, "Thunderstorms produced heavy rain that caused flash flooding leading to two high water rescues in Austin. One at Stassney Ln. and Palo Blanco Ln. and the other at Pleasant Valley Rd. and Onion Creek Dr. in southern Austin," illustrates this point with little information on the magnitude of the hydrologic hazard provided making it difficult to assess the contribution of an extreme hydrologic hazard versus societal response. Contrast this with tornadoes where *Storm Data* contains explicit fields for tornado damage rating, tornado path length and tornado width. As such if one wishes to attempt to correlate severity of hydrologic response with severity of impacts then additional data collection is necessary.

Similar efforts to create compilations of flash floods such as those documented in Llasat et al. (2010) and Gourley et al. (2013) also lack information on the magnitude of the hydrologic hazard for many of the events and data sources. Llasat et al. (2010) compiles existing databases including the International Disaster Database, the

European Severe Weather Database, databases from reinsurance companies, newspapers, and scientific case studies into a single flood and flash flood database focused on documenting numbers of fatalities and damage costs. Gourley et al. (2013) integrates U.S. specific databases such as flash flood data from Severe Hazards Analysis and Verification Experiment (SHAVE) (Gourley et al. 2010a; Ortega et al. 2009), USGS discharge gauging stations, and NWS observations of flash flooding from *Storm Data* into a single website for ease of download. Only the USGS discharge gauging station database provides information on hydrologic parameters of flash floods including timing and peak discharge. In Europe there have been continental and regional databases created indexing only extreme flood events and including estimates of flood peak discharge, flood duration, and rainfall accumulation.

Gaume et al. (2009) compiled flash flood data for the entire continent with an aim to capture the top 30 flash floods in each region using all available data sources. For an event to be contained inside the database an estimate of peak discharge must be available from at least one cross-section. This makes this database one of the few with hydrologic information but it is still limited to major flash flood events only. Marchi et al. (2010) expanded on the work of Gaume et al. (2009) by including additional information such as soil moisture in the previous 30 days and digital elevation models for impacted basins. Again this compilation was limited to only the most extreme flash flood events available in the existing database. Mediero et al. (2015) use observed discharge time series to build a comprehensive set of flood events over Europe for a time period from 1900 to 1999. Ruiz-Villanueva et al. (2013) builds a database of flash flood events in ungauged basins in Spain by using existing documentation to examine flood events and then compute rainfall-runoff relationships from daily rainfall to estimate the peak flood discharges. Another reconstruction of flash flood events in Spain is conducted by Rodriguez-Morata et al. (2016) using dendrogeomorphic

techniques. Bryndal (2015) generated a database of flash flood events over Poland, but does not attempt to quantify the peak discharge associated with the floods.

Costa (1987a) compares flood envelopes, maximum peak discharges by basin area, from the U.S. and China, compiling information from China based on personal communication. A database of flood fatalities in Australia was compiled by Coates (1999) where the database contains physical characteristics of some of the flooding events. The paper notes a limitation in differences of information from event source to event source suggesting that a comprehensive database with information compiled in a similar manner would increase the overall utility of the data. Adhikari et al. (2010) creates a global flood inventory by combining information from multiple sources. The data for this inventory contains a discrete severity class based on the recurrence interval for the flood event. However, there are only three severity classes which define small to medium flood events, large events and extreme events.

Regardless of the area of the world the information available on flash flood events is lacking in quality and completion. The peak discharges are often estimated through reconstruction (high water marks) and extrapolation of stage-discharge relationships. This method is suitable for analyzing events that have occurred hours or days ago but over time high water marks fade making reconstruction months or years after an event difficult. In basins equipped with stream gauges, the stream gauge itself may yield measurements of the peak discharge, however Ruin et al. (2008) notes that high storm intensity often affect gauge measurement reliability and integrity. Smith et al. (2014) and Le Boursicaud et al. (2015) both developed unique methods for retrieving flood discharge from recorded images and videos using photogrammetry but are limited to events where this information is available. Costa (1987b) uses a slope-area relationship to estimate peak flood discharges over the CONUS from a form of Manning's equation but requires surveyed channel cross-sections for estimation. Given the lack of recorded physical characteristics of flash flood events and the difficulty in

reconstructing the record from the environment another method is needed for creating retrospective information on flash flood events.

Herschy (2002), which updates maximum flood envelope curves for data through 1999, states "The estimation of floods by statistical and mathematical analysis will always be important especially where no measurements exist but actual measurement, where possible, will always be preferable." Distributed hydrologic and hydraulic models, which are one form of mathematical analysis, have been used partially or fully in reconstruction efforts to estimate the peak discharge of flash flood events and build databases of hydrologic variables (Koutroulis and Tsanis 2010; Braud et al. 2010; Ballesteros Cnovas et al. 2010; Smith et al. 2014). This study expands on these works and creates a climatology of flash flood events for the 2002–2011 period when MRMS forcing data are available.

2.2 Storm Data Flash Flood Events

NCEI *Storm Data* is an official publication to document storms and significant weather phenomena which have the intensity to cause loss of life, injuries, significant property damage or disruption to commerce (NWS 2007). The publication is also expected to include rare or unusual weather in which there is media coverage and significant meteorological events such as temperature minima and temperature and precipitation maxima that occur in connection with another event. *Storm Data* allows for forty eight different types of events to be included in the publication. The period of coverage for all forty eight event types runs from January 1996 to present with a ninety day lag to allow for research into recently occurring events. *Storm Data* events are recorded based on a specified point, however for many flash floods early in the study period the point is left out of the data set and the event is considered to be "countywide." Starting in October of 2006 the events switched to being storm based where a set of coordinates defining a polygon around the impacted area are also stored in the database. The accuracy of the storm based polygons is unknown at this time, especially for flash flood events, and there is a desire to include as much data as possible so the county locations will be used for this study.

The data used in *Storm Data* is collected by the NWS. The NWS gathers information from many places, including county, state and federal emergency management officials, law enforcement officials, spotters and storm chasers, official NWS damage surveys, reports from the general public including social media, and information collected by insurance companies. The NWS does not have the resources to verify the information reported to them in terms of damage amounts and injuries so the data are considered to be the best easily available data set in terms of accuracy. The damage amounts are specifically referred to as the "best guess" by the NWS. *Storm Data* is used as the official verification source for warnings issued by the NWS so there is an incentive for offices to capture events for which they issue warnings. This is both a

good and bad thing, but given the frequency of warning issuance will tend to insure that every damaging event is captured.

For the period from 2002 through 2011 there are 35,240 flash flood events reported in *Storm Data*. The damage from these events is reported at $5,103,429,787 and 518 lives were lost. There are 528 reported injuries due to flash flooding in the database during this time period. Figure 2.1 shows the distribution of *Storm Data* recorded flash flood events from 2002 through 2011 normalized by the area of the reporting county. Notable hot spots include the Texas hill country with many counties seeing over one event a year. South-western Missouri also has a noticeable maximum in flash flood events with many of the counties in the region also seeing over one event a year.

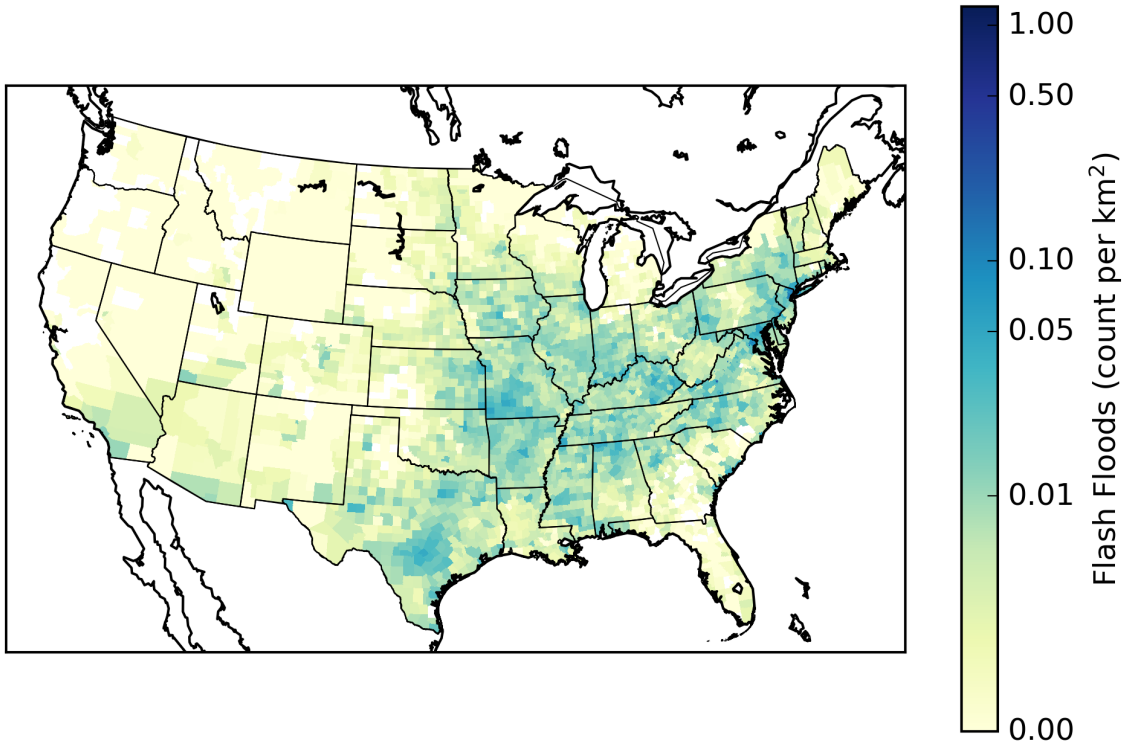

Figure 2.1: The number of *Storm Data* flash flood event reports for each county normalized by the area of the county for the period from 2002 through 2011.

Figure 2.2 shows the distribution of *Storm Data* recorded damage costs from flash flood events from 2002 through 2011 normalized by the area of the reporting county. Local maxima are present over central Mississippi, northern Ohio, and southern New

York. The locations of the maxima are different for the damage costs compared to the number of flash flood events suggesting that the sheer number of events does not drive the distribution of costs of flash flood events. There may also be a reporting bias present by the NWS where more detailed surveys of impacts are conducted in areas with fewer overall flash flood events. The influence of population is visible in this figure with local maxima over Dallas, Chicago, and Birmingham. The exposure of more infrastructure to flash floods increases the relatively chance of damage so these maxima over populated locations make physical sense.

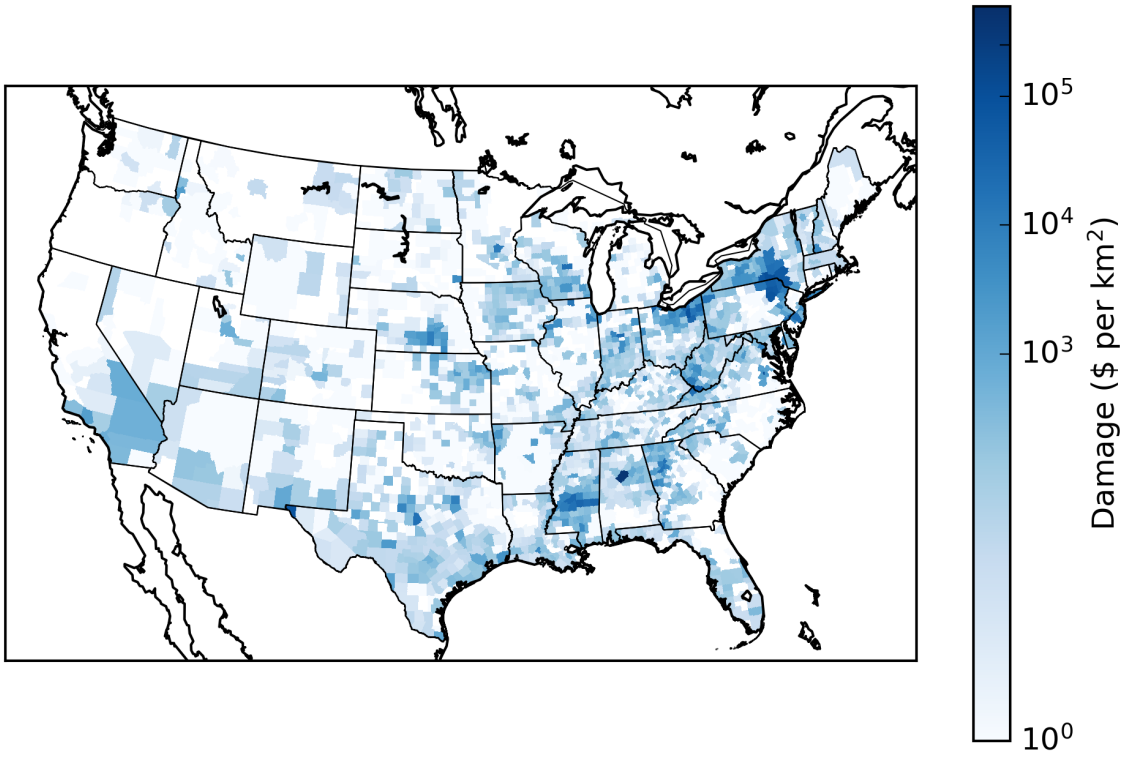

Figure 2.2: The damage costs of *Storm Data* flash flood events for each county normalized by the area of the county for the period from 2002 through 2011.

Figure 2.3 shows the *Storm Data* recorded deaths and injuries from flash flood events from 2002 through 2011 normalized by the area of the reporting county. Deaths and injuries are rare in a relative sense with few counties reporting significant multiples of fatalities. The Texas hill country features a local maximum in both deaths and injuries. Other local maxima are scattered through the southeast and midwest

for both deaths and injuries. In Arizona and southern California there is a signal that fatalities and injuries due to flooding occur there but the counties are so large it is not possible to narrow down on more problematic areas. Single events with multiple fatalities or injuries seem to be controlling the distribution of these impacts suggesting that these are rare enough occurrences that more data are needed to fully resolve locations with anomalously high numbers. Overall, the deaths and injuries look very similar in spatial distribution to the distribution of the total number of flash flood events. This is in direct contrast with the spatial distribution of the damage costs which are displaced from the spatial distribution of flash flood events.

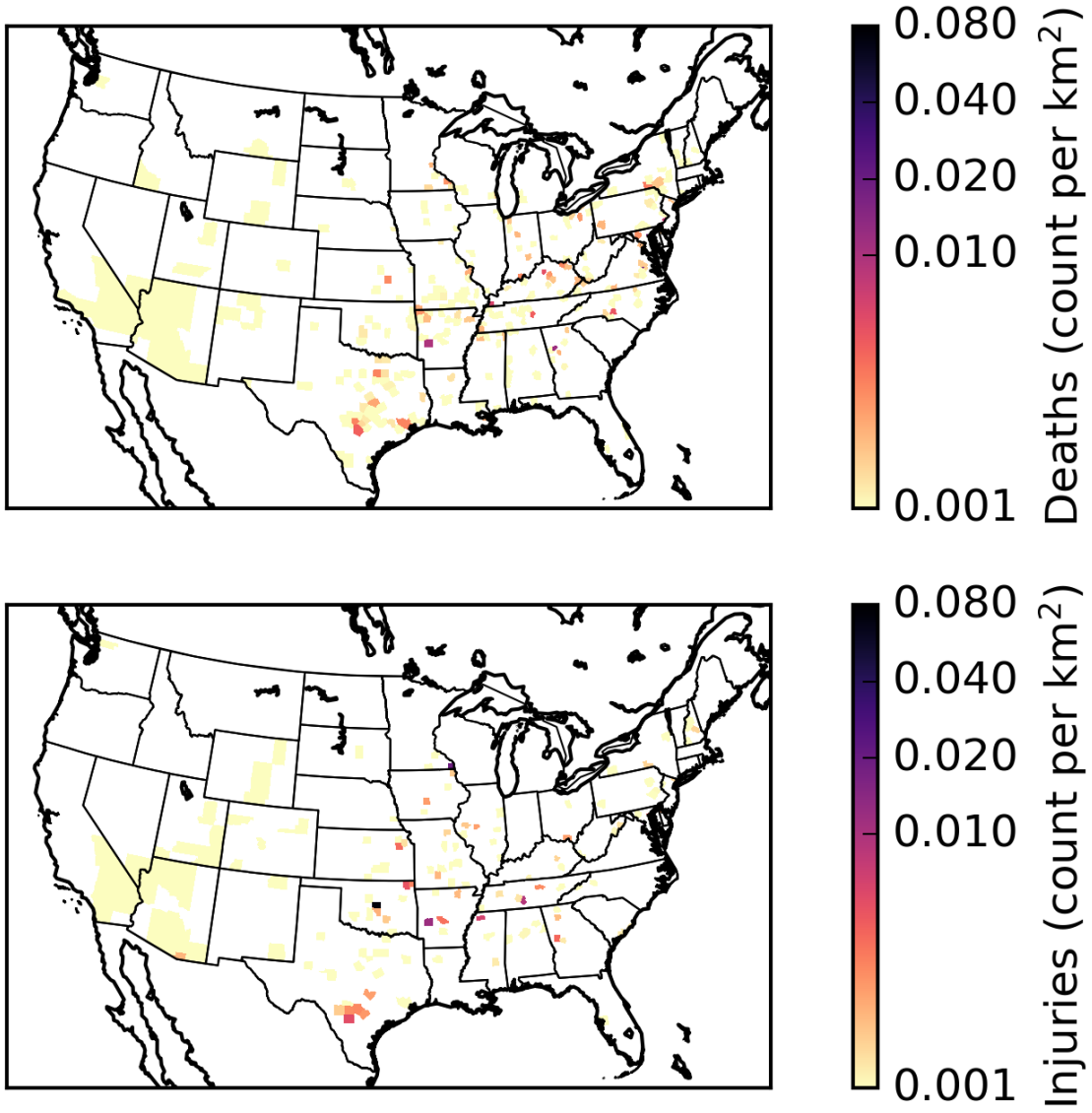

Figure 2.3: The top (bottom) panel shows deaths (injuries) from *Storm Data* flash flood events for each county normalized by the area of the county for the period from 2002 through 2011.

2.3 MRMS Precipitation Forcing

As hydrologic models have evolved so has the forcing information used to drive them. Rainfall data, once only available from rain gauges are now available from ground radars with spatially distributed maps updated in near real time. These rapidly updating radars have driven the creation of mosaic radar rainfall products over the CONUS. The U.S. NWS River Forecast Center (RFC) provide Stage IV hourly rainfall accumulations (Lin and Mitchell (2005)) for most of the CONUS utilizing a blend of rain gauges, radar rainfall estimates and human editing. The Stage IV QPE is available with a resolution of 16 km^2 at 1-, 6-, and 24 hour accumulation periods. However, because of the human-in-the-loop nature of the rainfall estimates they are not updated as frequently as possible given radars with volume coverage pattern updates on the order of five minutes and low elevation scan revisit times on the order of a single minute in newer operating modes (Chrisman 2009; Daniel et al. 2014). The MRMS project started by the National Oceanic and Atmospheric Administration (NOAA) National Severe Storms Laboratory (NSSL) has revolutionized the realm of radar based quantitative precipitation estimates by generating rapidly updating QPE without human intervention giving new precipitation estimates every five minutes. This study will utilize the rapidly updating QPE from the MRMS project for modeling of flash floods using a distributed hydrologic model over the CONUS.

Zhang et al. (2016) describes the MRMS system as a whole and in particular the QPE generation process as derived from the predecessor National Mosaic and Multi-Sensor QPE (NMQ) system (Zhang et al. 2011a). The MRMS system utilizes advances in networking and computational power to centralize collection of level II radar data from 160 radars across the CONUS (Kelleher et al. 2007). After the data are collected at a central location the first step in processing the radar data are quality control. The radar data are processed to remove non-precipitation echoes which may include ground clutter, biological objects such as birds and bats, sun strobes,

and electronic interference. This quality control procedure is carried out in three steps. First using heuristic rules to remove obvious ground clutter and anomalous propagation where the Doppler velocity is zero, as well as easy to identify features such as sun strobes and speckles. Second, a neural network classification trained on the mean, median, and, variance of the reflectivity, Doppler velocity and spectrum width helps identify non-precipitation echoes (Lakshmanan et al. 2007, 2010). Finally, another set of spatiotemporal image filters and rules is applied to remove any remaining non-precipitation echoes such as hardware testing signals. These rules can combine information from numerical weather prediction models such as the surface temperature to completely remove all radar echoes when the radar is operating in clear air mode and the surface temperature is above 5°C. The vertical profiles of reflectivity (VPR) from each single radar are then examined to determine and correct for issues such as radar bright banding (Zhang et al. 2008; Zhang and Qi 2010). This correction process is essential if the data in the bright band must be used to generate the precipitation estimate. The VPR are also examined to determine the type of precipitation regime that is occurring in each range bin such as convective, or warm rain in order to apply the appropriate Z-R relationship (Xu et al. 2008; Grams et al. 2014). The radar data from each single radar is then interpolated from polar coordinates on to 2D Cartesian coordinates on a grid with a horizontal resolution of 0.01°. The polar coordinate data are selected such that the lowest altitude radar that are not blocked by terrain or other obstacles are used in the analysis. This product is equivalent to the hybrid scan reflectivity (HSR) product generated in Fulton et al. (1998) and so named because it consists of data from different elevation angles for each azimuth and range bin. An exponential weighting scheme defined in Zhang et al. (2011a) is used to mosaic the HSR from multiple radars onto a single common Cartesian grid. This weighting scheme was picked because it produces better continuity than a nearest neighbor approach. Figure 2.4 shows the height of the radar beam used

in the hybrid scan reflectivity computation over the CONUS. Poor radar coverage is visible in the western CONUS with large areas of high radar beam height.

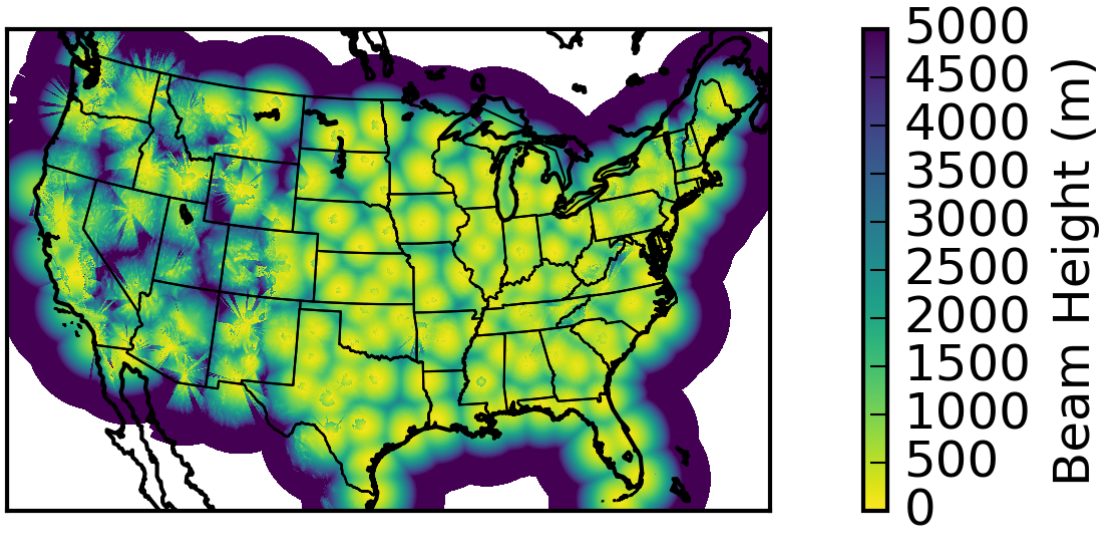

Figure 2.4: Height of the radar beam (m) in the hybrid scan reflectivity mosaic produced by MRMS.

Where MRMS really differentiates from existing rain rate algorithms is the ability to determine on a per grid cell basis which Z-R relationship is most applicable. The system does this with a simple decision tree based on the 3D reflectivity data, surface temperature, surface wet bulb temperature, the column vertically integrated liquid density, and if a warm rain process was identified in the VPR. Figure 9 in Zhang et al. (2011a) details the entire decision tree with resulting classifications as either snow, hail, warm rain, convective rain, or stratiform rain. Qi et al. (2013) examines the segregation between stratiform and convective rain modes in the decision tree and improves upon the classification results. The resulting Z-R relationships are as listed where convective rain uses $Z = 300R^{1.4}$ (Fulton et al. 1998), stratiform rain uses $Z = 200R^{1.6}$ (Marshall et al. 1955), warm rain uses $Z = 230R^{1.25}$ (Rosenfeld et al. 1993), and snow uses $Z = 75R^{2.0}$ where Z is the radar reflectivity in $mm^6\ m^{-3}$ and R is the rain rate or snow water equivalent in $mm\ h^{-1}$.

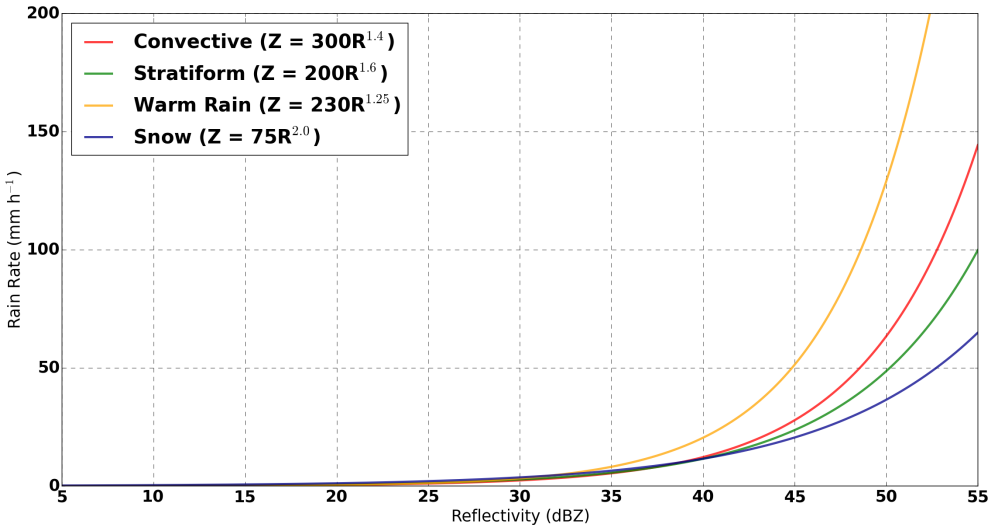

Figure 2.5: The Z-R relationships used in the MRMS system for different precipitation regimes as a function of radar reflectivity.

Figure 2.5 shows in graphical form the differences between the Z-R relationships as a function of radar reflectivity. The separation between the relationships is most evident for higher reflectivity values illustrating the need for correct identification of the precipitation regime.

Several studies have looked to quantify the performance of MRMS QPE both in terms of comparing to raw rain gauge measurements and the impact on hydrologic modeling. Kitzmiller et al. (2011) focused on the impact of MRMS QPE on discharge prediction in the Hydrology Laboratory-Research Distributed Hydrologic Model (HL-RDHM) (Koren et al. 2004). The study focuses on three wet periods including Hurricane Isabel in September of 2003. The conclusions drawn from the study show that the MRMS QPE products are uniquely capable of capturing the dynamic Z-R relationship environments in tropical systems and cool season rain events. Chen et al. (2015) compared MRMS QPE to Stage IV QPE on a grid cell by grid cell basis for a two year period and found very favorable correlations across most of the CONUS. The biggest differences are in regions of complex terrain where the gauge adjustments and human modifications are increasingly important suggesting MRMS

may struggle in these areas due to its radar only nature. In Chen et al. (2016) the MRMS surface precipitation types are evaluated against data from mPING. mPING data are collected from citizen scientists who use an Android or iOS app to report the occurrence of rain, snow, or mixed precipitation types at the users' location (Elmore et al. 2014). In general there is good agreement between MRMS rain and snow precipitation classes and the data collected from mPING. In a few cases the MRMS system reports rain when the mPING observations are snow which suggests the thresholds used for delineation in the precipitation regime decision tree could be further optimized in the future.

The MRMS system has primarily been a research system focused only on processing incoming data in real time. To perform more comprehensive studies and analysis there was a desire for the MRMS QPE to be generated for a retrospective period. Subsequently collaboration between NCEI and NSSL yielded an agreement to produce an MRMS QPE reanalysis period going from 2001 through 2011. This period was selected because it covers the period from when installation of the WSR–88D over the CONUS was completed and data was archived at a centralized location through when the upgrade to dual polarization began for the network. With dual polarization radars it may be possible to get better precipitation estimates in the MRMS system (Gourley et al. 2010b) and better quality control (Tang et al. 2014) but that work has not yet been finalized.

The MRMS system is constantly evolving with new algorithms and improvements to old ones. As such, the MRMS algorithms used for this reanalysis are out of date with the operational MRMS system now in use. The newer MRMS algorithms do not pick deterministic Z-R relationships for each type class but use a linear combination of Z-R relationships based on the probability of each type class. This provides smoother transitions between types and allows for more variability in the overall rain rates produced.

The MRMS reanalysis domain is the same as the operational MRMS domain with products on a regular 0.01° grid spanning from –130.0 to –60.0 longitude and 20.0 to 55.0 latitude producing a grid with 7000 columns and 3500 rows for a total of 24,500,000 grid cells. The 5 minute precipitation rate products were produced for this entire period and then distributed to users. The archive of precipitation rate data totals 800 GB and 1,139,162 individual files.

Figure 2.6 shows the MRMS radar only precipitation rates accumulated for yearly average for the period from 2001 through 2011. The yearly average precipitation has a gradient from the east to west across the western two-thirds of the CONUS until the Rocky Mountains. The mountainous western region of the CONUS has many radar artifacts still present such as beam blockage, and ground clutter. Along the west coast of the CONUS the yearly average precipitation values are higher than anywhere else in the CONUS. The overall distribution of precipitation matches well with other climatologies such as Parameter Elevation Regressions on Independent Slopes Model (PRISM). Figure 2.7 shows the average precipitation accumulation for days with accumulations >1 mm for the period from 2001 through 2011. The daily average precipitation accumulation was averaged to 0.5° grid cells and then interpolated back to 0.01° grid cells using bilinear interpolation. The gradient from east to west is no longer present in the daily average precipitation map indicating that the gradient present in the annual average precipitation is created by having fewer rainfall events and not more events with less rainfall per event.

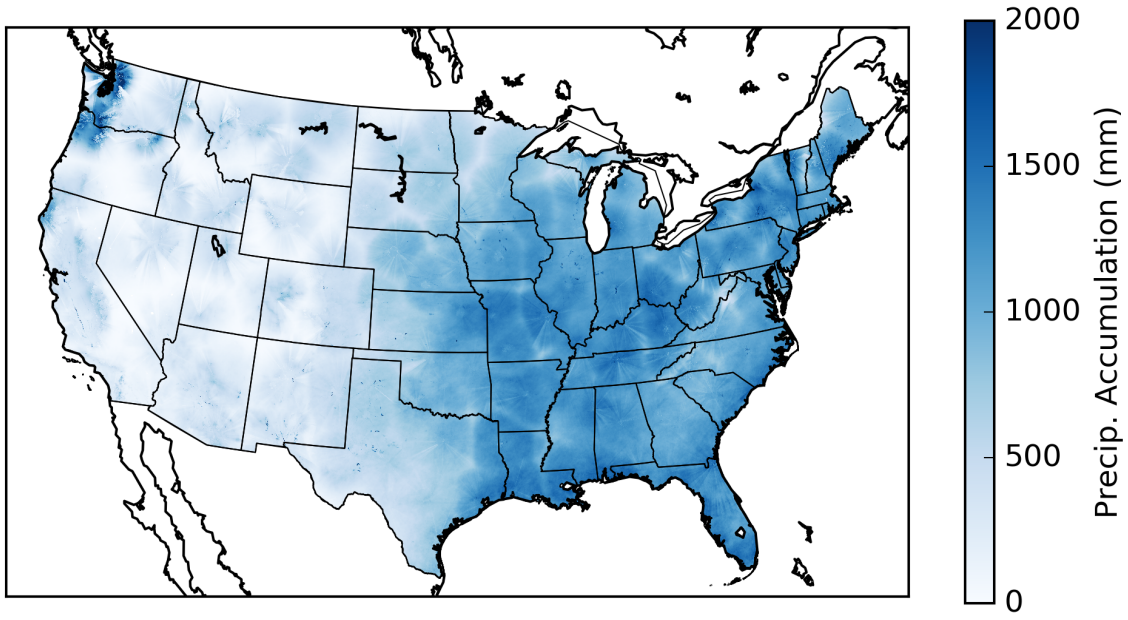

Figure 2.6: Yearly average MRMS radar only precipitation rate accumulated for the period from 2001 through 2011.

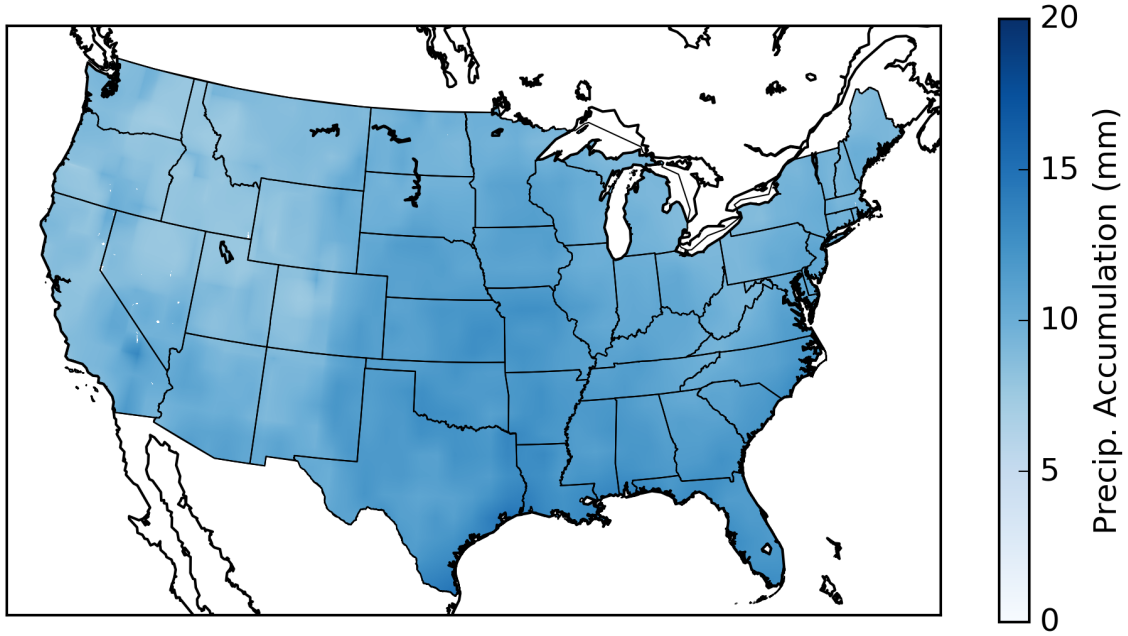

Figure 2.7: MRMS radar only average daily precipitation accumulation for days with >1 mm of precipitation.

2.4 mPING Flash Flood Reports

The mPING project started as a way to collect reports of the precipitation type falling at the surface, particularly for winter weather events where transition zones between rain and snow may be quite small (Elmore et al. 2014). The reports were collected in order to improve the surface precipitation type classifications produced by the weather radar network. The reports were collected by crowd-sourcing, where individuals download an app on their phones and then submit a report when there is precipitation falling. The reports are automatically tagged using the phones GPS to provide the location of the report and the time. The iOS application was developed by the author of this dissertation. As of July, 2016, mPING applications had been downloaded over 100,000 times and over 1 million reports had been collected. Figure 2.8 shows the iOS mPING app interface. Notable features include the simple interface with emphasis on collecting the report.

The mPING applications were first released in December of 2012 and focused only on precipitation type. Shortly there afterwards in May of 2013 the apps were expanded to collect reports of other weather hazards such as wind, floods, tornadoes and reduced visibility. As of July, 2016 there have been 3,883 flood reports collected out of a total of 1,000,000+ reports. The reports are loosely classified by severity with table 2.1 showing the flood levels, associated descriptive text, and number of reports. The data collected so far seems unbiased with the more severe and rarer classes of flash flooding seeing fewer overall reports.

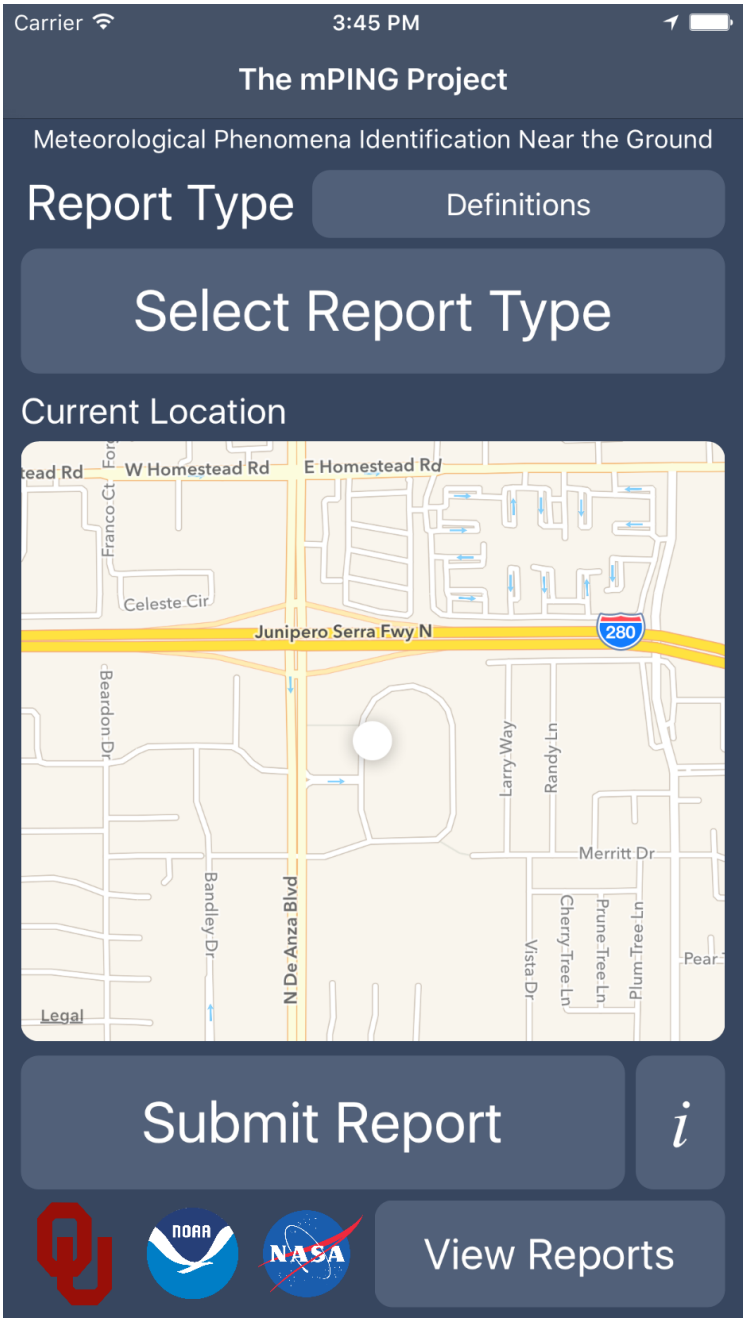

Figure 2.8: The iOS interface for the mPING app which collects crowd sourced reports of precipitation types and weather hazards.

mPING has been translated into 10 different languages, French, Chinese, Spanish, Estonian, Hungarian, Vietnamese, Polish, Greek, Portuguese, and Serbian. This in an effort to increase the exposure around the world and enable the collection of reports in the future from anywhere in the world by making it available in a language native to a majority of the people in the world. The reports already collected by mPING are

Table 2.1: mPING Flood Reports

Flood Level	Description	Number of Reports as of July 2016
1	River/Creek overflowing; Cropland/Yard/Basement Flooding	2563
2	Street/road flooding; Street/road closed; Vehicles stranded	1228
3	Homes or buildings filled with water	52
4	Homes, buildings or vehicles swept away	40

waiting for analysis to determine their significance. The reports could also be used by hydrologic models as a source of data for data assimilation, especially if the reports can be linked to inundated locations using a digital elevation model (DEM). Future databases for flash flood information may rely heavily on crowd sourced reports to identify the locations, time and impacts of the flash floods.

mPING is now a collaborative project between the University of Oklahoma (OU), NSSL, NASA, and commercial partner AccuWeather who owns the patent on crowd sourcing weather reports. The AccuWeather press release available at `http://www.accuweather.com/en/press/58766354` provides more details on the ongoing collaboration between the two organizations. mPING is a shining example of successful crowd sourcing and collaboration between public, private and academic partners. The project has been featured twice on the White House Blog as an example of successful federal government crowd sourcing.

The future for mPING is very promising, but the number of reports is not yet enough to develop climatologies of flash flooding. The reports are also biased towards areas with larger populations, as well as populations with more weather savvy citizens. This results in few reports in the western U.S. because of small population density limiting the overall utility right now. Future developments and more work to

promote mPING may change the distribution of reports making it more suitable for climatological studies.

Chapter 3

Ensemble Framework For Flash Flood Forecasting (EF5)

3.1 Introduction

To fully capture flash flood events distributed hydrologic models need to be run at fine spatial resolution on the order of 100 m to 2 km with a temporal step that is sub-hourly (Rafieeinasab et al. 2015). Given this requirement to run with fine spatiotemporal resolution several distributed hydrologic models were evaluated for their potential to be run in this fashion to capture flash flood events over the CONUS. The Two-Dimensional Runoff Erosion and Export (TREX) distributed hydrologic model was one option, however the model attempts to be fully physical meaning that it requires very fine spatial resolution and time steps on the order of seconds in order to properly solve the equations (Velleux et al. 2008). Running it over the CONUS would require computational resources unavailable at present time to OU and NSSL. Given the obvious choice for a full physics hydrologic model was out of the running one had to decide if any fully physical hydrologic model would be suitable to this problem domain at the present time. There is a wide body of literature asking the question of just how accurate are the physically based hydrologic models and can we produce equal forecasts and understanding with a conceptual simple model?

Devia et al. (2015) provides an overview of the differences between empirical (statistical), conceptual (parametric), and fully physical hydrologic models. The authors provide valuable dialog recognizing that each formulation of a hydrologic model has strengths and weaknesses and there is no one answer for the entire problem domain

in hydrology right now. Empirical models are considered to be useful only for the specific watershed they are developed on and cannot be easily extrapolated into new water sheds. Conceptual models are defined as simple and easily to implement in software but require large amounts of data for calibration. Physically based models require extensive amounts of data on processes often not observed by current sensor networks and suffer from an inability to scale to large collections of watersheds. They further state that, "Each model has various drawbacks like lack of user friendliness, large data requirements, absence of clear statements of their limitations etc. In order to overcome these defects, it is necessary for the models to include rapid advances in remote sensing technologies, risk analysis, etc. By the application of new technologies, new distributed models can be developed for modelling gauged and ungauged basins." This belief is held strongly at OU and NSSL too, which will lead ultimately to the creation of EF5.

Beven et al. (2014) addresses the ever increasing spatiotemporal resolutions of hydrologic models and particularly the land surface models coupled to atmospheric weather prediction models. They argue that there is a lack of information available to validate hypothesizes made in hyper resolution models which may lead to mistake beliefs about the processes. Information from hyper resolution models is often presented to stakeholders but without adequate quantification of the uncertainty leading to misunderstandings. Further the information is presented where only part of the model is hyper resolution and for example the precipitation forcing may not support the ability to resolve details at the resolutions being presented on maps. Kuczera et al. (2010) address the problem of uncertainty in the forcing information used for hydrologic models and model structural error. They argue that because of uncertainties in the forcing information, averaging methods applied to obtain it, and hydrologic model structural error that no conceptual model should be presented in a deterministic way. The argument about model structural error suggests that future modeling systems

should be able to account for these uncertainties with different model structures. Micovic and Quick (2009) look at the complexity of model representation needed as the temporal resolution of the hydrologic model decreases. So as simulations move from long term climate simulations at a daily time step to simulations for individual days with extreme flood events is there a need for more hydrologic model complexity? The results from the study are only valid over a single watershed but suggest that important hydrologic processes for extreme flooding are different than the processes yielding good prediction skill at long time ranges.

Given the evidence above the choice of a hydrologic model for CONUS flash flood prediction seems to fall to multiple conceptual models which are computationally efficient. The Coupled Routing and Excess Storage (CREST) distributed hydrologic model developed by OU and NASA for global flood modeling seems like a natural choice for inclusion into such work (Wang et al. 2011). Given the ties between NSSL and the NWS the other logical choice is to include the Sacramento Soil Moisture Accounting (SAC-SMA) model in a distributed fashion similar to HL-RDHM (Koren et al. 2004; Burnash 1995). The available implementations of both CREST and SAC-SMA featured very user unfriendly software. The input forcing were required in different formats for each model, as well as parameter grids. The output predictions from HL-RDHM is in a format unfriendly to any software written in the last 30 years. Further HL-RDHM uses a projection system and raster grid storage solution that are not used in any other software outside of the NWS making it impossible to utilize community development and improvements. The CREST hydrologic model is better with the output formats, producing American Standard Code for Information Interchange (ASCII) text files that can be opened in common geographical information systems (GIS) software. However the choice of text files means the data are not stored in a compressed fashion and so file sizes quickly grow as domain sizes increase. Neither HL-RDHM or CREST are friendly towards new users as both have confusing

error messages (if you even get an error message). CREST did not have the ability to load distributed parameter grids when EF5 was developed. CREST has poor handling of units for both parameters and forcing information requiring input files to be converted to different units instead of allowing for unit conversion multipliers to be supplied by the end user. All of these factors made it desirable to produce a new piece of software which could allow for multi-model hydrologic simulations with common input data sets and tried to be as user friendly as possible.

The ideas behind EF5 were to incorporate the CREST water balance model, SAC-SMA water balance model, and then couple the runoff output from either of those to a linear reservoir routing scheme. As work on EF5 evolved it became apparent that there was a need for more routing options so kinematic wave routing was added as well. Applying EF5 in different locations made it apparent that there was a need for snow parameterization so the Snow–17 parametric temperature index snow model was added to EF5. Additionally it was identified that for some use cases calibration of the hydrologic models was desirable so the DREAM automatic calibration scheme was incorporated into EF5. EF5 also has limited data assimilation capabilities supporting only direct insertion which can also be used as a boundary condition to model a smaller area of a large watershed (Houser et al. 2012) . Figure 3.1 is the flow chart for EF5 showing the various modules and options that can be utilized for distributed hydrologic modeling.

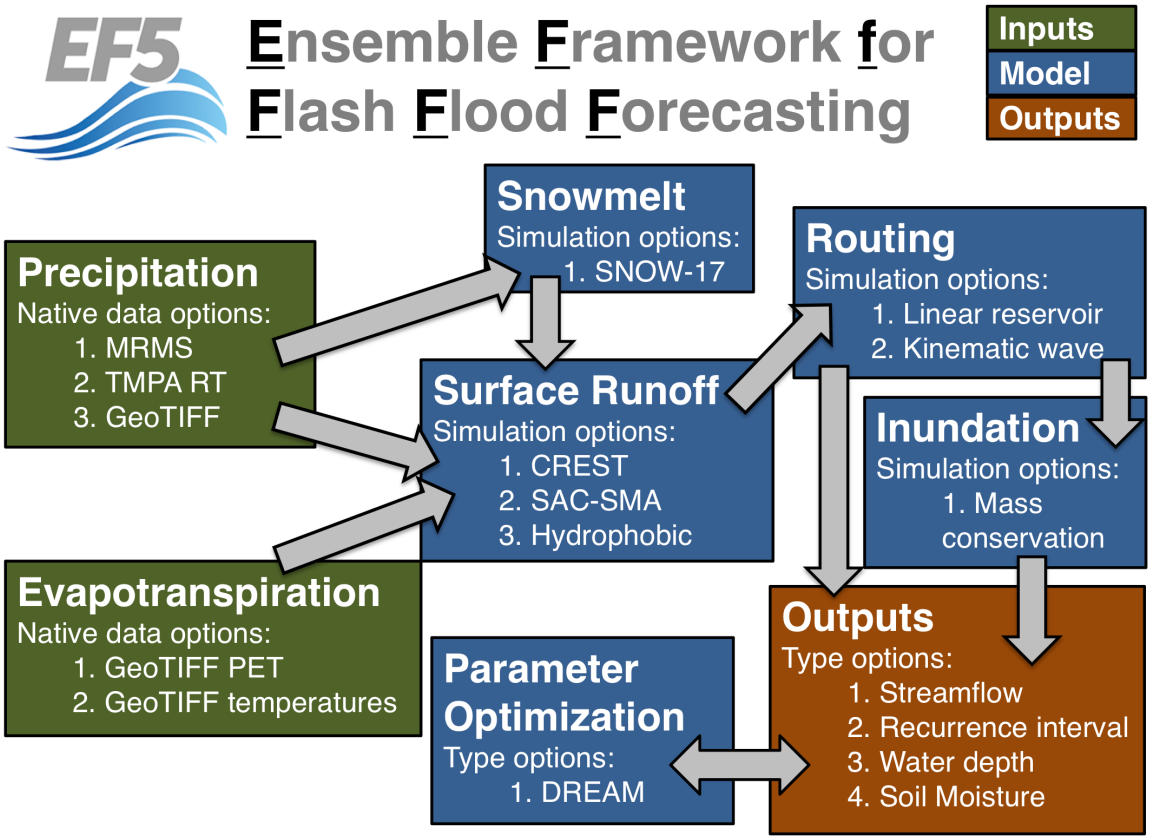

Figure 3.1: Flow chart illustrating the different modules and options available in EF5.

EF5 is designed with the concepts of watersheds in mind. To pick an area to model the basic files must first be provided which includes DEM, flow direction map (FDM), and flow accumulation map (FAM). The downstream point to model is then identified as a "gauge" which may or may not also correspond to an observation measurement location. Groups of gauges can be collected into a "basin" which is fundamentally just a collection of gauges one wishes to model on and not necessarily a collection of gauges in the same physical watershed. Parameters for the models are specified on a per gauge basis and then applied everywhere upstream of the gauge, until the next gauge if there is one. The parameters are specified either as a distributed grid and then a multiplier value or as a single value that is applied uniformly across the watershed.

EF5 is written in C++ and currently contains 20,388 lines of code while supporting Linux, Mac OS X and Windows operating systems. Linux and Mac OS X are supported via binaries run from the shell command prompt while Windows features a fully-fledged Graphical User Interface (GUI). The Windows GUI provides very similar feedback when compared to the Linux and Mac OS X versions but in an easier to work with package. The source code to EF5 is available on GitHub and documented in Flamig et al. (2016).

EF5 currently supports several different options for file formats and map projections. The preferred file format for use with EF5 is Geotiff, which has the distinct advantage of including native compression capabilities reducing file sizes greatly. ESRI Arc ASCII grids are also supported as input options for all gridded fields. For precipitation input, MRMS binary, Tropical Rainfall Measurement Mission (TRMM) TRMM Multi-Satellite Precipitation Analysis (TMPA) 3B42 realtime binary are all supported input options.

EF5 was created to be model physics agnostic and to do so implements virtual base classes for the snow melt, water balance, and routing physics. The water balance base class is detailed below, and thus it is possible for any water balance model that can conform to this specification to be implemented into EF5. EF5 provides two input forcing variables for the water balance component, precipitation and potential evapotranspiration. The output variables are a fast flow (typically surface) component, slow flow (typically subsurface) component, and a soil saturation value.

```
class WaterBalanceModel {
public:
  virtual bool InitializeModel(std::vector<GridNode> *nodes,
      std::map<GaugeConfigSection *, float *> *paramSettings,
      std::vector<FloatGrid *> *paramGrids) = 0;
  virtual void InitializeStates(TimeVar *beginTime,
```

```
    char *statePath) = 0;
  virtual void SaveStates(TimeVar *currentTime, char *statePath,
    GridWriterFull *gridWriter) = 0;
  virtual bool WaterBalance(float stepHours,
    std::vector<float> *precip, std::vector<float> *pet,
    std::vector<float> *fastFlow, std::vector<float> *slowFlow,
    std::vector<float> *soilMoisture) = 0;
  virtual bool IsLumped() = 0;
  virtual const char *GetName() = 0;
  };
```

The base class contains methods for initializing the model, initializing model state variables that may have been saved to file, saving model state variables to file and finally performing the water balance physics itself. For completeness the base classes for the routing and snow components are included below. The routing and snow components contain similar methods to be implemented as the water balance component with functionality for initialization, state loading and saving, and the main method for executing the physics. The routing virtual class takes a fast flow and slow flow input components and provides a single discharge output variable. The snow module takes as input precipitation, and temperature while providing melted runoff (or just passing through precipitation in the no snow case) and snow water equivalent as the output variables.

```
class RoutingModel {
public:
  virtual bool InitializeModel(std::vector<GridNode> *nodes,
    std::map<GaugeConfigSection *, float *> *paramSettings,
    std::vector<FloatGrid *> *paramGrids) = 0;
  virtual void InitializeStates(TimeVar *beginTime,
```

```
        char *statePath, std::vector<float> *fastFlow,
        std::vector<float> *slowFlow) = 0;
    virtual void SaveStates(TimeVar *currentTime,
        char *statePath,
        GridWriterFull *gridWriter) = 0;
    virtual bool Route(float stepHours, std::vector<float> *fastFlow,
        std::vector<float> *slowFlow,
        std::vector<float> *discharge) = 0;
    virtual float GetMaxSpeed() = 0;
    virtual float SetObsInflow(long index, float inflow) = 0;
};
class SnowModel {
public:
    virtual bool InitializeModel(std::vector<GridNode> *nodes,
        std::map<GaugeConfigSection *, float *> *paramSettings,
        std::vector<FloatGrid *> *paramGrids) = 0;
    virtual void InitializeStates(TimeVar *beginTime,
        char *statePath) = 0;
    virtual void SaveStates(TimeVar *currentTime, char *statePath,
        GridWriterFull *gridWriter) = 0;
    virtual bool SnowBalance(float jday, float stepHours,
        std::vector<float> *precip, std::vector<float> *temp,
        std::vector<float> *melt, std::vector<float> *swe) = 0;
    virtual const char *GetName() = 0;
};
```

This implementation of the model physics allows for EF5 to be easily expanded in the future to contain more options for treatment of basic hydrologic functions. This

expandability is a unique feature because many modeling implementations claim to be frameworks for supporting multiple sets of model physics none (to this authors knowledge) actually contain more than a single set of physics options.

3.2 Water Balance Models

Currently EF5 contains three water balance options. All three options are conceptionally based and rely on parameters loosely based on properties measured in existing data sources. The three options described in this section are CREST, SAC-SMA and Hydrophobic (HP). The most detailed description will be provided for the CREST model because the underlying model has been modified from previous publications.

The HP option is by far the simplest, as there are no parameters to be specified for the land surface. The HP option treats the surface as completely impervious so all rain immediately runs off and flows down slope. The HP water balance option is included for the ability to diagnose processes and errors when running in an ensemble with the other water balance models. Underestimation with the HP model indicates that the precipitation is likely biased. When everything is operating correctly the HP model produces an upper bound on the expected discharge values.

Another water balance option, CREST, is a derivation of the Xinanjiang model developed for use in China which features a variable infiltration curve for partitioning rainfall into direct runoff and infiltration. (Ren-Jun 1992; Liang et al. 1996; Liu et al. 2009). The first version of CREST was documented in (Wang et al. 2011) and the version used here is an adaptation of that. The EF5/CREST implementation has only a single soil layer, further simplifying the model and reducing the input data requirements. EF5/CREST also contains partitioning for impervious area. Figure 3.2 shows a schematic for the various processes represented in EF5/CREST to convert rainfall into runoff.

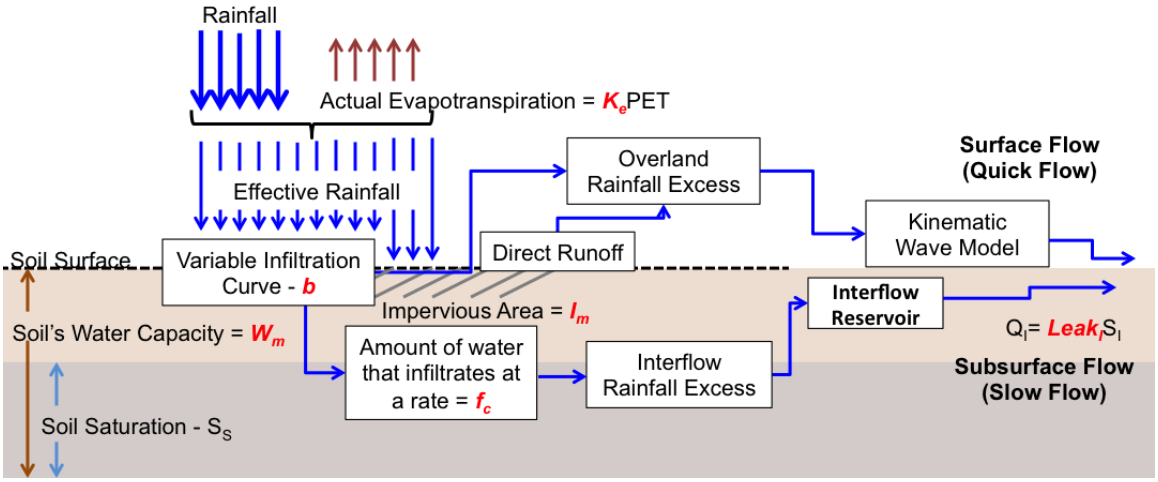

Figure 3.2: A schematic showing the progression of processes represented in the EF5/CREST water balance component (Vergara 2015).

Since EF5/CREST differs significantly from previous versions of CREST a detailed description of EF5/CREST will be provided here. The first step is converting potential evapotranspiration to effective transpiration using the user configurable scalar parameter K_e as shown in equation 3.1.

$$EET_t = K_e * PET_t \tag{3.1}$$

Where PET_t is input forcing data into EF5 and EET_t is the effective potential evapotranspiration.

$$EP_t = \begin{cases} 0, & \text{for } EET_t \geq P_t \\ P_t - EET_t, & \text{for } EET_t < P_t \end{cases} \tag{3.2}$$

Where P_t is the input forcing rainfall into EF5. From the effective rainfall (EP_t) the direct runoff portion is calculated with the rest falling to the soil and then the infiltration process. The rainfall is then partitioned into a portion reaching the soil (SP_t), a portion contributing to actual ET and a portion contributing to direct runoff (DP_t).

$$DP_t = EP_t * I_m \tag{3.3}$$

$$SP_t = EP_t * (1 - I_m) \tag{3.4}$$

Where I_m is a scalar parameter representing the percent impervious area. The infiltration is then modeled using:

$$I_t = \begin{cases} 0, & \text{for } P_t \leq EET_t \vee SM_t \geq W_m \\ W_m - SM_t, & \text{for } (i_t + SP_t) \geq I_m \\ W_m - SM_t - W_m * [1 - \frac{i_t + SP_t}{i_m}]^{1+b}, & \text{for } (i_t + SP_t) < I_m \end{cases} \tag{3.5}$$

Where W_m represents the maximum water capacity, and b represents the exponent of the variable infiltration curve. Both W_m and b are user defined parameters in EF5/ CREST. i_m represents the maximum infiltration capacity defined by:

$$i_m = W_m * (1 + b) \tag{3.6}$$

The infiltration capacity at the current time, i_t, is defined as:

$$i_t = i_m * [1 - (1 - \frac{SM_t}{W_m})^{\frac{1}{1+b}}] \tag{3.7}$$

Where SM_t is the soil moisture state variable. The soil precipitation is then partitioned into excess rainfall (ER_t) based on the infiltration.

$$ER_t = \begin{cases} 0, & \text{for } SP_t = 0 \vee SP_t \leq I_t \\ SP_t - I_t, & \text{for } SP_t > I_t \end{cases} \tag{3.8}$$

The excess rainfall is then divided into overland (OER_t) and subsurface (SER_t) flow components by:

$$SER_t = \begin{cases} 0, & \text{for } EP_t = 0 \\ temX_t, & \text{for } ER_t > temX_t \\ ER_t, & \text{for } ER_t \leq temX_t \end{cases} \tag{3.9}$$

With $temX_t$ is defined as:

$$temX_t = \begin{cases} SM_t + W_t 2W_m * F_c, & \text{for } EP_t > 0 \\ (EET_t - P_t) * \frac{SM_t}{W_m}, & \text{for } EP_t = 0 \end{cases} \tag{3.10}$$

Using F_c to represent the hydraulic conductivity and with W_t as:

$$W_t = \begin{cases} 0, & \text{for } EP_t = 0 \\ W_m, & \text{for } SM_t + I_t \geq W_m \\ SM_t + I_t, & \text{for } SM_t + I_t < W_m \end{cases} \tag{3.11}$$

The overland flow component is then calculated by taking a difference between the amount that infiltration and the excess rain plus adding in the direct runoff.

$$OER_t = \begin{cases} 0, & \text{for } EP_t = 0 \\ ER_t - SER_t + DP_t, & \text{for } EP_t > 0 \end{cases} \tag{3.12}$$

The new soil moisture value is then computed using:

$$SM_{t+1} = \begin{cases} SM_t - temX_t, & \text{for } EP_t = 0 \\ W_t, & \text{for } EP_t > 0 \end{cases} \tag{3.13}$$

Finally the actual evapotranspiration, AET_t, is given as:

$$AET_t = \begin{cases} temX_t & \text{for } EP_t = 0 \\ EET_t, & \text{for } EP_t > 0 \end{cases} \tag{3.14}$$

EF5/CREST has six user configurable parameters. W_m is the cell's maximum water capacity and is closely related to the soil porosity. This parameter controls how much water is necessary for a grid cell to become saturated and can be viewed as a bucket that fills up. F_c is the maximum amount of water allowed to infiltrate into the subsurface flow when the grid cell is saturated. This parameter is closely related to saturated hydraulic conductivity. K_e is a linear adjustment to potential evapotranspiration and controls how efficiently potential evapotranspiration is converted into actual evapotranspiration. The b parameter is related to the soil texture. Figure 3.3 shows the sensitivity of the variable infiltration curve as a function of soil saturation and the b parameter. I_m is the percent of rain that will be converted directly into

overland runoff. This parameter is related to the impervious area of the grid cell. The final parameter, I_{wu} is the percent of W_m that is water initially in the grid cell. This is really a model state, but to allow for more thorough model calibration is classed as a parameter value.

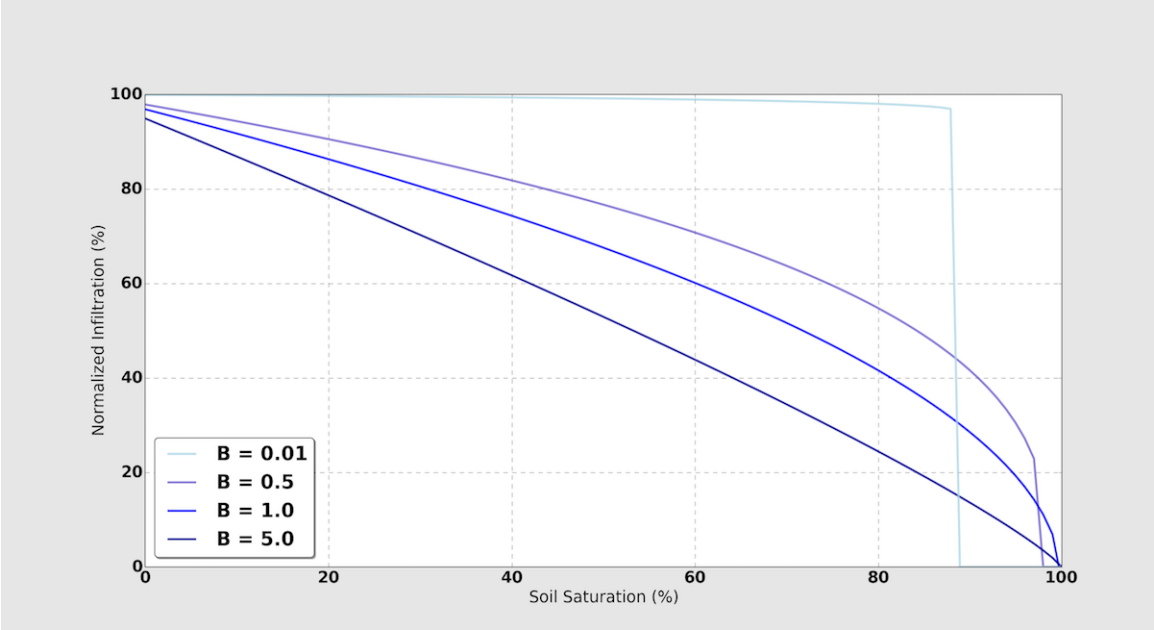

Figure 3.3: Curves showing how the infiltration rate changes as a function of soil saturation and the b parameter, the exponent of the variable infiltration curve.

The SAC-SMA water balance option is the most complex one featured in EF5 currently. The implementation of SAC-SMA in EF5 is based off the works of Koren et al. (2004) and Yilmaz et al. (2008) so the model structural details are not described here. Figure 3.4 is a schematic of the processes represented in the SAC-SMA water balance component. Multiple zones with significantly more complex interactions are include in SAC-SMA than when compared with CREST. The twenty one parameters for EF5/SAC-SMA are listed and briefly described in table 3.3. The SAC-SMA uses a saturation excess process to generate runoff differing from the infiltration excess process used in CREST.

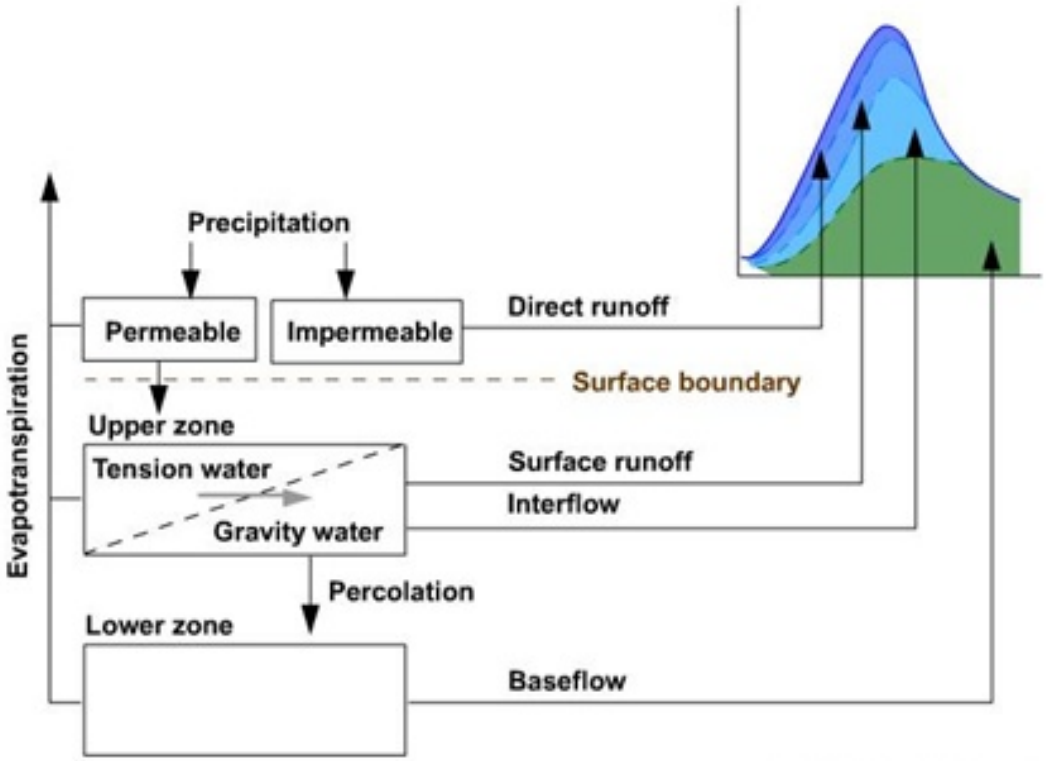

Figure 3.4: A schematic showing the progression of processes represented in the EF5/SAC-SMA water balance component. Figure adapted from UCAR COMET MetEd (UCAR 2009).

3.3 Routing Options

The routing options available in EF5 are a lumped routing model conceptualized as a series of linear reservoirs and a kinematic wave approximation of the Saint-Venant equations for one-dimensional open channel flow. The linear reservoir option is adapted from the original CREST model (Wang et al. 2011) and has been well described and used in many hydrologic projects (Nash 1957; Moore 1985; Chow et al. 1988; Vrugt et al. 2002). The EF5 linear reservoir option features two separate reservoirs where their depths are computed as:

$$OR_{t+1} = OR_t + OER_t + \sum_{i=1}^{N} OER_t^i \tag{3.15}$$

$$SR_{t+1} = SR_t + SER_t + \sum_{i=1}^{N} SER_t^i \tag{3.16}$$

Where OR_t and SR_t are the overland and subsurface reservoirs. OER_t and SER_t are the excess rainfall components from EF5/CREST representing the fast and slow flow components. The N represents the number of adjacent grid cells that flow into the current grid cell. The discharge out of each reservoir is based on the linear equations:

$$OQ_t = LeakO * OR_t \tag{3.17}$$

$$SQ_t = LeakI * SR_t \tag{3.18}$$

$$Q_t = OQ_t + SQ_t \tag{3.19}$$

Where $LeakO$ and $LeakI$ are parameters defining the rate of discharge. The total discharge Q_t is based on the summation of the fast (OQ_t) and slow (SQ_t) discharge rates. At each time step the fast and slow discharges are routed downstream following the FDM into the reservoir of the downstream grid cell.

The implementation of the kinematic wave routing is based on an approximation to the one-dimensional unsteady open channel flow equations. The full one-dimensional unsteady open channel flow equations were developed in 1871 by Barr de Saint-Venant and represent a physical description of the movement of water in a watershed

(Chow et al. 1988). The full equations have a number of assumptions which must be true in order for the Saint-Venant equations to work including that the flow is one-dimensional, that the flow varies gradually along the channel implying vertical accelerations can be neglected, that the channel is approximately a straight line, that the channel does not experience scour and deposition, and that the flow fluid is incompressible implying a constant density. The kinematic wave model further simplifies the equations and requires that bed slopes be steep. In the steep slope case the kinematic wave approximation reasonably describes the unsteady flow phenomena (Ponce 1986). The work by (Ponce 1991) claims that even in most overland cases the criterion for the kinematic wave approximation hold. The kinematic wave model is widely used in hydrology and has been implemented in systems such as the Hydrologic Engineering Center's Hydrologic Modeling System (Feldman 2000), the Storm Water Management Model created by the Environmental Protection Agency (Huber 1995), HL-RDHM previously mentioned here and described in Koren et al. (2004), and finally already coupled to the Xinanjiang model (Liu et al. 2009).

Deriving the kinematic wave approximation starts with the Saint-Venant equations in the Eulerian frame of reference where we model fluid as it passes by a control point, or in this case as it passes through a control volume. The time rate of change of the fluid is model as a function of the external forces acting on it as in Reynolds transport theorem (Chow et al. 1988). The external forces in this case are derived from Newton's second law of motion while neglecting lateral inflow, eddies and wind shear. The Saint-Venant continuity equation is given as:

$$\frac{\partial Q}{\partial x} + \frac{\partial A}{\partial t} = q \tag{3.20}$$

Where Q is the discharge, x is the horizontal distance, q is the lateral inflow into the channel, t is time, and the channel cross-sectional area is A. The equation of momentum is defined by:

$$\frac{1}{A}\frac{\partial Q}{\partial t} + \frac{1}{A}\frac{\partial}{\partial x}(\frac{Q^2}{A}) + g\frac{\partial y}{\partial x} - gS_o + gS_f = 0 \tag{3.21}$$

Where gravity is g, S_o is the bottom channel slope, and S_f is the friction slope. The terms in equation 3.21 have been named such that $\frac{1}{A}\frac{\partial Q}{\partial t}$ is the local acceleration, $\frac{1}{A}\frac{\partial}{\partial x}(\frac{Q^2}{A})$ is the convective acceleration, $g\frac{\partial y}{\partial x}$ is the pressure force, gS_o is the gravity force, and gS_f is the friction force. Simplifications to equation 3.20 and 3.21 represent different schemes commonly used in distributed hydrologic models. When no simplifications are made the routing is referred to as dynamic wave, when the acceleration terms are neglected the resulting wave model is called diffusive wave, and when the acceleration terms are neglected and the gravity force and friction force are assumed to be equal the result is the kinematic wave routing. In the kinematic wave assumption the resulting equation for momentum is:

$$Q = \alpha A^{\beta} \tag{3.22}$$

Where α and β are the kinematic wave parameters. This can be substituted back into the continuity equation and solved for Q which yields:

$$\frac{\partial Q}{\partial x} + \alpha\beta Q^{\beta-1}\frac{\partial Q}{\partial t} = q \tag{3.23}$$

Chow et al. (1988) also provides an implicit solution to the equations for distributed routing which is implemented into EF5. The kinematic wave routing in EF5 is applied only to the overland discharge, the subsurface discharge is routed with linear reservoir routing as described above. The equations above describe the kinematic wave routing for channel routing. For overland routing process is the same as above but for q instead of Q. The resulting equation is as follows:

$$\frac{\partial q}{\partial x} + \alpha_0\beta_0 q^{\beta_0-1}\frac{\partial q}{\partial t} = i - f \tag{3.24}$$

where α_0 is the overland conveyance parameter, and the β_0 parameter is fixed at $\frac{3}{5}$. The $i - f$ forcing term is the surface excess rainfall passed in from the water balance model. Table 3.5 details the parameter options for kinematic wave routing used by EF5.

3.4 Setup Over CONUS

The EF5 was set up over the CONUS to run CREST, SAC-SMA and HP water balance models all coupled with Kinematic Wave (KW) routing. No snow module was used for these simulations. The modeling domain was set to exactly match the MRMS domain with a regular 0.01° grid spanning from –130.0 to –60.0 longitude and 20.0 to 55.0 latitude. This grid was picked to fully exploit the resolution provided by the MRMS precipitation estimates. The basic files, which are the DEM, FDR, and FAM, were derived from the National Elevation Dataset (NED) (Gesch et al. 2009). The NED data was resampled to the 0.01° resolution using an arithmetic mean and then FDR and FAM were derived using ESRI ArcGIS and the ArcHydro toolbox. Figure 3.5 shows the resulting FAM where large rivers and streams are clearly visible. A priori distributed parameter maps were preferred where available. The models were run in an uncalibrated mode because robust calibration is not currently feasible over CONUS due to computational constraints. The models were also run uncalibrated because there are not enough observation points over the CONUS to adequately calibrated distributed hydrologic models.

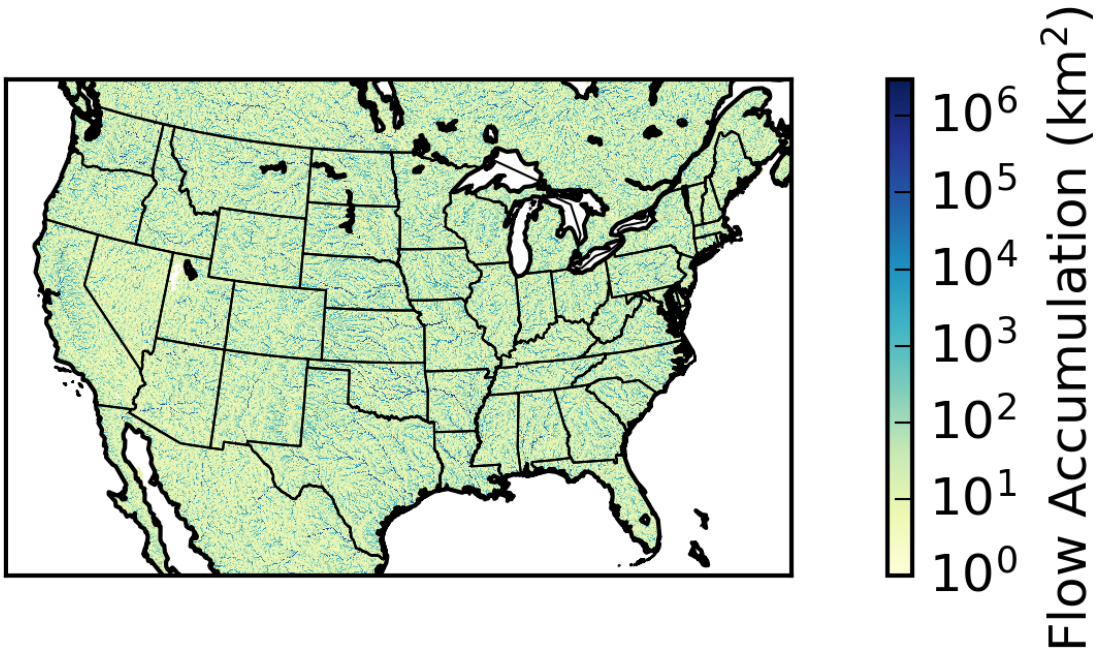

Figure 3.5: The flow accumulation map derived at 0.01° horizontal resolution from the National Elevation Dataset.

The CREST parameters used for this study are largely based on a priori maps of soil information generated by Miller and White (1998) utilizing the STATSGO dataset. Table 3.2 summarizes the EF5/CREST parameters and the values used in this study. The b parameter was derived from the soil texture map provided by Miller and White (1998) with a lookup table from Cosby et al. (1984) then used to convert from the soil texture into the exponent parameter. The lookup table for b is provided in Table 3.1. The values for b over the CONUS are shown in Figure 3.6. The W_m parameter map was generated from resampling the available water capacity 250 cm depth map in Miller and White (1998) to the domain used here with bilinear interpolation. The resulting map is shown in Figure 3.7. The F_c parameter for EF5/CREST was produced using the permeability map from Miller and White (1998) where Figure 3.8 shows the spatial variability over the CONUS. The percent impervious area was derived from the National Land Cover Database (NLCD) 2011 edition impervious area from Xian et al. (2011) resampled using average interpolation onto the study

domain. Figure 3.9 shows the resulting map of impervious area percentage over the CONUS. The KE and IWU are the only EF5/CREST parameters without distributed aprior parameter maps.

Table 3.1: Soil Texture and b Value from Cosby et al. (1984)

Soil Texture	b
Sandy loam	4.74
Sand	2.79
Loamy sand	4.26
Loam	5.25
Silty loam	5.33
Sandy clay loam	6.77
Clay loam	8.17
Silty clay loam	8.72
Sandy clay	10.73
Silty clay	10.39
Light clay	11.55

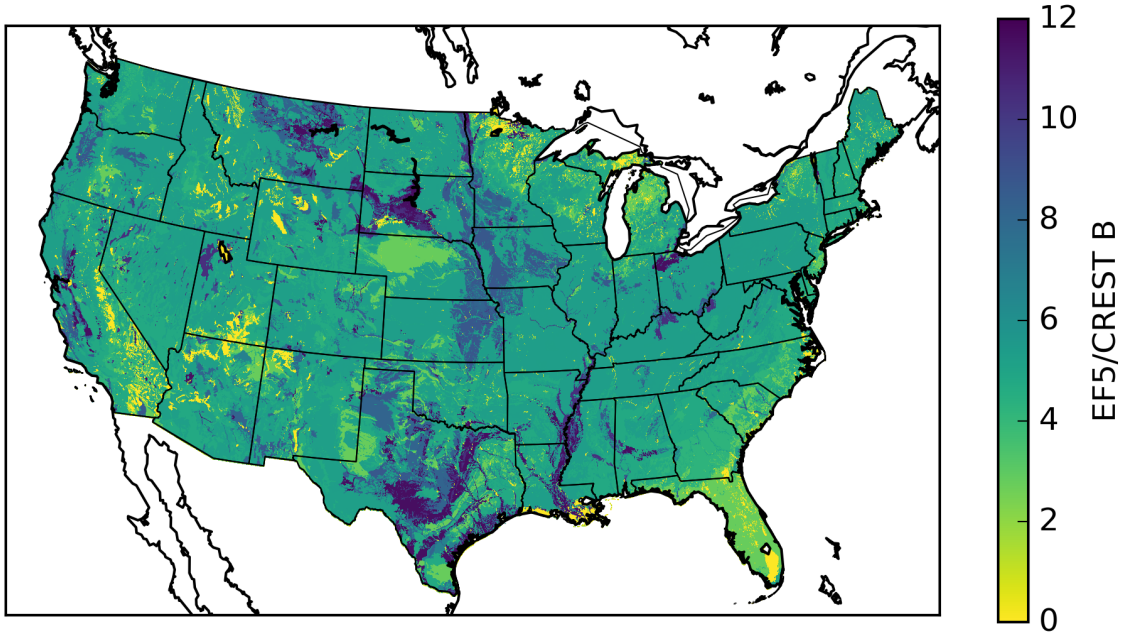

Figure 3.6: The EF5/CREST b parameter shown over the CONUS.

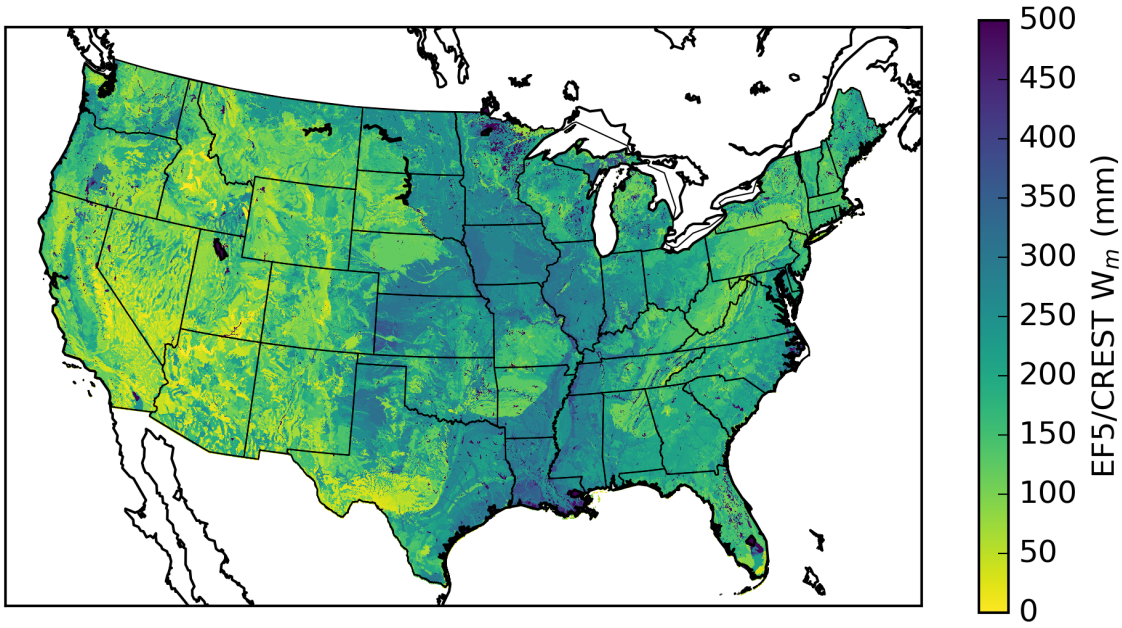

Figure 3.7: The EF5/CREST W_m parameter shown over the CONUS.

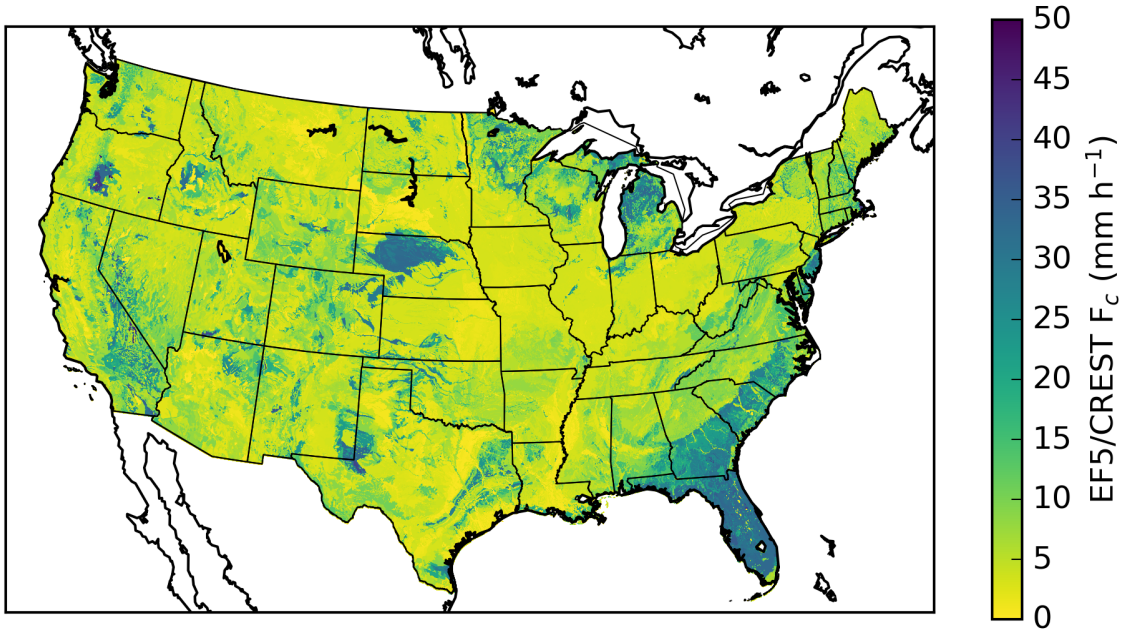

Figure 3.8: The EF5/CREST F_c parameter shown over the CONUS.

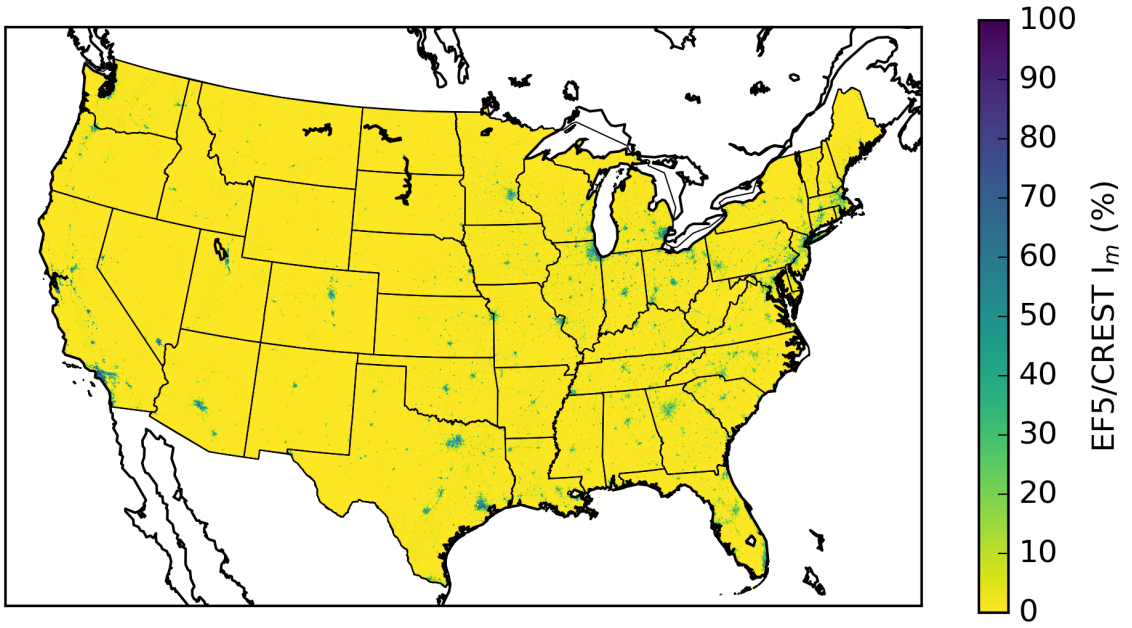

Figure 3.9: The EF5/CREST I_m parameter shown over the CONUS.

Table 3.2: CREST Parameter Values

Parameter	Description	Value	Grid Source	Min	Mean	Max
WM	Water capacity of soil in mm	1	Miller and White (1998)	0	206	2500
FC	Saturated hydrologic conductivity in mm h^{-1}	1	Miller and White (1998)	0	8	51
B	Exponent of the infiltration curve	1	Miller and White (1998)	0	5	12
IM	Percentage impervious area in %	1	Xian et al. (2011)	0	1	96
KE	Potential evapotranspiration adjustment factor	1	NA	NA	NA	NA
IWU	Initial soil water content	75	NA	NA	NA	NA

The EF5/SAC-SMA parameters were taken directly from work done by Zhang et al. (2011b) because this work is most comparable to what is used operationally by the NWS. Table 3.3 lists the parameters and their respective values used in this study. PCTIM, ADIMP, SIDE, and RIVA are using lumped values defined in the tables as a priori grids were not made available.

The kinematic wave parameters used by EF5 are listed in Table 3.5. These parameter values are used for all model combinations when coupled with CREST,

Table 3.3: SAC-SMA Parameter Values

Parameter	Description	Value	Grid Source
UZTWM	Upper zone tension water capacity in mm	1	Zhang et al. (2011b)
UZFWM	Upper zone free water capacity in mm	1	Zhang et al. (2011b)
UZK	Depletion rate from upper zone free water storage from interflow in day^{-1}	1	Zhang et al. (2011b)
LZTWM	Lower zone tension water capacity in mm	1	Zhang et al. (2011b)
LZFSM	Lower zone supplemental free water capacity in mm	1	Zhang et al. (2011b)
LZFPM	Lower zone primary free water capacity in mm	1	Zhang et al. (2011b)
LZSK	Rate of depletion of the lower zone supplemental free water storage in day^{-1}	1	Zhang et al. (2011b)
LZPK	Rate of depletion of the lower zone primary free water storage in day^{-1}	1	Zhang et al. (2011b)
ZPERC	Maximum and minimum percolation rate ratio	1	Zhang et al. (2011b)
REXP	Shape parameter of the percolation curve	1	Zhang et al. (2011b)
PFREE	Percolation fraction that goes directly to the lower zone free water storage	1	Zhang et al. (2011b)
PCTIM	Percentage impervious area in %	0.1	NA
ADIMP	Maximum fraction of additional impervious area from saturation	0.1	NA
RIVA	Riparian vegetation fractional area	1.0	NA
SIDE	Ratio of deep percolation from lower zone free water storage	0.0	NA
ADIMC	Initial additional impervious area from saturation	1.0	NA
UZTWC	Initial filled amount of upper zone tension water	0.55	NA
UZFWC	Initial filled amount of upper zone free water	0.14	NA
LZTWC	Initial filled amount of lower zone tension water	0.56	NA
LZFSC	Initial filled amount of lower zone supplemental free water	0.11	NA
LZFPC	Initial filled amount of lower zone primary free water	0.46	NA

SAC-SMA and HP water balance options for this study. The parameters are a priori based on statistical relationships with geomorphological, precipitation and soil parameters developed in Vergara et al. (2016). Observed α and β values were computed from the cross-sections and discharge values measured by the USGS. These observed values were then modeled using generalized additive models for location, size, and shape (GAMLSS) which allows for the extrapolation of information collected at the approximately 10,000 USGS discharge stations in the CONUS to everywhere on the hydrologic model grid. The parameters used are basin area, elongation ratio, relief ratio, slope index, slope to outlet, mean annual precipitation, mean annual temperature, K factor, depth-to-rock, rock volume percentage, soil texture, curve number, and river length. Figure 3.10 shows the resulting model fit to the observed data for α and β. The α_0 parameter was computed using Manning's equation for overland flow:

$$\alpha_0 = \frac{1}{n} S^{\frac{1}{2}} \tag{3.25}$$

Where the S is the slope computed from DEM, n is Manning's roughness coefficient. The roughness coefficient was computed from University of Maryland (UMD) Moderate Resolution Imaging Spectroradiometer (MODIS) land cover type mosaics (Channan et al. 2014) and a lookup table from Chow et al. (1988) documented in Table 3.4. Figure 3.11 shows the resulting α parameter map for the CONUS. The β parameter is shown in Figure 3.12. Figure 3.13 shows the results for α_0 from Equation 3.25.

Table 3.4: UMD Land Cover Classes

UMD Class	Description	Manning's n
0	Water	0.001
1	Evergreen Needleleaf Forest	0.1
2	Evergreen Broadleaf Forest	0.1
3	Deciduous Needleleaf Forest	0.1
4	Deciduous Broadleaf Forest	0.1
5	Mixed Forest	0.1
6	Woodland	0.1
7	Wooded Grassland	0.3
8	Closed Shrubland	0.3
9	Open Shrubland	0.2
10	Grassland	0.17
11	Cropland	0.035
12	Bare Ground	0.01
13	Urband and Built	0.015

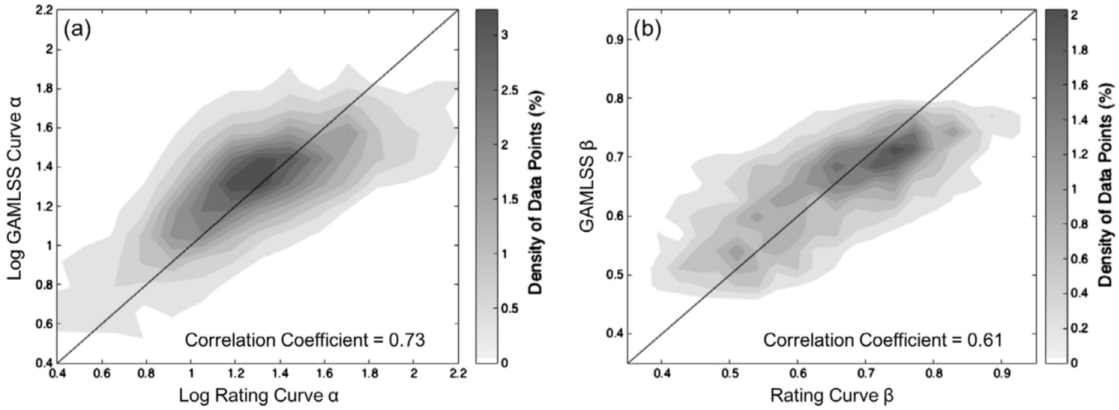

Figure 3.10: Density scatter plots showing GAMLSS modeled fits for (a) α and (b) β kinematic wave parameters. Figure adapted from Vergara et al. (2016).

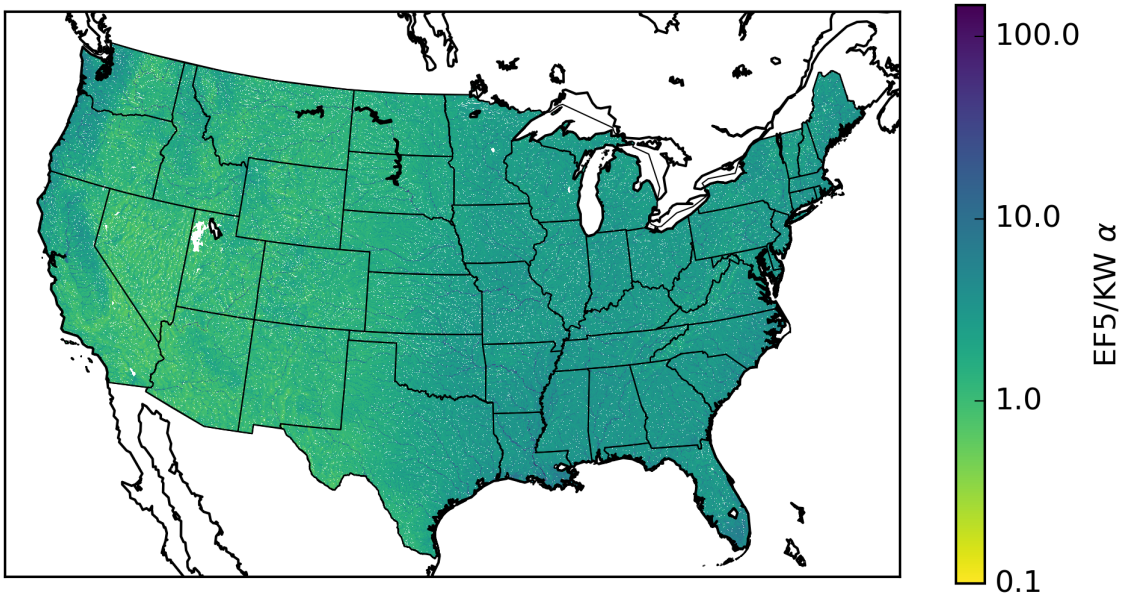

Figure 3.11: The α kinematic wave parameter derived in Vergara et al. (2016).

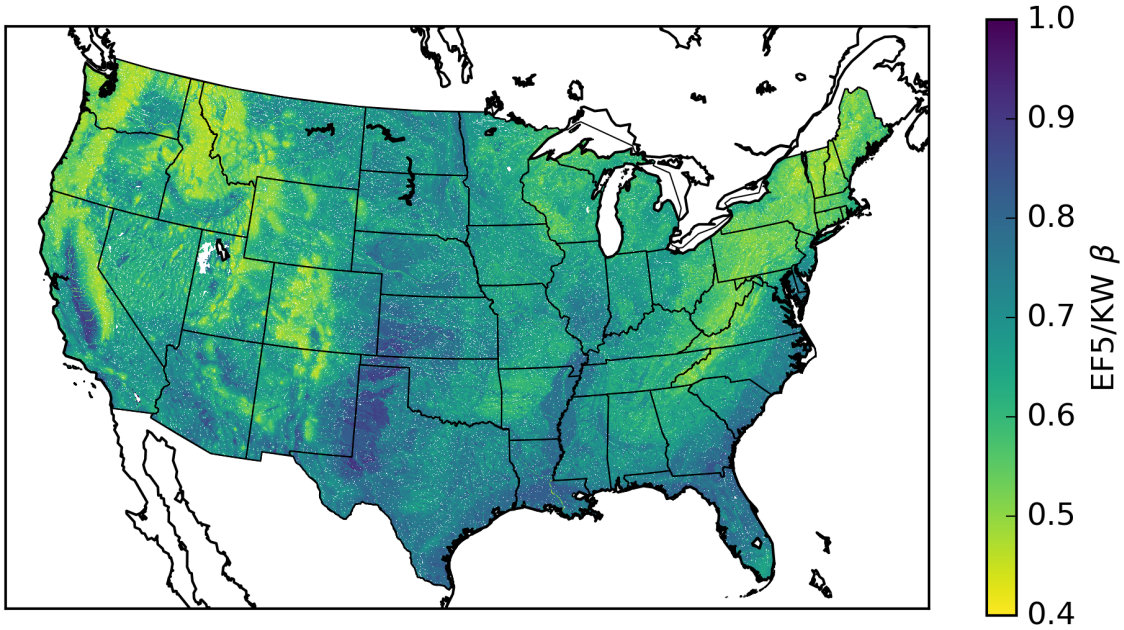

Figure 3.12: The β kinematic wave parameter derived in Vergara et al. (2016).

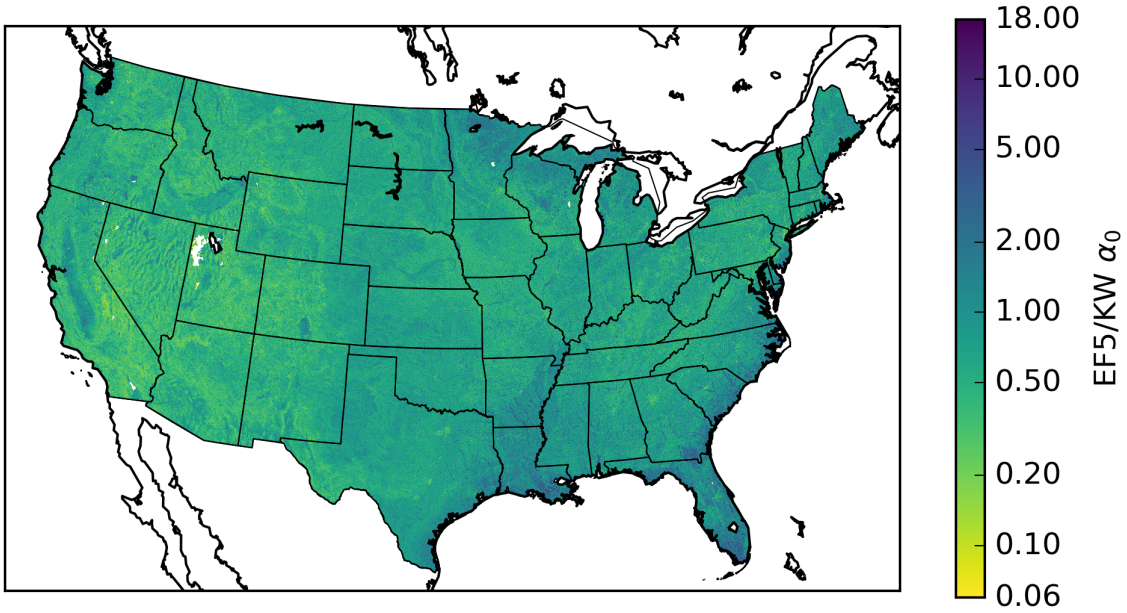

Figure 3.13: The α_0 kinematic wave parameter derived in Vergara et al. (2016).

Table 3.5: Kinematic Wave Parameter Values

Parameter	Description	Value	Grid Source	Min	Mean	Max
α	Kinematic wave multiplier coefficient	1	Vergara et al. (2016)	0.4	3	149
β	Kinematic wave power coefficient	1	Vergara et al. (2016)	0.4	0.7	1.0
α_0	Kinematic wave conveyance parameter for overland	1	Vergara et al. (2016)	0.06	0.7	18
Under	Subsurface flow speed in m s^{-1}	0.0001	Miller and White (1998)	0	8	51
LeakI	Percentage reduction in interflow storage per time step in %	1	Zhang et al. (2011b)	0.127	0.128	0.129
Th	Area threshold for declaring a grid cell to contain a channel in grid cells	10	NA	NA	NA	NA
ISU	Initial water storage in channel grid cells	0.0	NA	NA	NA	NA

EF5 was run for the period from 2001 through 2011 for all USGS discharge gauges with a basin area under 1,000 km^2. There are 4,366 discharge gauges over the CONUS that meet this basin area threshold. The MRMS reanalysis precipitation rates every

five minutes were used as the precipitation forcing for EF5. The potential evapotranspiration (PET) data was climatological monthly mean data derived in Koren et al. (1998) and shown in Figure 3.14. EF5 was run with a five minute time step producing five minute output simulated time series. The resulting simulations took 1-week of computer time for the EF5/CREST combination and 2.5-weeks of computer time for EF5/SAC-SMA illustrating the relative differences in complexity and performance between the two water balance models. The year 2001 was used as a model warmup period and so results will only be presented from 2002 through 2011.

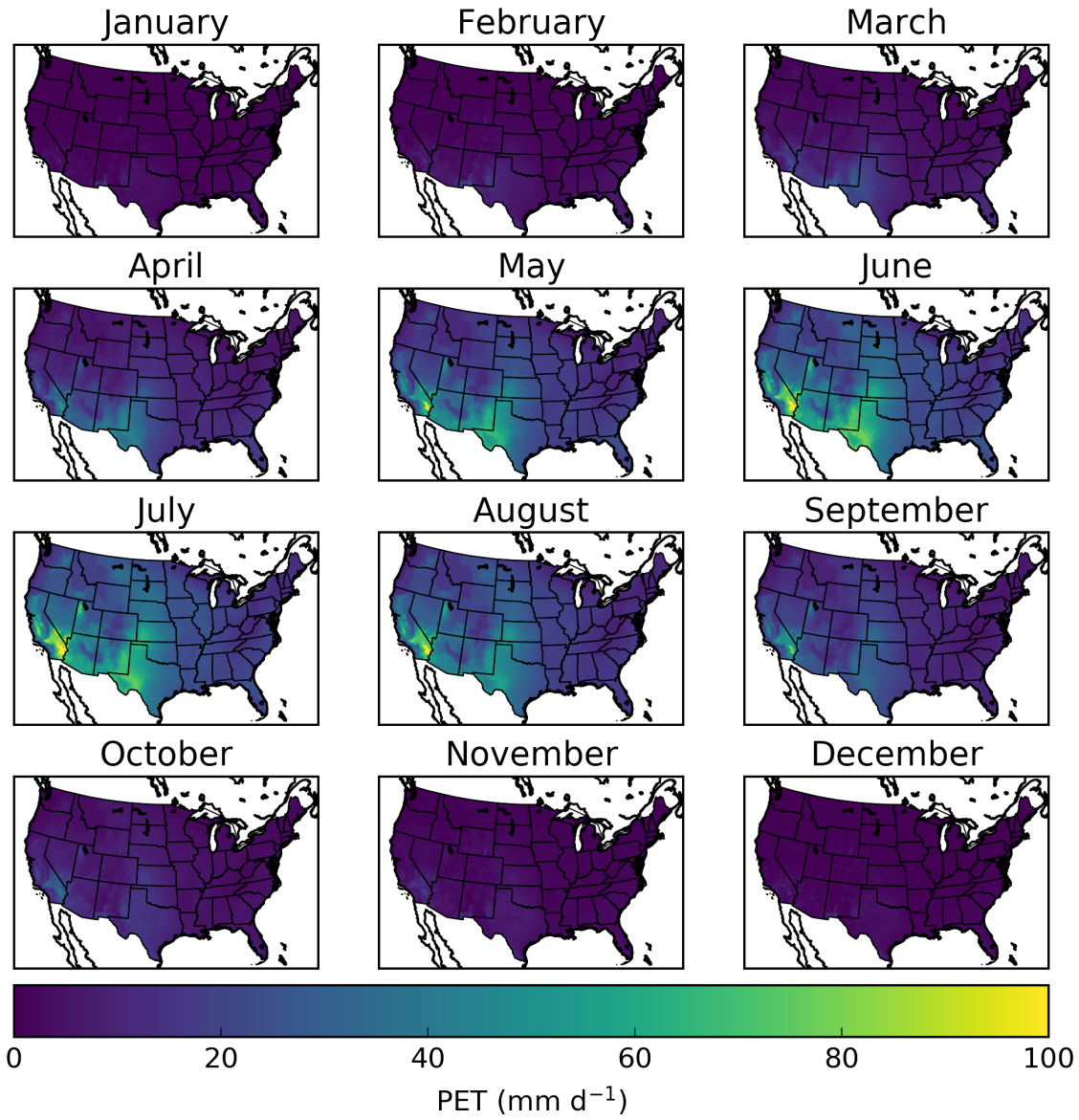

Figure 3.14: Maps of the mean daily PET variations by month derived from Koren et al. (1998).

3.5 CONUS Case Study Results

Before diving directly into bulk evaluations of the performance of the hydrologic models it is useful to view hydrographs for a flash flood event. The performance of the hydrologic models will be examined for the June 11th, 2010 flash flood in Arkansas because this event had the most fatalities during the study time period. 20 campers at the Albert Pike Recreational Area lost their lives 10 km northwest of the Little Missouri River discharge gauge when flood waters rapidly rose overnight while they were sleeping. Many of the campers were in tents, but even cabins near the river were destroyed in the flash flood. As many as 200 people were in the area when the flood occurred with many able to make it safely away from the disaster. Figure 3.15 shows the basin averaged accumulated precipitation for this event. The Little Missouri River, with a basin area of 177 km^2 is plotted upstream of USGS discharge gauge 07360200. For the Caddo River the basin upstream of the USGS discharge gauge 07359610 is plotted with a contributing basin area of 352 km^2. The MRMS precipitation reanalysis shows event total precipitation of 200 mm over a large area of the basins with some isolated areas receiving over 350 mm. The observed and simulated hydrographs for the Caddo River are shown in Figure 3.16. All three model simulations overestimate the peak and are three hours earlier with the timing of the peak for this gauge. At the Little Missouri River, shown in Figure 3.17, the EF5/ CREST and EF5/SAC-SMA simulations underestimate the peak but are very close on the timing being only an hour early while the EF5/HP simulation has similar peak timing but overestimation of the magnitude.

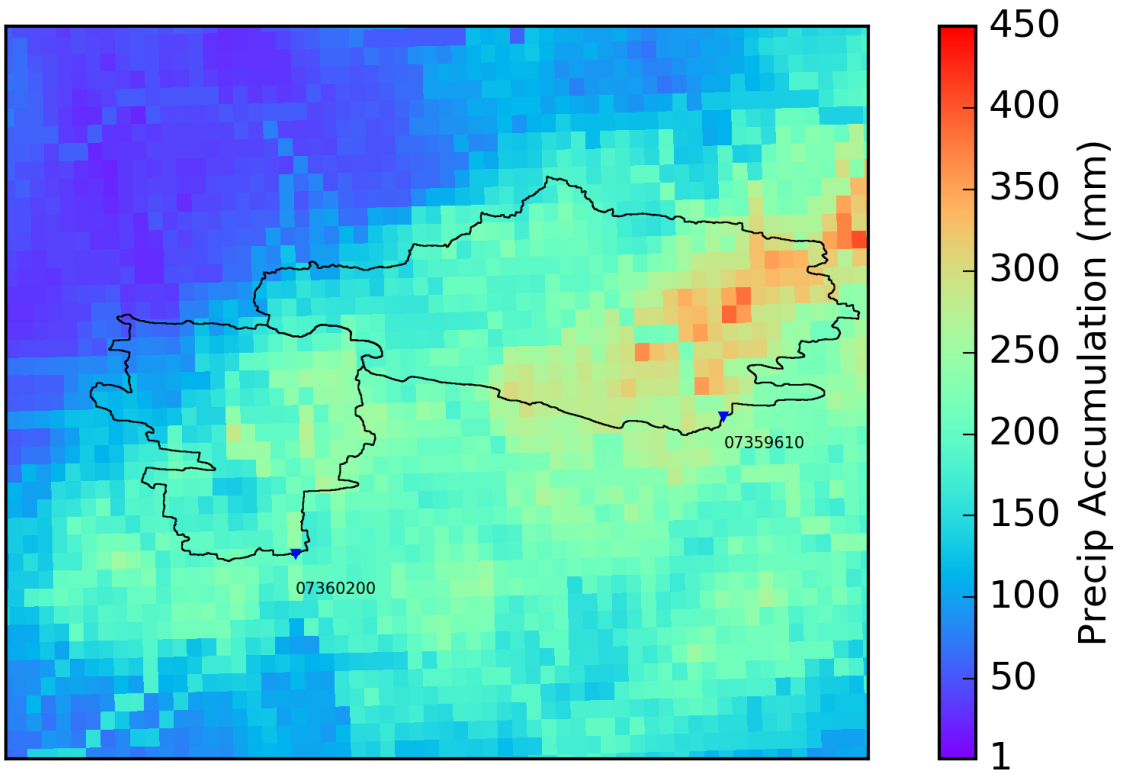

Figure 3.15: 24 hour precipitation accumulation ending 2010-06-12 00 UTC over the Caddo and Little Missouri Rivers in Arkansas. The blue triangles are USGS discharge measurement locations.

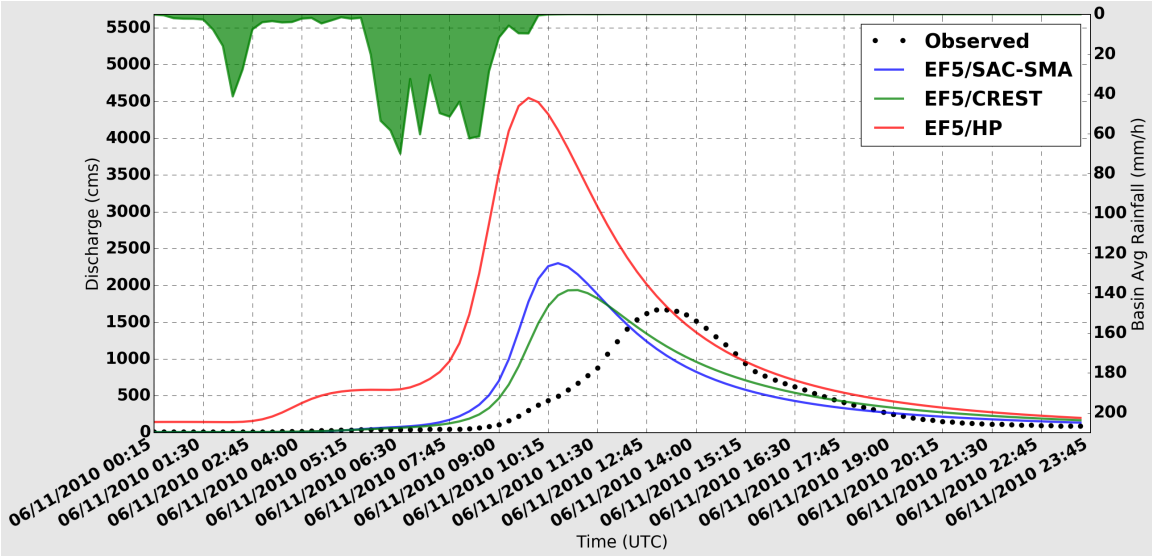

Figure 3.16: Observed and simulated hydrographs from Caddo River near Caddo Gap, AR. The contributing basin area at this point is 352 km^2.

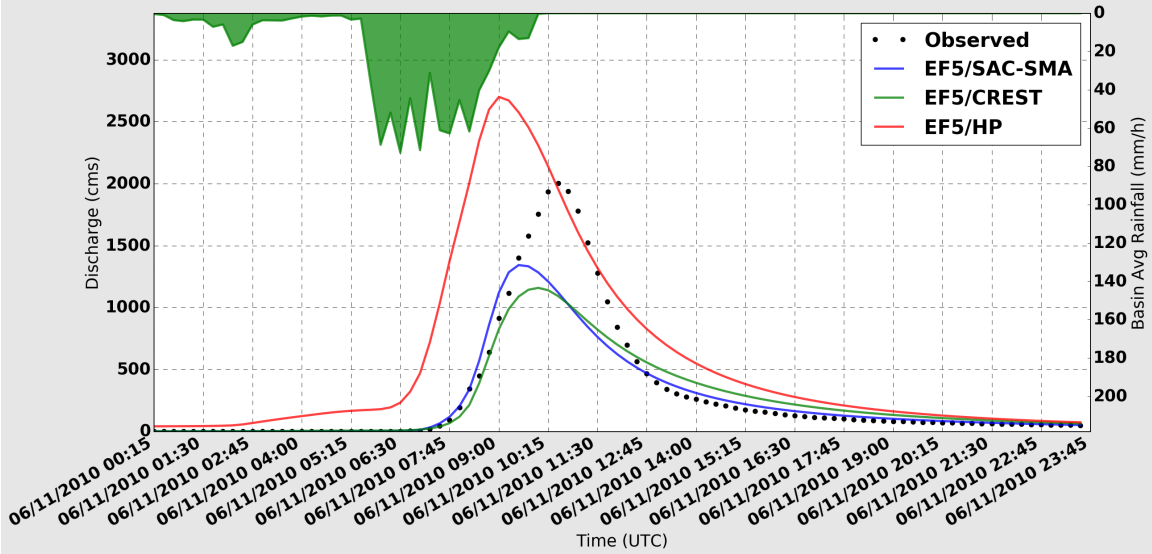

Figure 3.17: Observed and simulated hydrographs from Little Missouri River near Langley, AR. The contributing basin area at this point is 177 km^2.

3.6 CONUS Bulk Results

While the analysis for a single extreme event determined the EF5 simulations capable of producing reasonable hydrologic simulations, more analysis is needed to determine the overall ability of the modeling system. A bulk analysis was performed to evaluate the skill of the modeling system at every USGS gauge with a basin area less than 1,000 km^2. The time series from the EF5 simulations can be evaluated as a function of the performance at each individual discharge gauge. This information can then be viewed in bulk to gather of a sense of how the system performs spatially in terms of the overall mass of water, and the correlation between events. The accuracy of the simulations will be judged using Pearson's linear correlation coefficient, CC, defined as:

$$CC = \frac{\mathbf{Cov}(Q_{sim}, Q_{obs})}{\sqrt{\mathbf{Var}(Q_{sim})\mathbf{Var}(Q_{obs})}} \tag{3.26}$$

Where Q_{sim} is the simulated discharge value and Q_{obs} is the USGS measured discharge value. The values for correlation coefficient can range from –1 to 1 with 1 being the best. The normalized bias of the simulations will be computed using:

$$bias = \frac{\sum_{i=1}^{N}(Q_{sim}^{i} - Q_{obs}^{i})}{\sum_{i=1}^{N} Q_{obs}^{i}} * 100 \tag{3.27}$$

Where N is the number of observations in the discharge time series. Normalized bias ranges from –100 % to ∞ with 0 % being the best. Finally the Nash Sutcliffe Efficiency (NSE) (Nash and Sutcliffe 1970), commonly used as a skill metric to define simulations that have better skill than the mean of the observations would have, will be computed as:

$$nse = 1 - \frac{\sum_{i=1}^{N}(Q_{sim}^{i} - Q_{obs}^{i})^2}{\sum_{i=1}^{N}(Q_{obs}^{i} - \overline{Q_{obs}})^2} \tag{3.28}$$

Where $\overline{Q_{obs}}$ is the mean of the discharge observations for this station. The values for NSE range from $-\infty$ to 1 with 1 being a simulation perfectly matching the observations.

Figure 3.18 shows the spatial distribution of normalized bias for the EF5/CREST simulations. The bias is close to 0 % over most of the eastern CONUS but with severe underestimation in the mountain west. The median bias for these simulations is 9 % Figure 3.19 shows the spatial distribution of normalized bias for the EF5/SAC-SMA simulations. The bias shows a very similar spatial pattern to the EF5/CREST results but with a tendency towards more slight underestimation in the central and eastern CONUS. The median bias for the EF5/SAC-SMA simulations is –8 %. The EF5/HP normalized bias shown in Figure 3.20 shows significant overestimation for a majority of the CONUS except for the mountainous areas in the west. The EF5/HP median bias is 248 %. These results show that the multi-model ensemble is working as intended with EF5/HP providing a worst case scenario result that typically overestimates while EF5/CREST and EF5/SAC-SMA have subtle differences. The results also show the underestimation resulting from a lack of MRMS radar coverage in the mountain west shown in Figure 2.4.

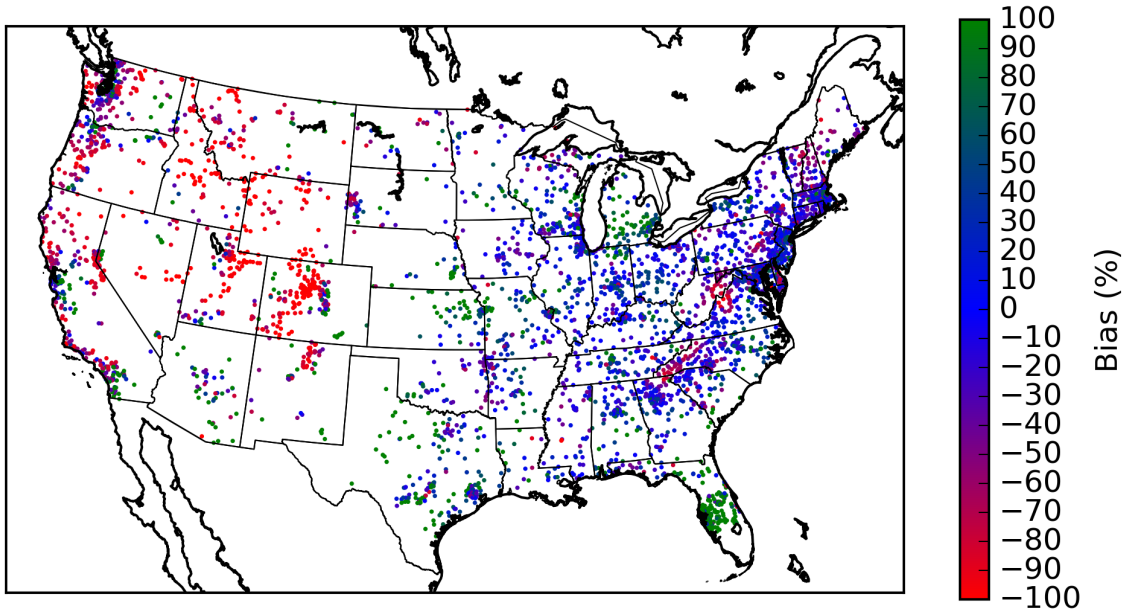

Figure 3.18: The normalized bias for the EF5/CREST simulations over the CONUS for USGS basins with areas less than 1,000 km^2.

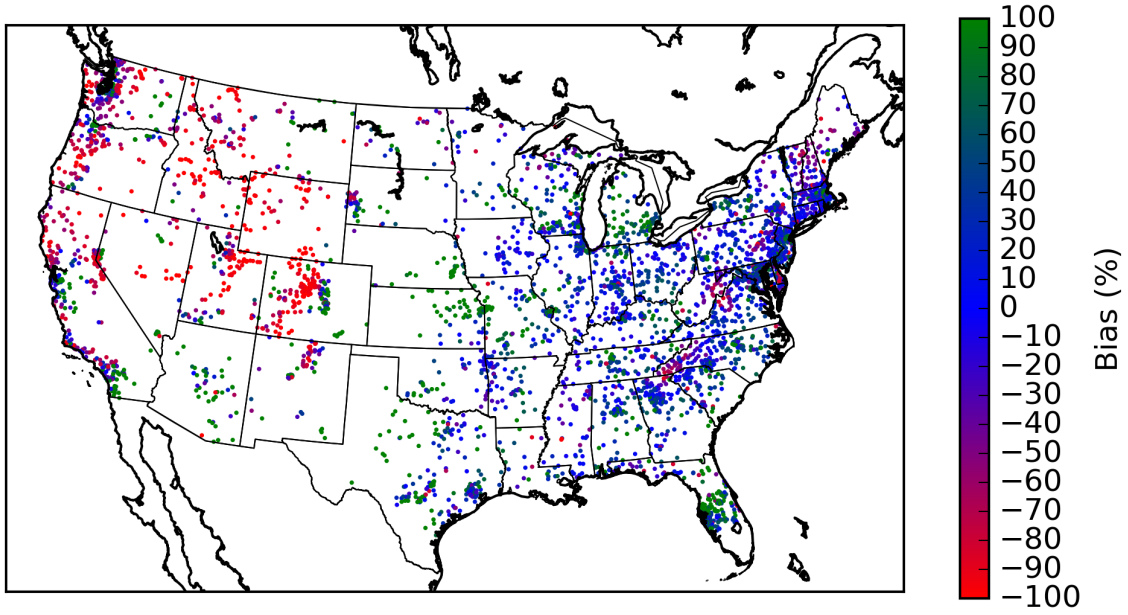

Figure 3.19: The normalized bias for the EF5/SAC-SMA simulations over the CONUS for USGS basins with areas less than 1,000 km^2.

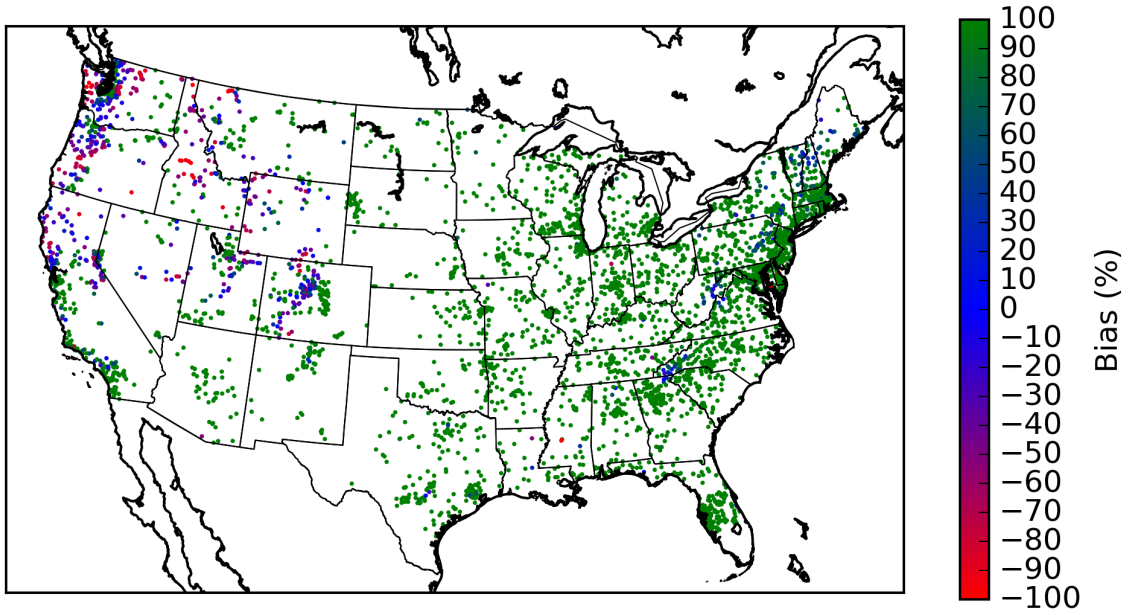

Figure 3.20: The normalized bias for the EF5/HP simulations over the CONUS for USGS basins with areas less than 1,000 km^2.

Figure 3.21 plots the correlation coefficient for the EF5/CREST simulations over the CONUS while Figure 3.22 and Figure 3.23 are for the EF5/SAC-SMA and EF5/HP respectively. The maps are all very similar with higher correlation coefficients in the eastern CONUS and along the west coast. The correlation coefficients are near 0 for the mountain west where the simulations are again plagued by a lack of good radar coverage. Cities with clusters of gauges such as Dallas, Houston and Atlanta have higher CC with EF5/CREST and EF5/HP compared to EF5/SAC-SMA. The EF5/CREST simulations have a min, median, max CC of –0.47, 0.40, and 1.0 respectively. The simulations for EF5/SAC-SMA have a min, median, max CC of –1.0, 0.35, and 0.92 respectively. The EF5/HP simulations have a min, median, max CC of –0.25, 0.36, and 0.83 respectively.

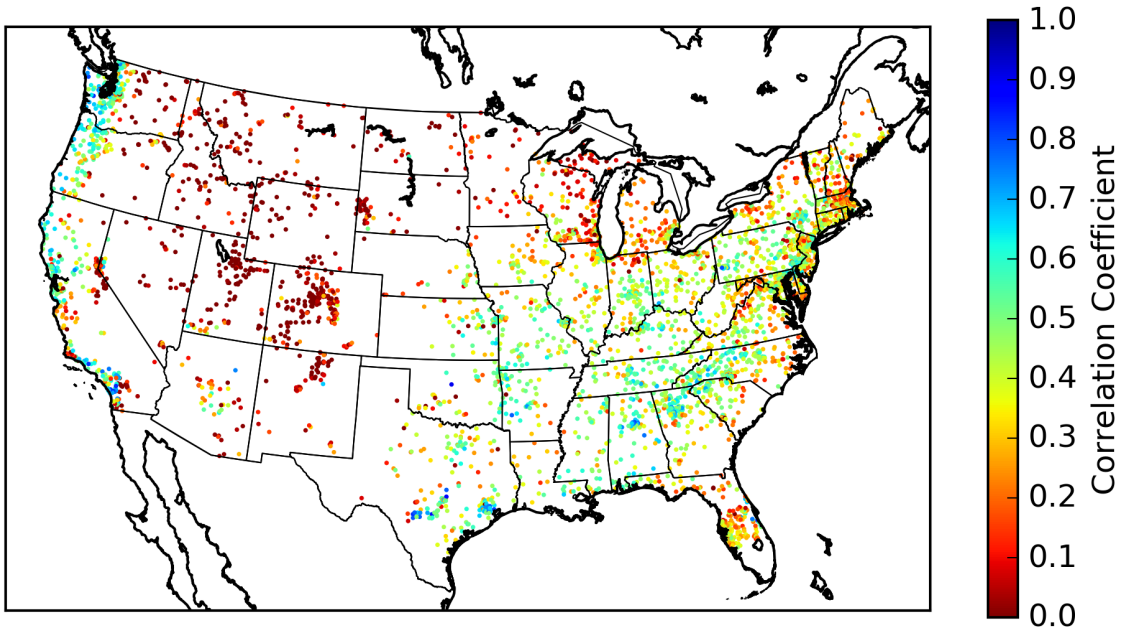

Figure 3.21: The correlation coefficient for the EF5/CREST simulations over the CONUS for USGS basins with areas less than 1,000 km^2.

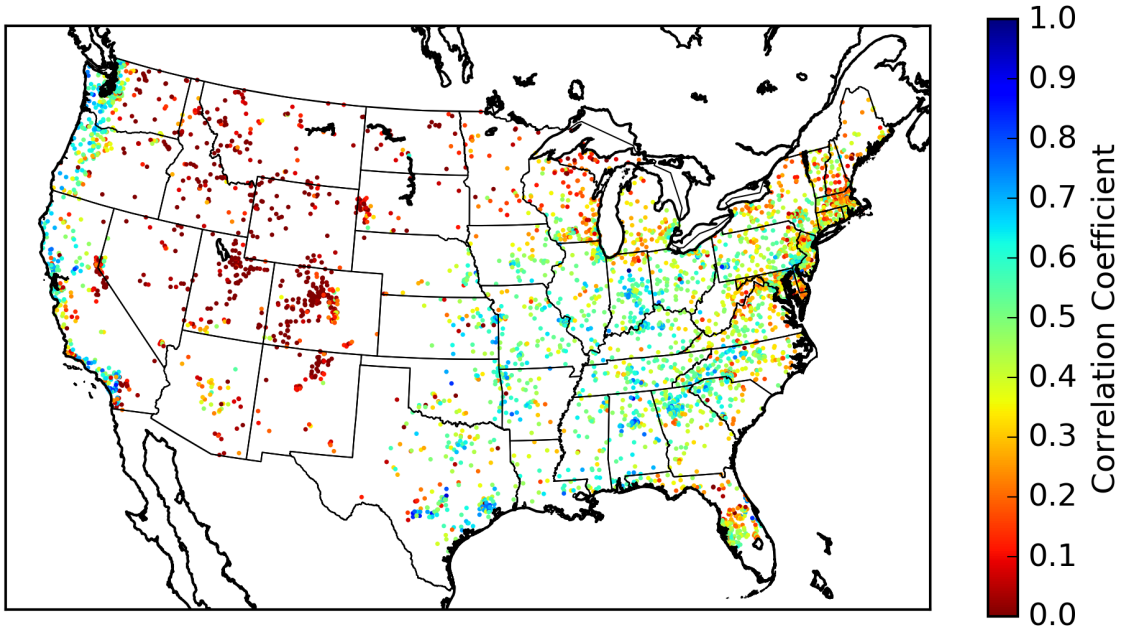

Figure 3.22: The correlation coefficient for the EF5/SAC-SMA simulations over the CONUS for USGS basins with areas less than 1,000 km^2.

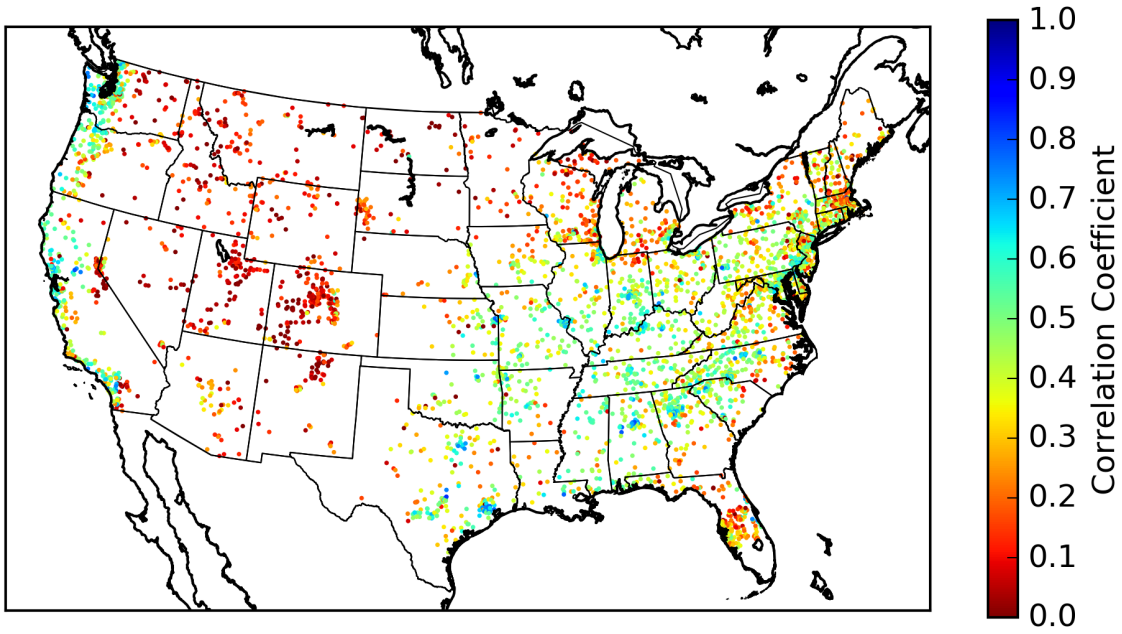

Figure 3.23: The correlation coefficient for the EF5/HP simulations over the CONUS for USGS basins with areas less than 1,000 km^2.

Figure 3.24, Figure 3.22, and Figure 3.23 plot the NSE for the EF5/CREST, EF5/SAC-SMA, and EF5/HP simulations respectively. The maximum, median, and minimum NSE are 0.71, –0.06, and –313 for the EF5/CREST simulations. 1,825 out of the 4,366 simulated basins have NSE values greater than 0. For the EF5/SAC-SMA simulations the maximum, median, and minimum NSE values are 0.76, –0.03, and –631. The EF5/SAC-SMA simulations have 1,982 basins with NSE greater than 0. And finally for the EF5/HP results the maximum, median, and minimum NSE values are 0.59, 0.08, and –20. The EF5/HP runs have 3,642 out of the 4,366 basins with NSE greater than 0.

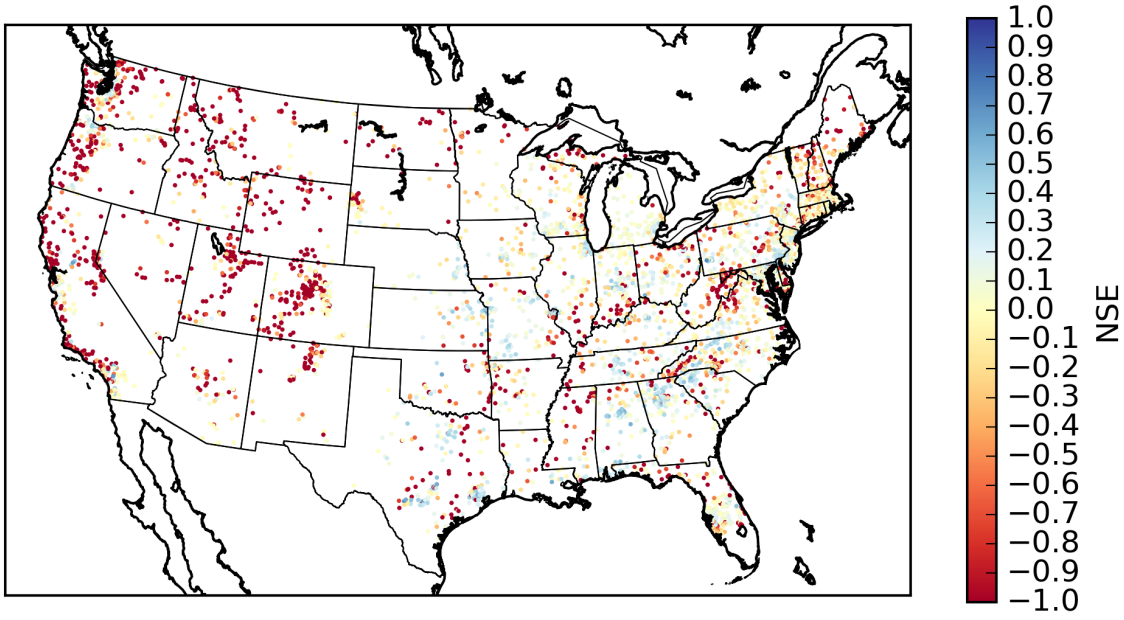

Figure 3.24: The NSE for the EF5/CREST simulations over the CONUS for USGS basins with areas less than 1,000 km^2.

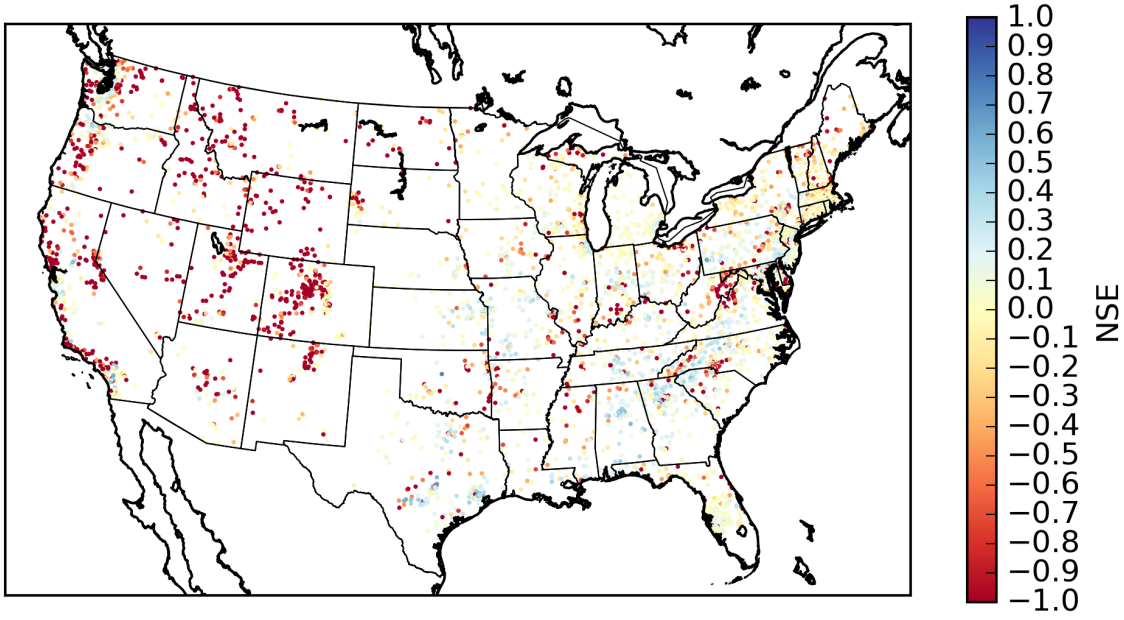

Figure 3.25: The NSE for the EF5/SAC-SMA simulations over the CONUS for USGS basins with areas less than 1,000 km^2.

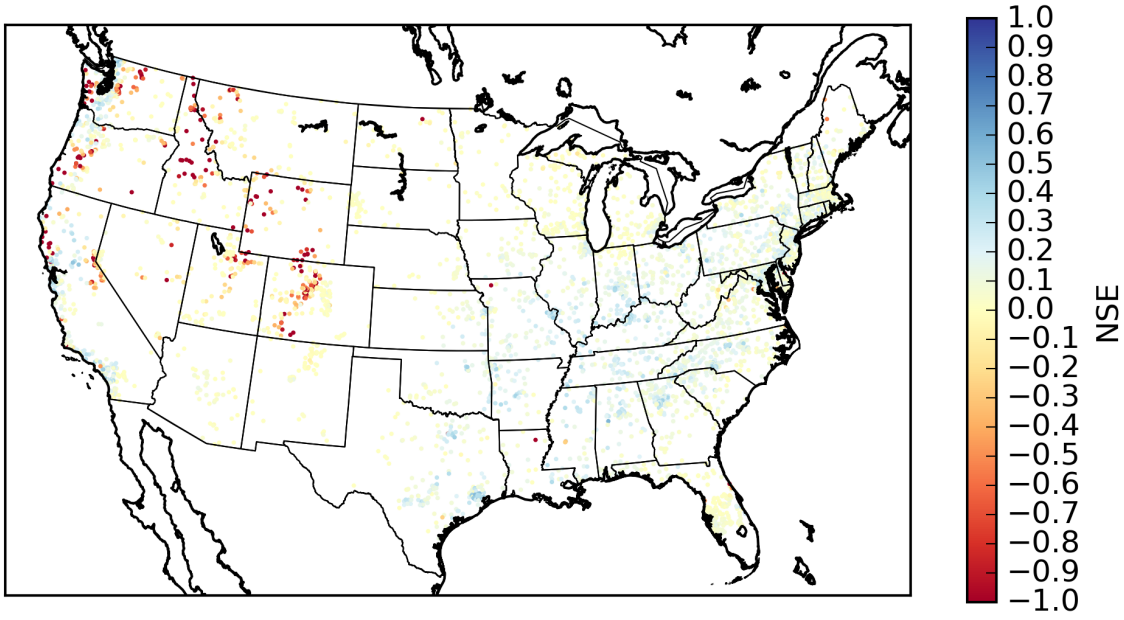

Figure 3.26: The NSE for the EF5/HP simulations over the CONUS for USGS basins with areas less than 1,000 km^2.

Table 3.6: Stastical Summary of EF5 Performance

	EF5/CREST	EF5/SAC-SMA	EF5/HP
Max NSE	0.71	0.76	0.59
Median NSE	–0.06	–0.03	0.08
Min NSE	–313	–613	–20
# basins NSE > 0	1,825	1,982	3,642
Max CC	1.0	0.92	0.83
Median CC	0.40	0.35	0.36
Min CC	–0.47	–1.0	–0.25
Median Bias	9 %	–8 %	248 %

Figure 3.27, Figure 3.28, and Figure 3.29 plot the CC as a function of basin area with bias color coded for the EF5/CREST, EF5/SAC-SMA, and EF5/HP simulations respectively. The plots show significant scatter as a function of basin area. There is a common trend among the models of performance decreasing with increasing basin area suggesting the routing may play a role as it is the only common model

structural component between the three sets of simulations. The EF5/CREST and EF5/SAC-SMA plots have a cluster of very negatively biased simulations which also exhibit poor CC while the EF5/HP simulation does not have this feature.

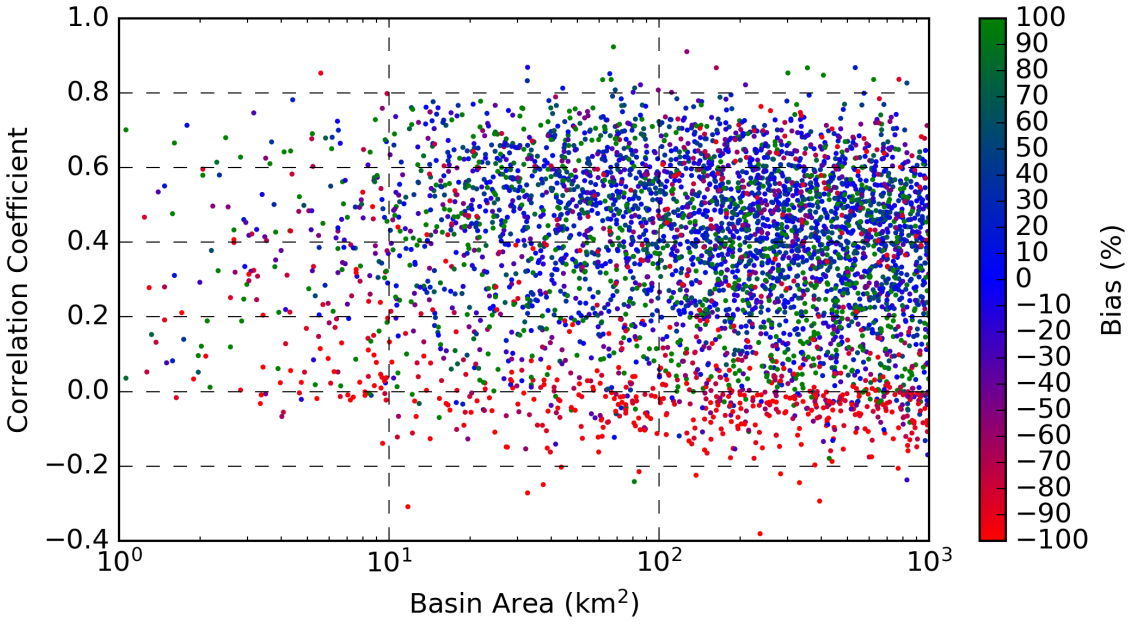

Figure 3.27: The CC from the EF5/CREST simulation plotted as a function of basin area for USGS basins with areas less than 1,000 km^2.

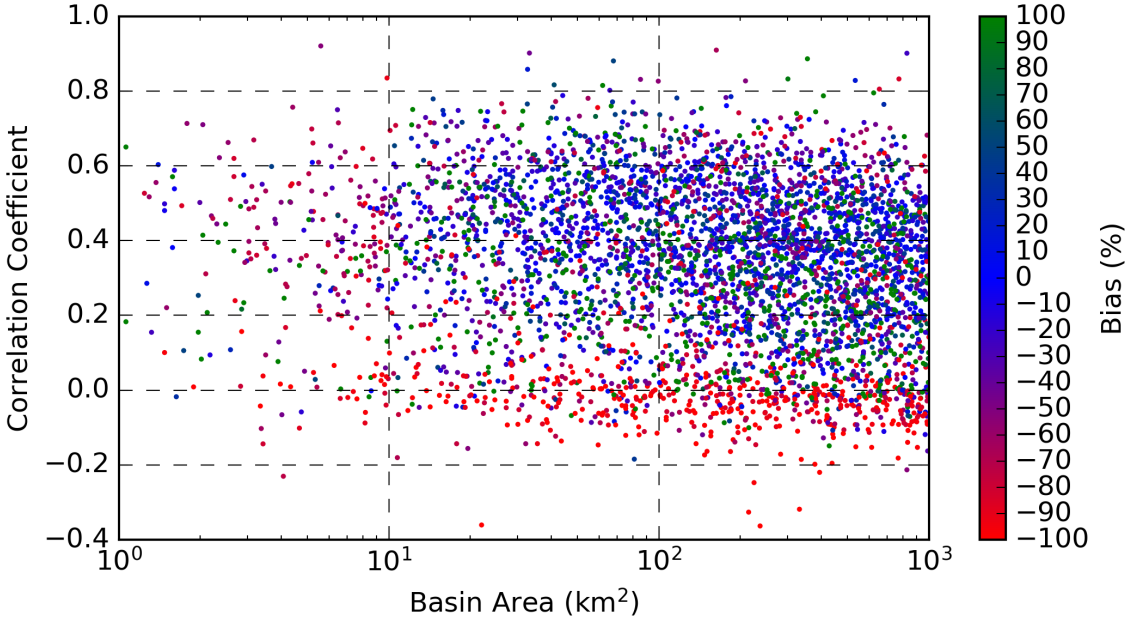

Figure 3.28: The CC from the EF5/SAC-SMA simulation plotted as a function of basin area for USGS basins with areas less than 1,000 km^2.

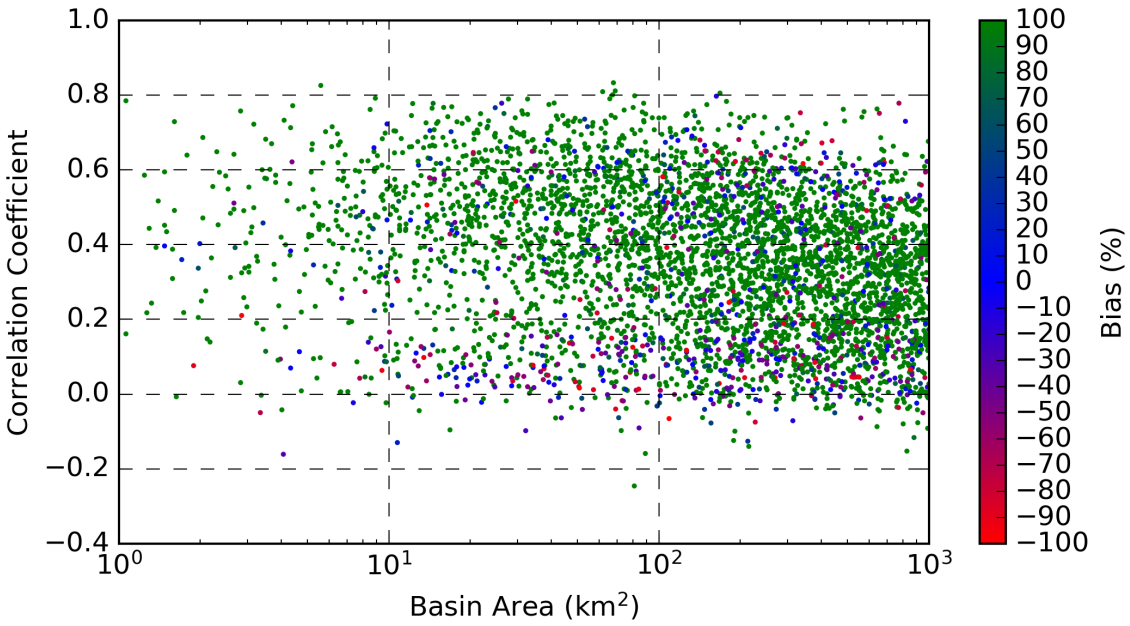

Figure 3.29: The CC from the EF5/HP simulation plotted as a function of basin area for USGS basins with areas less than 1,000 km^2.

The EF5/CREST a priori parameters are new compared to the rigorous validation work done with the EF5/SAC-SMA parameters, as such there is interest in the skill of EF5/CREST as a function of the parameter values. Figure 3.30 shows the correlation coefficient and bias plotted as a function of the basin averaged b parameter. There is no noticeable correlation between the skill of EF5/CREST and the b parameter. Figure 3.31 shows the comparison between the model skill and the basin averaged F_c parameter. There is also not obvious correlation between the parameter and the model skill. The relationship between skill and impervious area is shown in Figure 3.32. There is a trend with more impervious area leading to higher correlation coefficients but the bias also seems to increase at the same time. Figure 3.33 shows the skill between the model and the W_m parameter. There is not a clear signal in the relationship between model skill and this parameter. Finally, Figure 3.34 plots the model skill as a function of the percentage of precipitation that falls as snow. The higher the percentage of precipitation that is snow the lower the skill of EF5/CREST. This makes sense because the hydrologic model was run without a snow component.

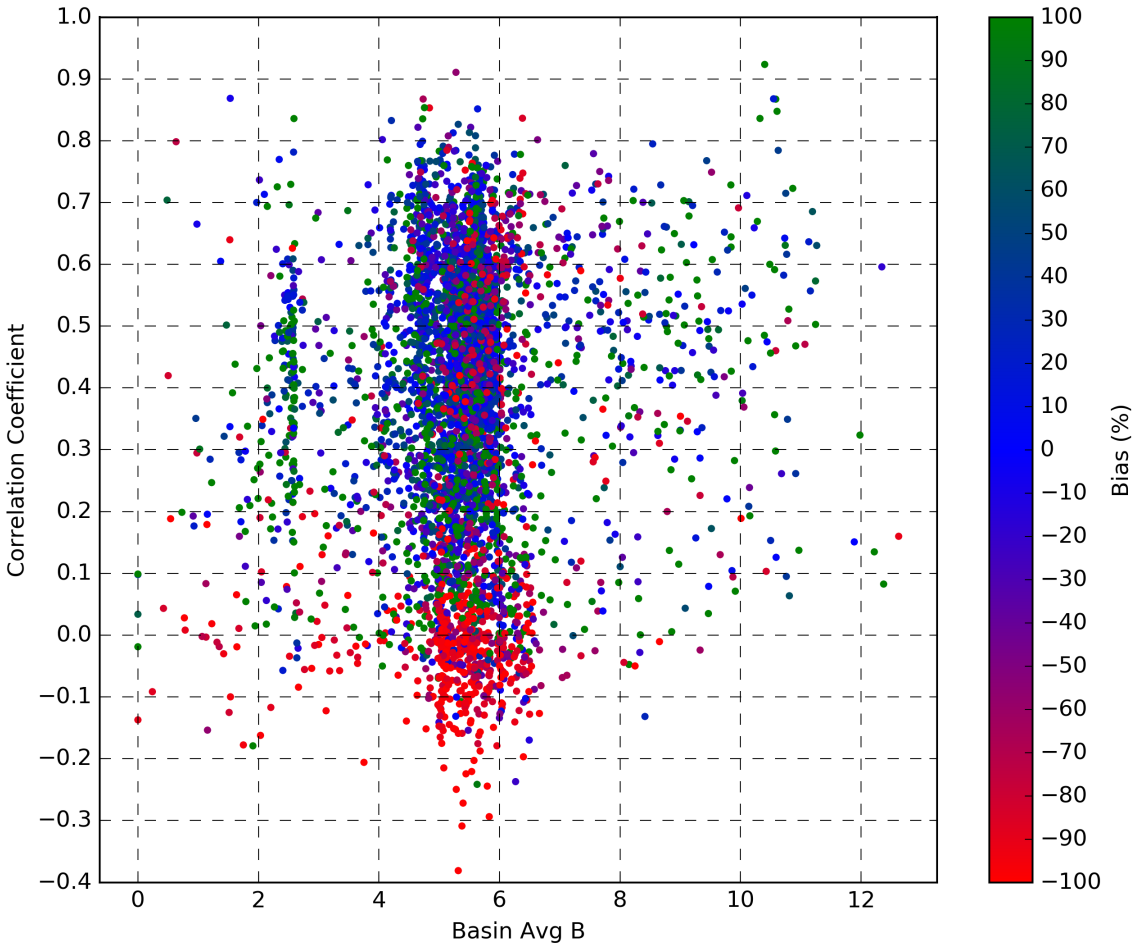

Figure 3.30: The CC from the EF5/CREST simulation plotted as a function of b for USGS basins with areas less than 1,000 km^2.

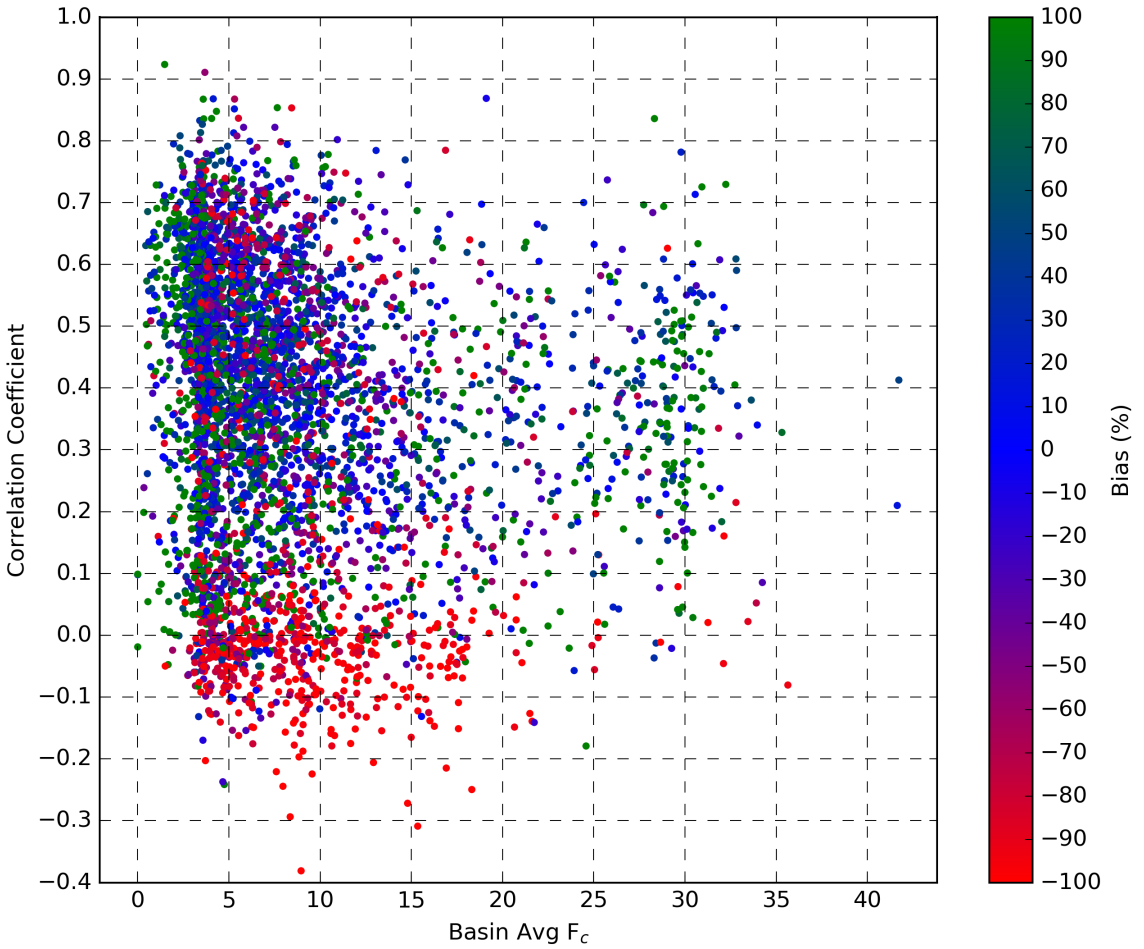

Figure 3.31: The CC from the EF5/CREST simulation plotted as a function of F_c for USGS basins with areas less than 1,000 km^2.

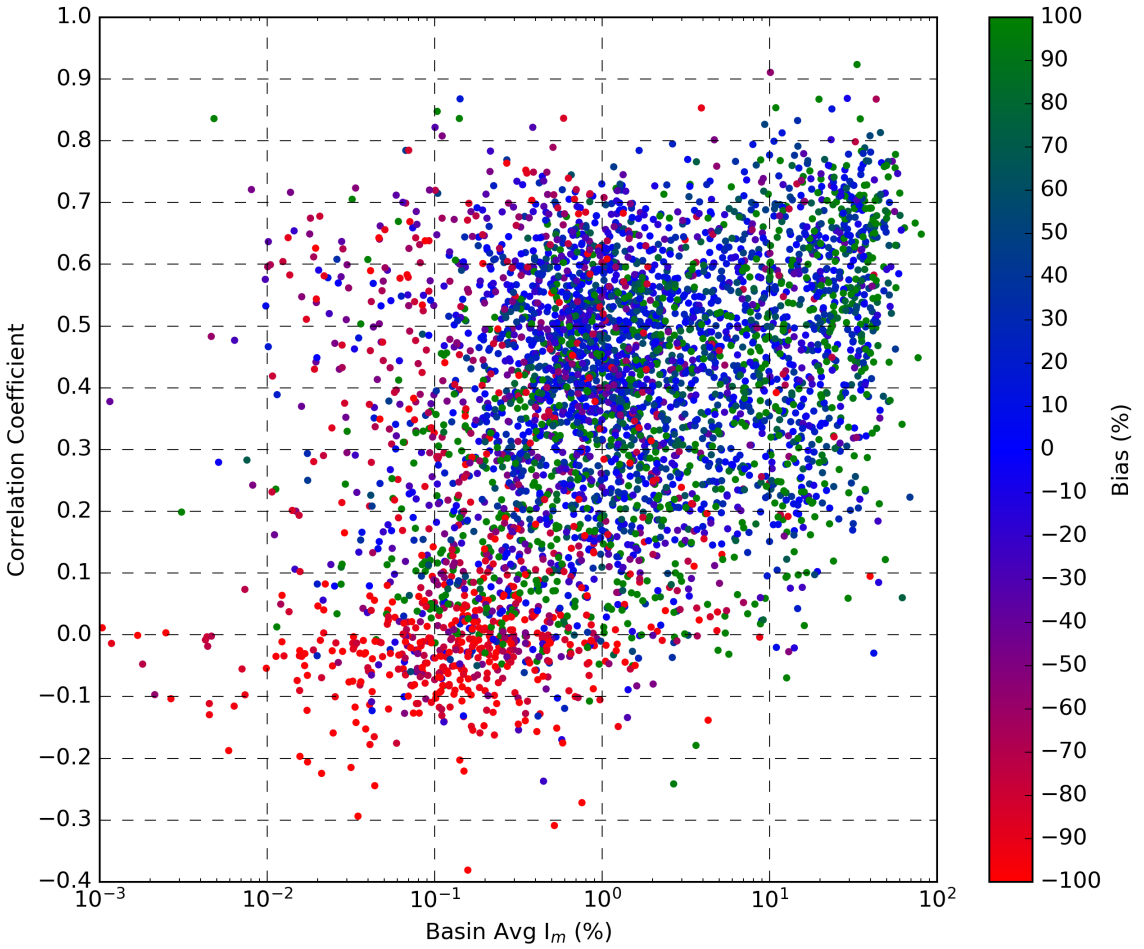

Figure 3.32: The CC from the EF5/CREST simulation plotted as a function of I_m for USGS basins with areas less than 1,000 km^2.

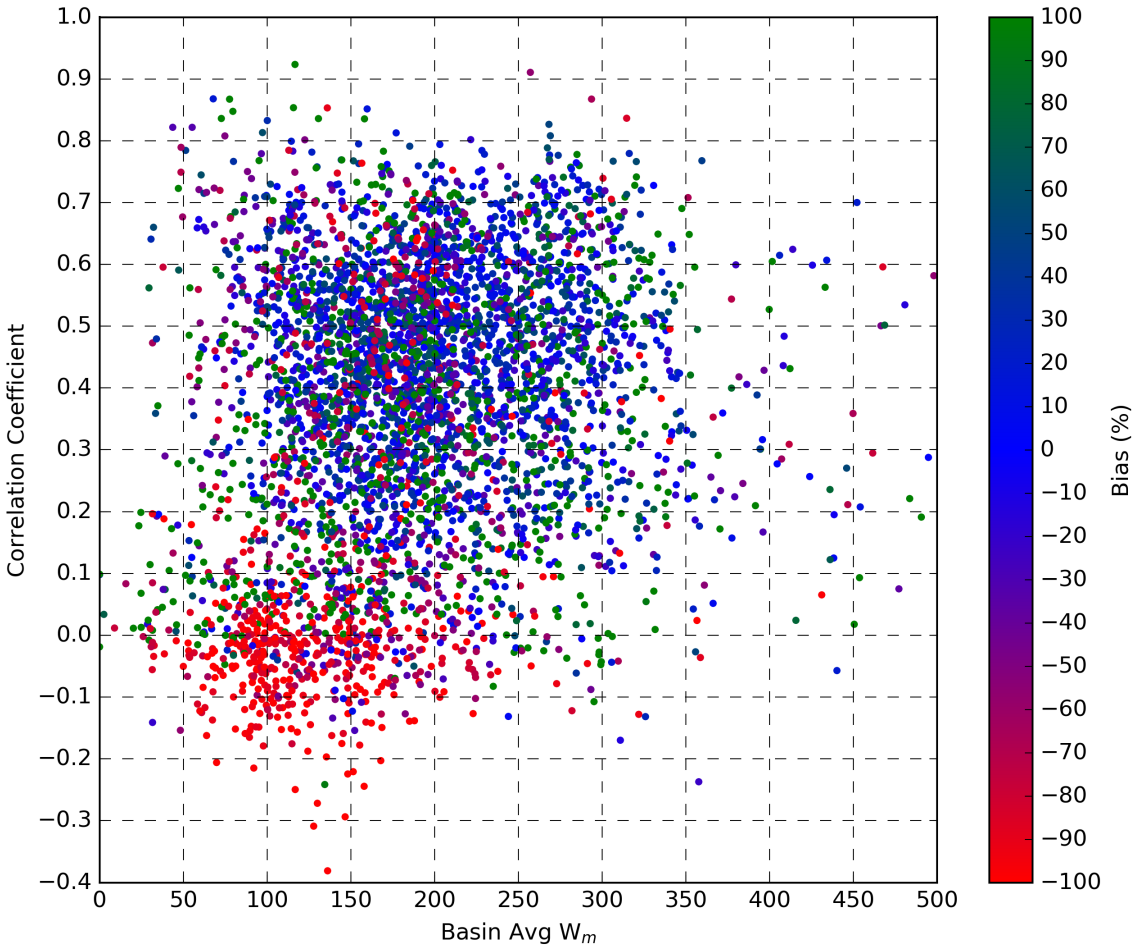

Figure 3.33: The CC from the EF5/CREST simulation plotted as a function of W_m for USGS basins with areas less than 1,000 km^2.

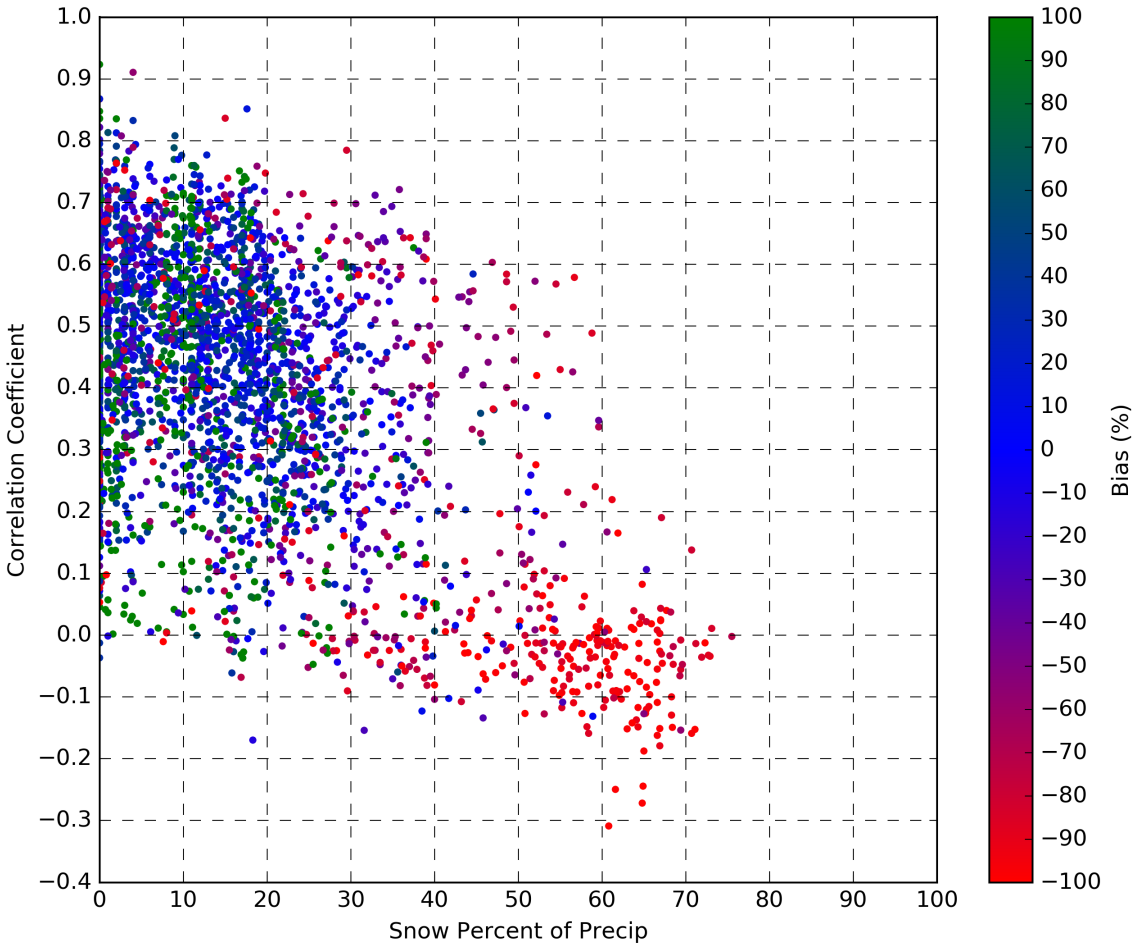

Figure 3.34: The CC from the EF5/CREST simulation plotted as a function of snow percentage for USGS basins with areas less than 1,000 km^2.

The results from this study using EF5/CREST, EF5/SAC-SMA, and EF5/HP all coupled with kinematic wave routing and a priori uncalibrated parameters for all models are acceptable showing no significant trends in skill related to basin averaged values. EF5 is able to ingest MRMS five minute precipitation rate files and a ten year simulation completed in a week of computer time is a reasonable expectation given the high resolution of the basic grids. The overall skill of the system is reasonable given its uncalibrated nature and on some watersheds the skill is good even for a calibrated hydrologic model. The results show no significant trend in accuracy versus basin area for the range of flash flood basins from 1 km^2 to 1000 km^2. The EF5/

HP model works as a worst case scenario and exhibits large positive bias for most watersheds which is expected behavior for a completely impervious land surface.

3.7 Training, Capacity Building, and the Future

As part of ensuring that EF5 is user friendly, a detailed user manual has been developed. This user manual explains purely the operation of EF5 leaving explanations of the science to journal articles. The user manual also gives detailed examples of different configuration file options so that they can be copy and pasted to run. Learning from experiences with user training, EF5 is also designed to give friendly error messages telling you what line of the configuration file has a problem and the source of the error. If a field with a fixed number of options is incorrectly specified then EF5 will list the valid options and what option was input in order to help users locate a potential misconfiguration. EF5 also tries to infer as much information as possible from the provided data files. This is useful because it simplifies and reduces the configuration options that must be specified in order to successfully run EF5.

EF5 has also been used for capacity building activities support by NASA SERVIR, the Secure World Foundation, and the Mexican Space Agency. For this role a week long training course was developed. This course covers an introduction to hydrologic modeling, an introduction to precipitation measurement via remote sensing satellites and radars, an introduction to GIS using the freely available and open source Quantum GIS software, and finally an overview of EF5 with sample cases ready to run. This workshop has been viewed as very valuable by the participants who have taken it because the workshop starts from the very beginning and builds skills. One of the lessons we have learned over the development of the workshop is to provide hands on time with the models and other tools every day so that the trainees can build actual experience with how to run the software packages. This is invaluable as a tool for increasing engagement from the workshop participants.

The training workshops are invaluable for the improvement to EF5 alone. Many features are requested, built, and tested by end users during the week long workshops. This rapid integration of user feedback is essential for improving the experience for

everyone involved. Having the model developer working directly with end users and feeling their pain plus frustration with learning EF5 is a wonderful way to ensure friction points with hydrologic modeling are resolved quickly.

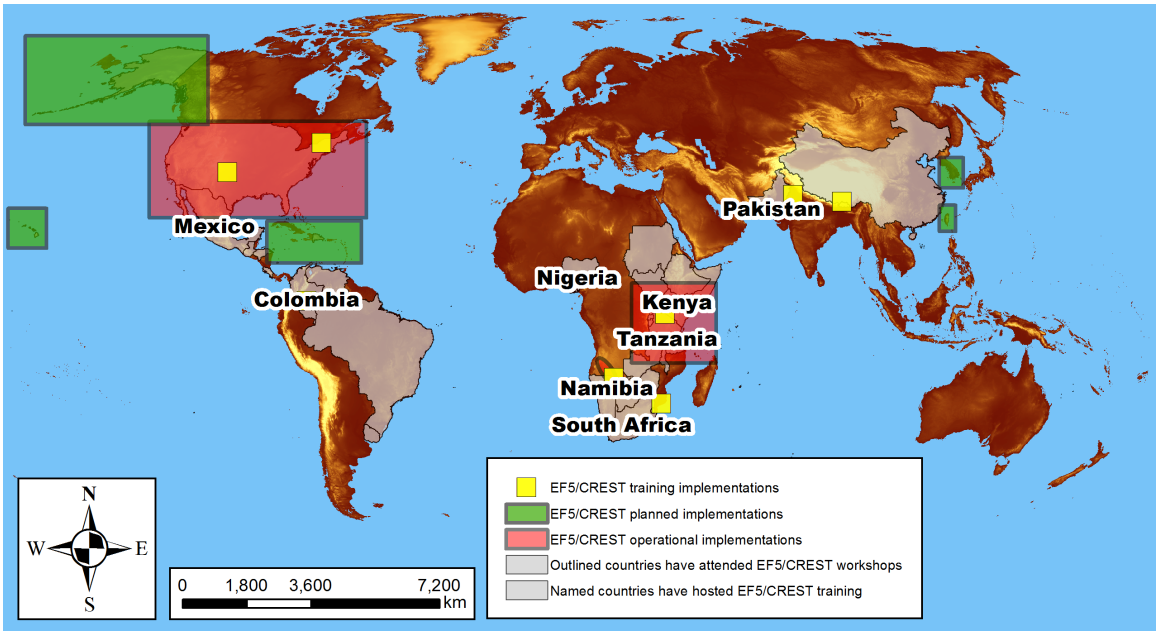

Figure 3.35: A map showing where EF5 training workshops have been conducted and where EF5 systems are currently running in operational or quasi-operational settings.

Figure 3.35 shows a map of all of the locations where EF5 training has been conducted or where EF5 is being run in a quasi operational fashion. African countries are the primary beneficiary from capacity building activities right now but there has been a growing EF5 presence in Central and South America as well. The year and location of EF5 workshops are listed in table 3.7. The training materials are all available online at `http://ef5.ou.edu/training` which includes 11 instructional modules. Video recordings of the first 5 training modules being presented are available at `http://ef5.ou.edu/videos/` . The videos were produced with the assistance of the OU School of Meteorology IT.

Table 3.7: EF5 Training and Capacity Building Workshops

Year	Workshop Location	Workshop Attendees
2012	Storrs, CT, USA	University of Connecticut
2015	Windhoek, Namibia	Namibia National Hydrologic Service
2015	Puebla, Puebla, Mexico	Colombia, Honduras, Uruguay, Brazil, Venezuela, Costa Rica, Mexico, Guatemala, and the Dominican Republic
2015	Bogata, Colombia	El Bosque University
2015	Villahermosa, Tabasco, Mexico	University of Tabasco, and the Mexican Space Agency
2016	Windhoek, Namibia	Namibia National Hydrologic Service

Chapter 4

Hydrologic Climatology Over the CONUS

4.1 EF5 Setup

The results in Section 3.6 show that the EF5 modeling system running EF5/CREST and EF5/SAC-SMA with uncalibrated a priori parameters over the CONUS produces reasonable skill on flash flood scale gauged basins. Given these results the next logical step is to extrapolate the hydrologic models to ungauged basins to examine a climatology of when these watersheds experience flash flooding. The goal is to produce a climatology of the number of days each grid cell experiences flash flooding. To do so the model setup will be described, a threshold to determine if a grid cell is flooding will be derived, and finally climatological maps produced.

In order to generate a climatology, the EF5 system was set up as described in Section 3.4. The EF5/HP model was not included in this analysis because the focus here is not on a worst case scenario. The modeling domain was again set to exactly match the MRMS domain with a regular 0.01° grid spanning from –130.0 to –60.0 longitude and 20.0 to 55.0 latitude. This produces 10,816,262 grid cells which will be modeled over the CONUS. The computation and storage requirements for storing five minute gridded data from the resulting model runs was too large for available capacity. It was determined that only specific variables should be kept and that they would be integrated through time to find a daily maximum or minimum value depending on the variable. For discharge, the daily maximum value and the time that the maximum occurred were kept so that the peak discharge for flash floods would be captured. For soil saturation, the daily minimum value was kept in order

to quantify the antecedent soil saturation conditions before flash flood events. Table 4.1 summarizes which variables were kept and what data reduction method was used.

Table 4.1: Climatology Variables Kept

Variable	What is Kept
Discharge	Daily Maximum Value & Time
Unit Discharge	Daily Maximum Value & Time
Soil Saturation	Daily Minimum

The simulations were again run for the 2001 through 2011 period when MRMS precipitation rate forcing was available. 2001 was used for a model warm up period and so results will be presented from 2002 through 2011. Both sets of simulations were run year-by-year, saving the states at the end of one year to use for the start of the next year. The EF5/CREST simulation took 6 days to complete a year of simulation while the EF5/SAC-SMA simulation took 7.5 days to complete a year. In total 3 months of computer time was spent to generate the simulations used here. Future reanalysis periods may be able to use the saved states generated here to hot start simulations for all of the years in parallel reducing the computational time to only a week. This may also be an elegant avenue for creating a five minute gridded time series for the hydrologic variables if there is a desire.

4.2 Flood Thresholds

Hydrologic models, especially those employing simplifying assumptions to the Saint-Venant equations, do not explicitly model the stream channel or channel cross-section. As such it is not possible for the hydrologic models to know when the water volume is so great that it can no longer be contained inside the channel banks. Therefore a threshold must be set on the discharge to approximate when the water will exceed the channel banks. This section will define the threshold used and show how it is estimated for ungauged locations.

Categories for flooding are defined at USGS stations by the USGS, NWS, and with input from the local community (NWS 2012). There are four stages of flood defined currently, action, minor, moderate, and major. The action stage is the stage that triggers mitigation action from the NWS for possible significant hydrologic activity. Often action stage is very similar or identical to the bankful condition. The minor flood stage is defined as minimal or no damage to property but possibly some threat to human life from for example inundated roads. Moderate flooding is classified as some inundation of structures/roads near stream, motivating some evacuation of people and/or transfer of property. The final category, major flooding, contains extensive inundation of structures and roads causing significant evacuations of people and transfer of property. In general the categories can be said to depend on the channel and bank conditions as well as the infrastructures near the river and the possible presence of levees.

For the purposes of this work the minor flood stage threshold will be used. Minor flood stage is appropriate because it is the first category with the potential for the loss of human life. Of the 10,000+ USGS stream gauges in the CONUS only 3,490 ($\sim$34%) of them have defined flood stages (Gourley et al. 2013). Figure 4.1 shows the minor flood threshold values and the locations where they are defined at across the CONUS. The lack of coverage for defined thresholds is apparent. It is hard to be

certain since discharge is dependent on basin scale but there are patterns visible such as higher threshold values over the eastern CONUS particularly over the Appalachian mountain range. Higher threshold values are also seen along the west coast and in south central Arizona.

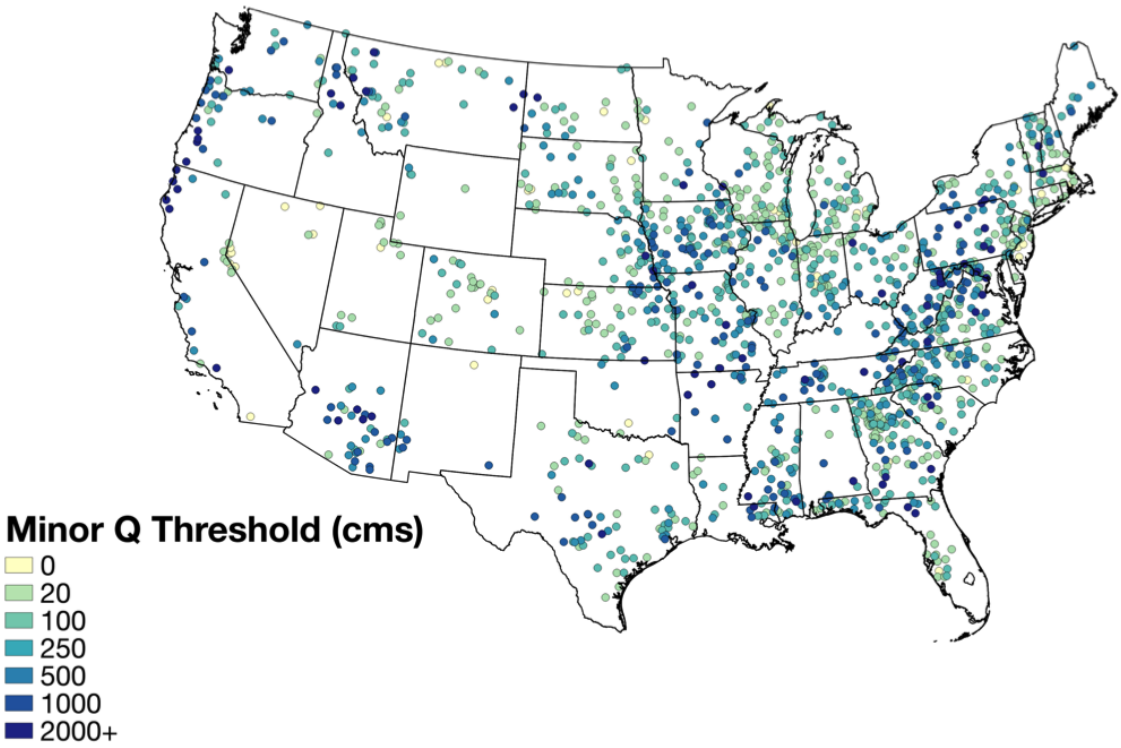

Figure 4.1: The minor flood thresholds defined by USGS, NWS, and local stakeholders for USGS stream gauge locations.

To define thresholds at ungauged basins the thresholds were modeled using the power law relationship shown in equation 4.1.

$$MinorFlood = aBA^{b}P^{c} \tag{4.1}$$

Where a, b, c are coefficients, BA is the basin area, P is the basin averaged mean annual precipitation. Here the basin area was defined by the model FAM and the basin average mean annual precipitation was generated from the PRISM dataset (Daly et al. 1994). The coefficients were found using ordinary least squares regression

and determined to be $a = 0.000784$, $b = -0.47$, and $c = 1.25$ with BA in units of km^2 and P in units of mm. As an example from this dataset, for grid cells with a basin area of 1 km^2 the mean threshold is 2.03 m^3 s^{-1} and the median threshold is 1.76 m^3 s^{-1}. Figure 4.2 shows a scatter plot of the predicted minor flood threshold versus the observed minor flood threshold. There is considerable scatter, but given the uncertainty implied by how the minor flood thresholds are defined this is considered to be a good fit.

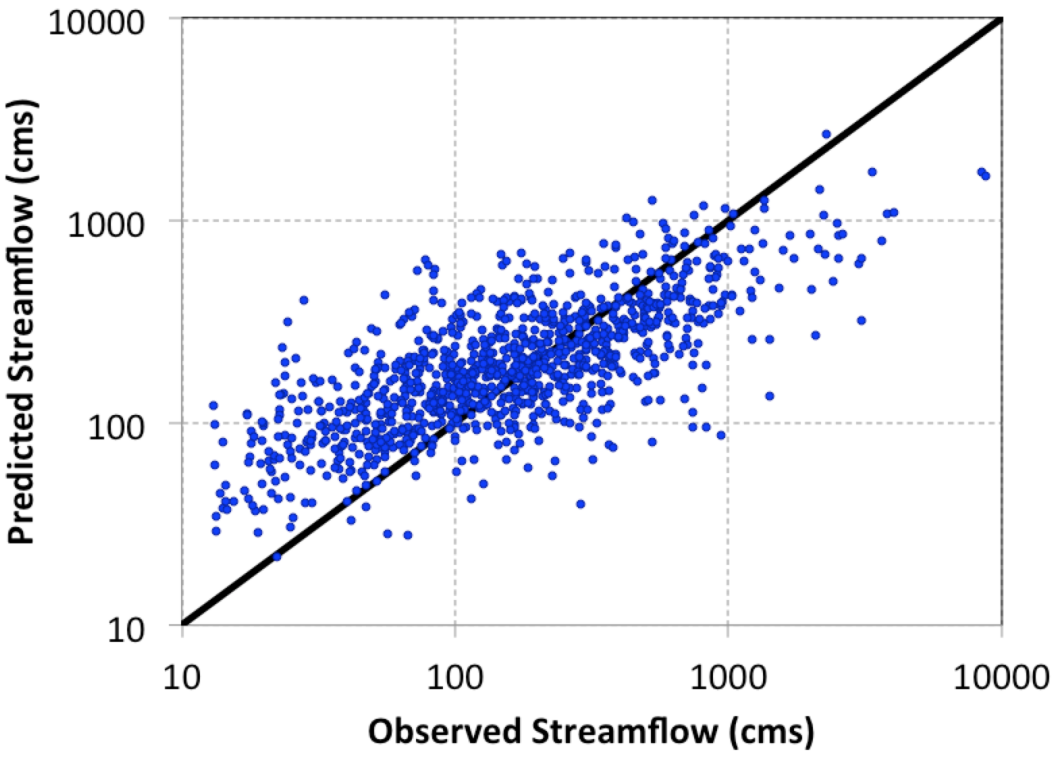

Figure 4.2: A scatter plot showing modeled minor flood thresholds using a power law with basin area and mean annual precipitation versus the observed minor flood thresholds.

After developing the model the next step is to use it to extrapolate flood thresholds for the entire CONUS. The same model FAM grid for basin area and PRISM grid for the basin averaged mean annual precipitation was used for this extrapolation process. The results of the extrapolation are shown in Figure 4.3 which is map of the distributed values for the minor flood threshold. The modeled map shows some of the

same trends as seen in the observed data in Figure 4.1. The higher values along the west coast of the US are well captured. The higher thresholds along the Appalachian mountains are not as apparent here. The gradually increasing values from east to west across the CONUS are visible here matching the mean annual precipitation pattern.

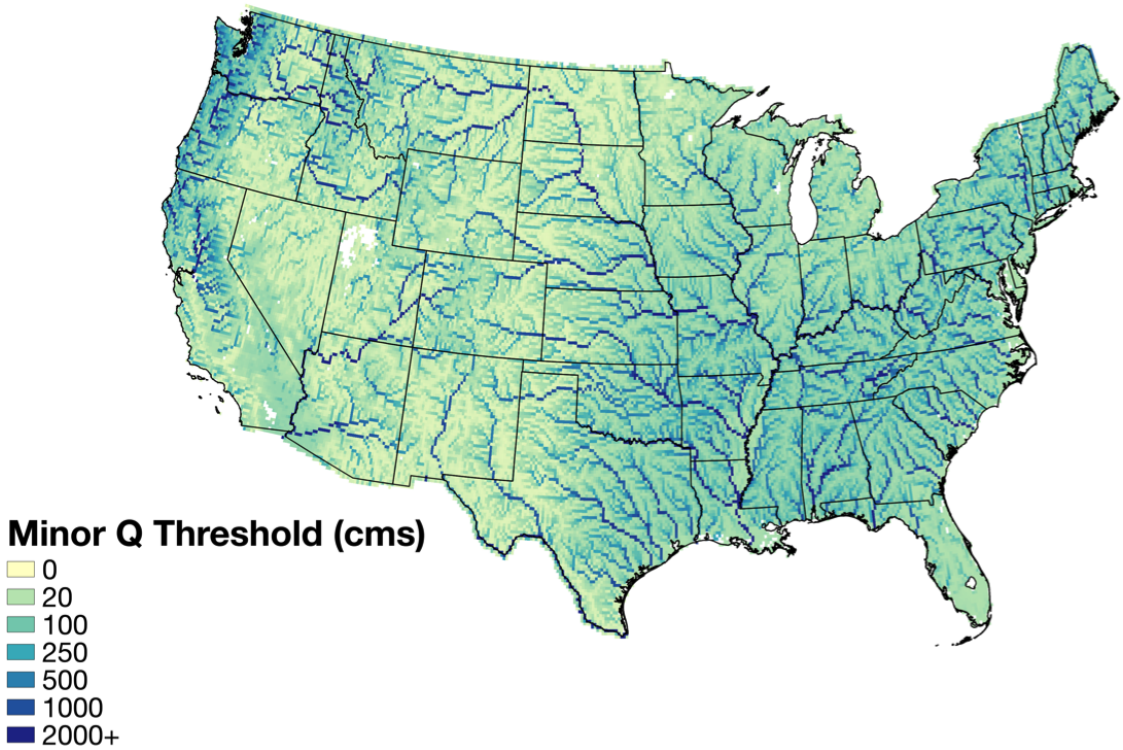

Figure 4.3: A map showing the modeled minor flood thresholds for the CONUS area.

While the minor flood threshold was used in this instance, it is possible to repeat this exercise for the action, moderate, or major thresholds if the need should arise. The following results which make reference to flood days are subject to the quality of these thresholds. If in the future, additional improvements to the flood thresholds are possible they should be undertaken because the improvements will yield significant dividends in the quality of research relating to flood climatology.

4.3 Quality Control

The quality of the resulting simulations is important to any conclusions hoping to be drawn from them. The MRMS quality control procedures greatly reduce the amount of bad data that could go into the hydrologic models but they are not perfect. As such three further steps will be taken to quality control the hydrologic output data.

First, grid cells with contributing basin areas $\geq$ 1,000 km^2 will be masked out. Figure 4.4 shows in red the areas removed for violating the basin area criteria which is visually only the large river networks in the CONUS. This step is necessary because the hydrologic models were run for the entire CONUS but we are only interested in flash flood grid cells as per the basin area definition.

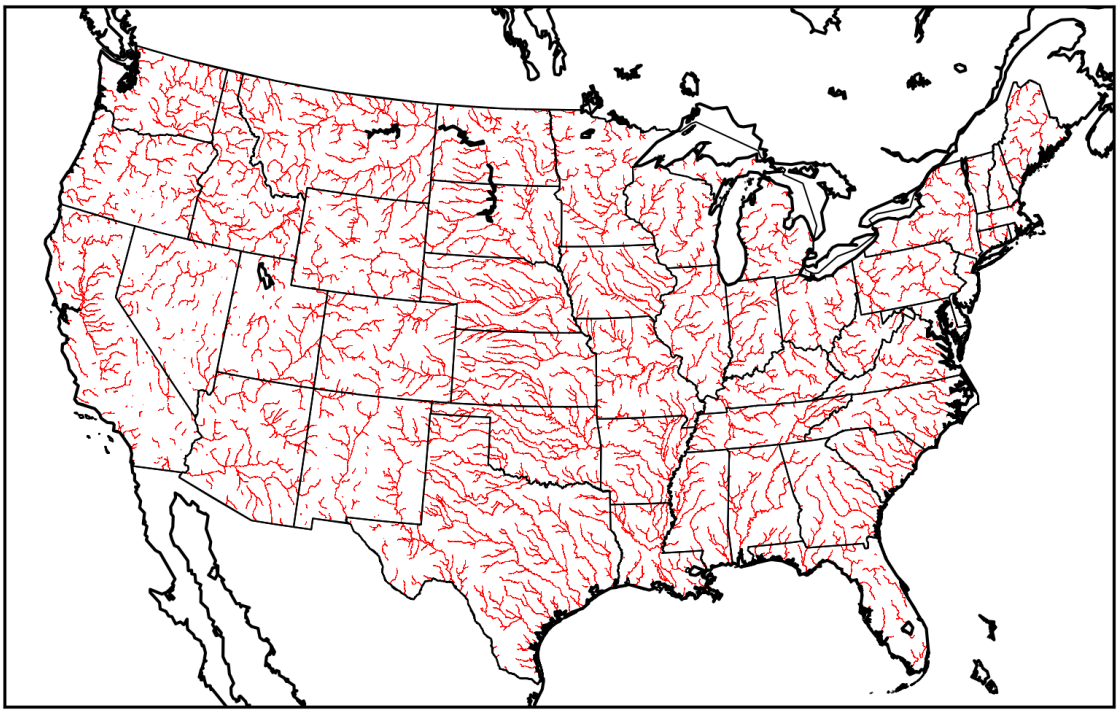

Figure 4.4: The areas shown in red were masked for having basin areas $\geq$ 1,000 km^2

Second, the MRMS precipitation accumulation grid was analyzed to remove grid cells that were consistently too high compared to surrounding neighbors. This may be the case when ground clutter or anomalous propagation is not fully removed by the MRMS quality control algorithms. This process was carried out by taking a

basin averaged MRMS precipitation accumulation for 2002–2011 and marking grid cells that were 200% greater than the average of all the grid cells in a 50 km radius from the cell of interest. This procedure is ideal for removing small areas that have a consistent overestimation when compared with the surrounding area. The results of this procedure are illustrated in Figure 4.5 with the red areas being areas that will be masked out. The mask here highlights several things such as wind farms in Kansas, and Texas, ground clutter from cities, highways and interstates (e.g. I–5 in California), and mountainous areas where the beam blockage was not fully mitigated (e.g. New Mexico, Colorado and Arizona) in the MRMS algorithms. The Pacific northwest and Vermont suffer heavily from the masking because the radars have beam blockage across many azimuths and elevations which limit good coverage to only a small area. The precipitation amounts over this area are large so the great change from an unblocked azimuth to a blocked azimuth gets caught in the masking procedure.

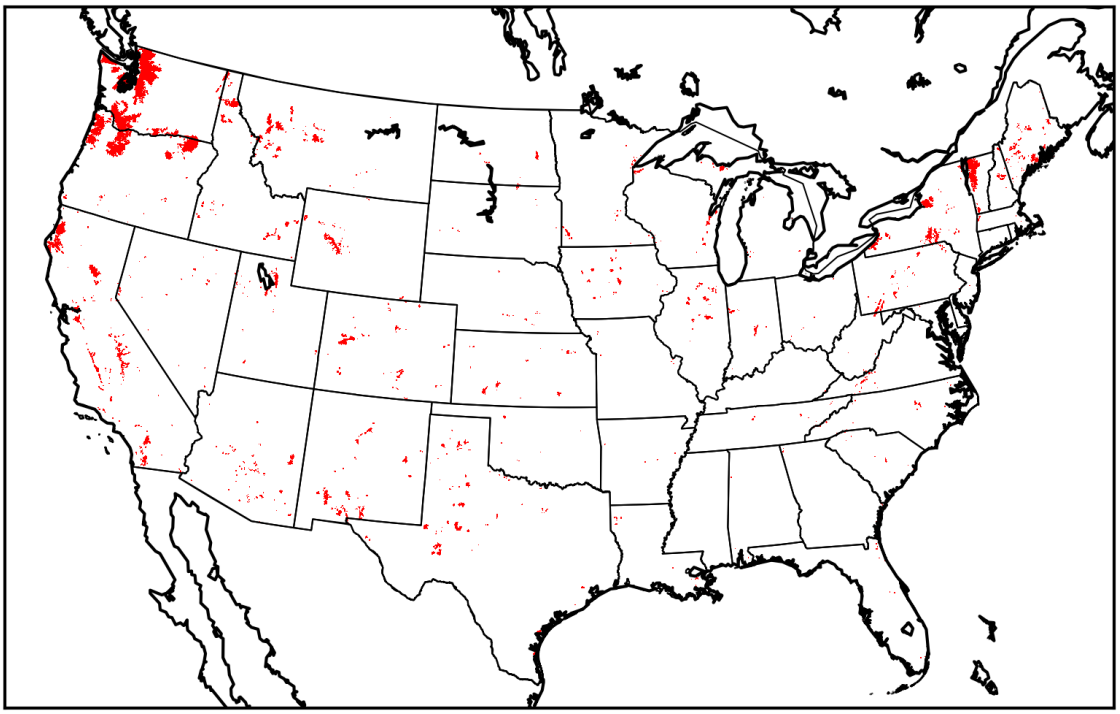

Figure 4.5: The areas shown in red were masked for having accumulated precipitation 200 % greater than the average of the grid cells in a 50 km radius.

Third, days with unit discharge values anywhere in the CONUS greater than 100 m^3 s^{-1} km^{-2} will be completely removed from the analysis procedure. This threshold value is appropriate based on the maximum envelope curves presented in Gaume et al. (2009) and Herschy (2002). It is necessary to remove the entire day and associated grid file because hydrologic routing propagates the impact of bad data down stream. This check helps control for spurious radar data that may have impacted a very limited temporal window. This check is performed for both the EF5/CREST and EF5/SAC-SMA simulations with the days removed being days where the threshold is violated for either model result. Table 4.2 contains a complete list of the 137 out of 3650 total days (4%) removed for violating this criteria. Figure 4.6 shows the maximum unit discharge for 2004 before (left panel) and after (right panel) this quality control step was implemented. The circular radar artifact visible in Texas in the before image is removed in the after image. The distribution of days that are removed due to this filter are skewed towards the winter cool season months, with four out of ten Christmas days being removed for example.This may suggest an issue with the algorithms employed in MRMS or enhanced radar hardware failure rates during the winter.

Table 4.2: Days Removed for Exceeding Unit Discharge Threshold

2002–01–25	2002–02–19	2002–06–06	2002–08–31	2002–11–17
2002–12–10	2002–12–11	2003–04–01	2003–04–14	2003–06–03
2003–08–29	2003–08–30	2003–11–06	2003–11–09	2003–11–11
2003–11–13	2003–11–18	2003–11–19	2003–11–21	2003–11–22
2003–11–13	2003–11–18	2003–11–19	2003–11–21	2003–11–22
2003–11–23	2003–11–24	2003–11–25	2003–11–26	2003–11–28
2003–11–29	2003–11–30	2003–12–15	2003–12–18	2003–12–23
2003–12–28	2004–03–26	2004–05–18	2004–05–19	2004–05–20
2004–12–11	2004–12–22	2004–12–25	2005–01–19	2005–01–27
2005–02–12	2005–02–17	2005–02–28	2005–04–01	2005–04–10
2005–04–11	2005–04–21	2005–11–14	2005–11–20	2005–11–21
2006–01–23	2006–01–29	2006–02–04	2006–03–17	2006–03–22
2006–05–07	2006–11–28	2006–11–29	2006–11–30	2006–12–05
2006–12–13	2006–12–19	2006–12–22	2006–12–25	2007–01–14
2007–01–31	2007–04–10	2007–11–02	2007–12–04	2007–12–10
2007–12–21	2008–01–02	2008–01–28	2008–02–11	2008–09–14
2008–11–13	2008–11–17	2008–12–21	2008–12–30	2009–01–05
2009–01–08	2009–01–16	2009–01–22	2009–01–28	2009–02–09
2009–02–10	2009–02–11	2009–02–12	2009–02–16	2009–02–18
2009–03–22	2009–03–28	2009–03–30	2009–04–04	2009–04–21
2009–10–10	2009–11–02	2009–11–16	2009–11–26	2009–12–19
2009–12–24	2009–12–25	2009–12–26	2009–12–31	2010–01–19
2010–02–03	2010–06–01	2010–11–21	2010–11–23	2010–11–26
2010–11–30	2010–12–11	2010–12–21	2010–12–22	2010–12–25
2011–01–10	2011–01–29	2012–02–04	2011–02–18	2011–03–02
2011–03–06	2011–03–07	2011–03–09	2011–03–11	2011–03–19
2011–03–22	2011–03–30	2011–04–06	2011–10–10	2011–10–29
2011–12–20	2011–12–23			

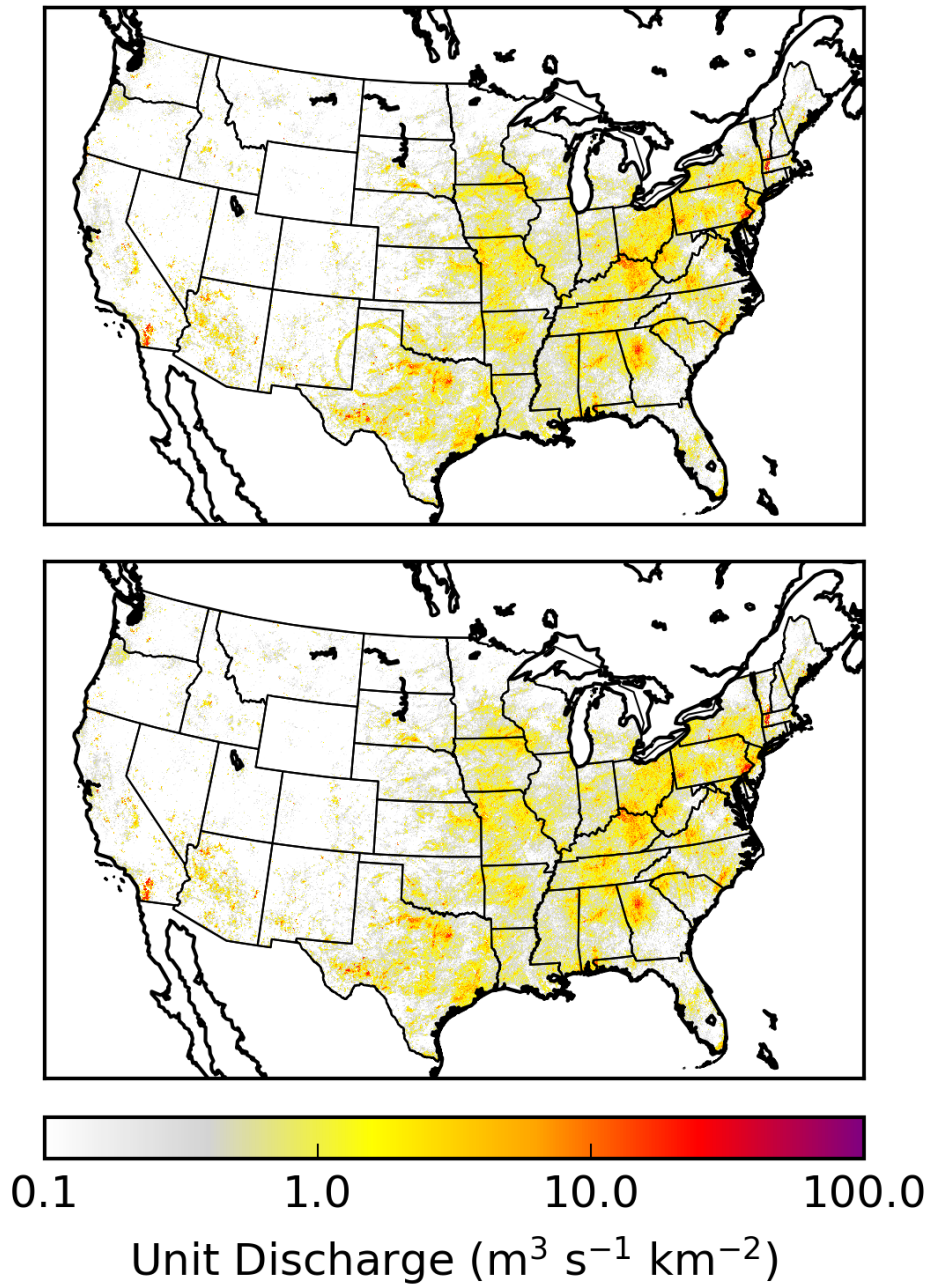

Figure 4.6: The maximum unit discharge for 2004 from EF5/CREST before (top panel) and after (bottom panel) it was quality controlled by removing 7 days with greater than 100 m^3 s^{-1} km^{-2} unit discharge.

Future efforts to quality control the data may be able to isolate specific areas that were negatively impacted on the above days and remove them. The ideal solution would be for the MRMS precipitation reanalysis to be corrected using information gleaned from above. This would prevent the impacts of hydrologic routing

from contaminating a large portion of the grid to an unknown extent. The dual-polarization upgrade to the weather radars should help significantly to cut down on non-precipitation echoes in the future. These polarimetric variables will remain unavailable for the 2001–2011 period analyzed here so additional work to quality control the data may be needed. It is possible a machine learning algorithm trained on automatic classifications produced with the aid of the polarimetric variables can be applied to the retrospective dataset. Gauge correction at hourly scale downscaled to the precipitation rates may be another effective mean for correcting the reanalysis precipitation dataset.

4.4 Results

Figures 4.7 and 4.8 show the mean annual maximum discharge simulated by EF5/CREST and EF5/SAC-SMA respectively. The basin areas greater than 1,000 km^2 were not removed for these figures so that the full extent of the hydrologic analysis is present. The differences between the models are readily apparent with EF5/CREST producing higher values overall and a more distinct spatial pattern. The EF5/CREST figure has a peaked areas all around the eastern US while the EF5/SAC-SMA figure lacks this pattern featuring a relatively uniform mean annual maximum discharge. These grids would be useful in the creation of model simulation return period estimates for this time period.

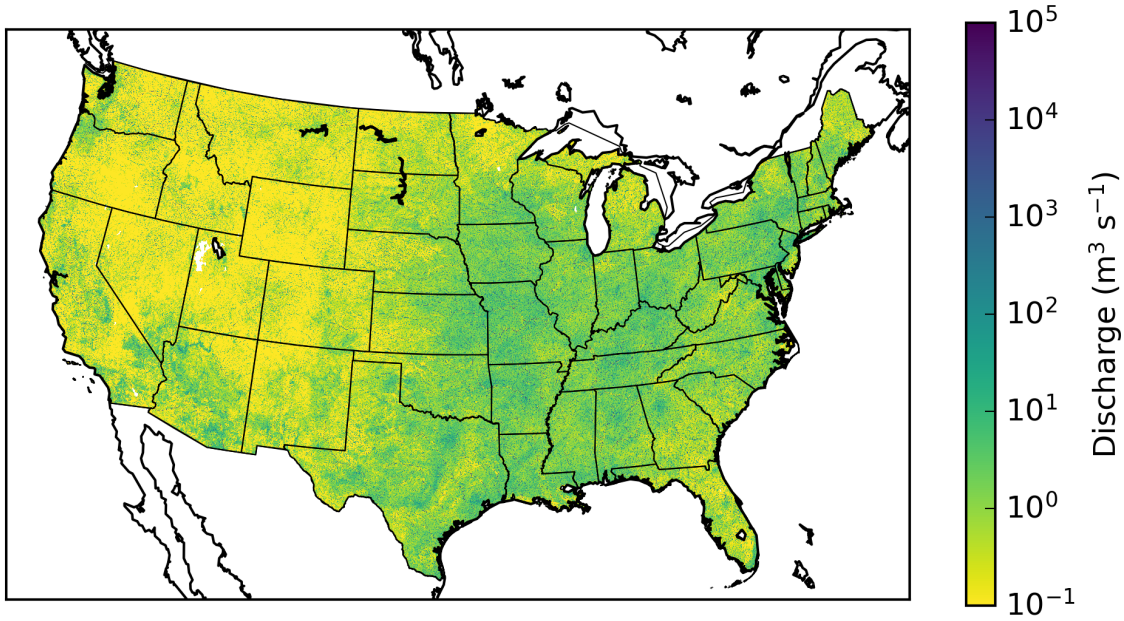

Figure 4.7: The mean annual maximum discharge simulated by EF5/CREST from 2002-2011.

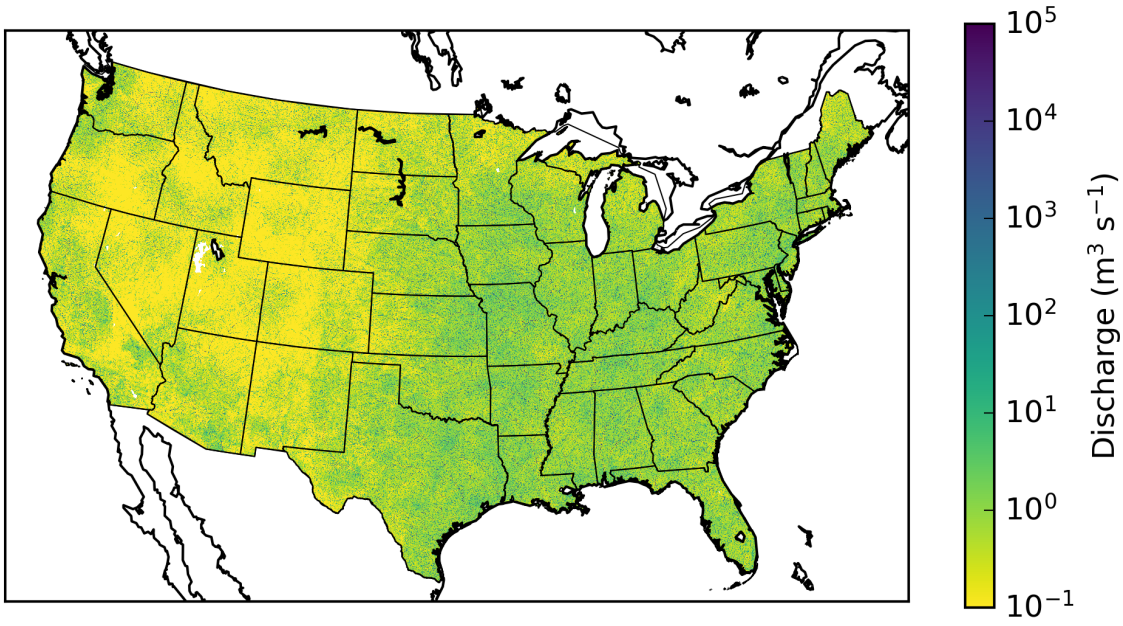

Figure 4.8: The mean annual maximum discharge simulated by EF5/SAC-SMA from 2002-2011.

The mean annual maximum unit discharge are shown in Figures 4.9 and 4.10 for EF5/CREST and EF5/SAC-SMA respectively. The differences between the models are again apparent with the same trend that the EF5/SAC-SMA amplitudes are not as high across the US. EF5/CREST has values greater than 10 m^3 s^{-1} km^{-2} in many cities such as Dallas, Texas; Atlanta, Georgia; Birmingham, Alabama, and Houston, Texas. The values from the EF5/SAC-SMA simulation for these cities is only around 1 m^3 s^{-1} km^{-2}. EF5/CREST has higher values in Arizona while EF5/SAC-SMA has higher values in Florida. The differences between the models here is likely due to land surface parameterization.

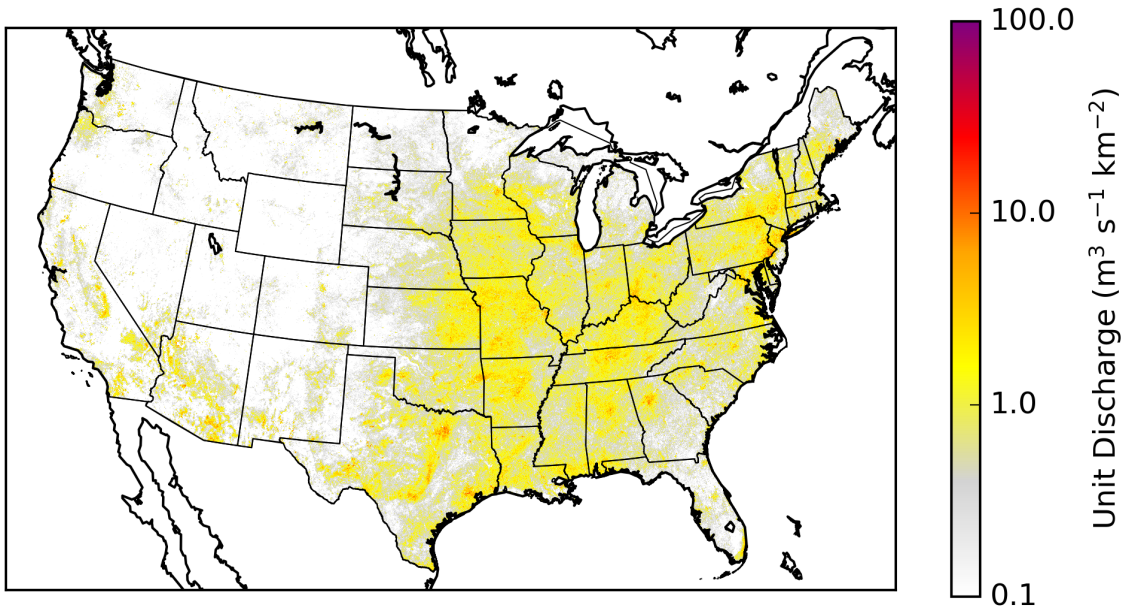

Figure 4.9: The mean annual maximum unit discharge simulated by EF5/CREST from 2002-2011.

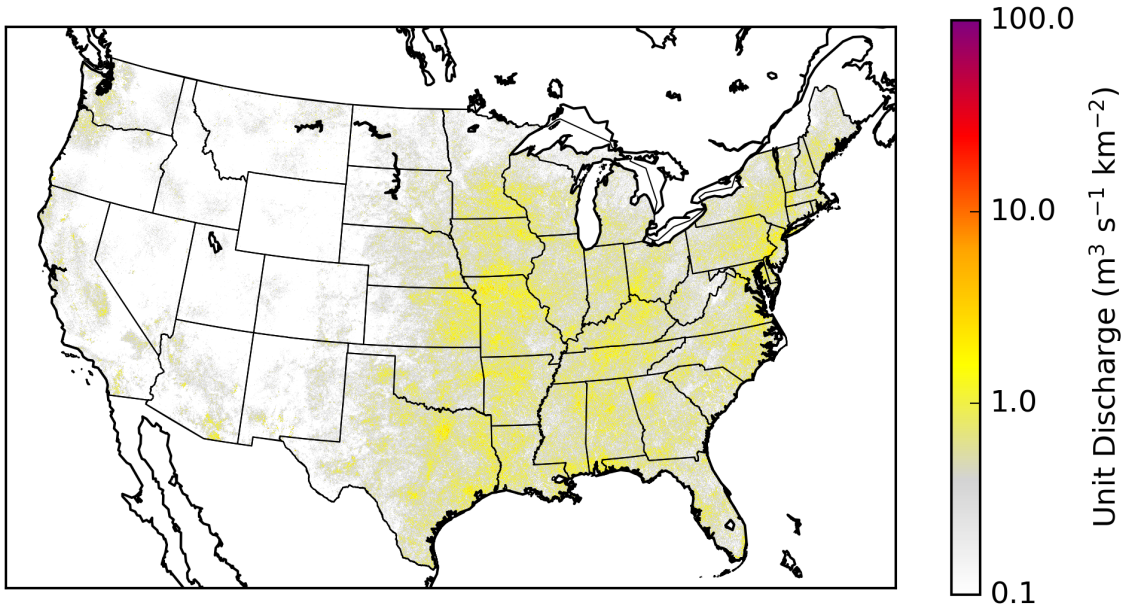

Figure 4.10: The mean annual maximum unit discharge simulated by EF5/SAC-SMA from 2002-2011.

The mean annual number of flash flood days are shown in Figures 4.11 and 4.12 for EF5/CREST and EF5/SAC-SMA respectively. The data for these plots was resampled to 0.25° using the average for display purposes. As might be expected

given the mean annual maximum unit discharge, EF5/CREST produces more flood days in cities than EF5/SAC-SMA with many cities seeing 2+ flash flood days a year in the EF5/CREST simulations. In Arizona there are significant differences between the two models with EF5/CREST producing several areas of 2+ flash flood days per year on average that are not present in the data from EF5/SAC-SMA. The EF5/ SAC-SMA data are relatively uniform across the eastern US in the number of flash flood days while the EF5/CREST simulations are very peaked over hot spots and then quickly trend towards nearly zero flash flood days. Both models agree on a zone of higher number of flash flood days over Missouri, eastern Kansas, northern Arkansas, Iowa, and into southern Minnesota. These region sees on average 0.5 flash flood days per year, or putting it another way each area sees a flash flood on average every other year. New York and Pennsylvania are another zone of increased average number of flash flood days that have agreement from both models with a comparable number of flash flood days here to the zone in the central US.

Comparing the mean annual number of flash flood days back to the original *Storm Data* dataset of the number of flash floods in Figure 2.1 there is a good spatial correspondence. Both the *Storm Data* and the model simulations capture the region of flash flooding in the southwest caused by the monsoon. The region of higher flash floods in Missouri is also well captured in both datasets. The peak in flash floods in central Texas observed in *Storm Data* is not well captured in either of the model simulations even though this region is a hot spot for flash flood fatalities and injuries. There does appear to be a signal in the mean annual maximum unit discharge figures over the region of interest in central Texas. This may mean that the flash floods in Texas have higher peak discharges which is why they are more deadly than the more numerous flash floods in the Missouri region.

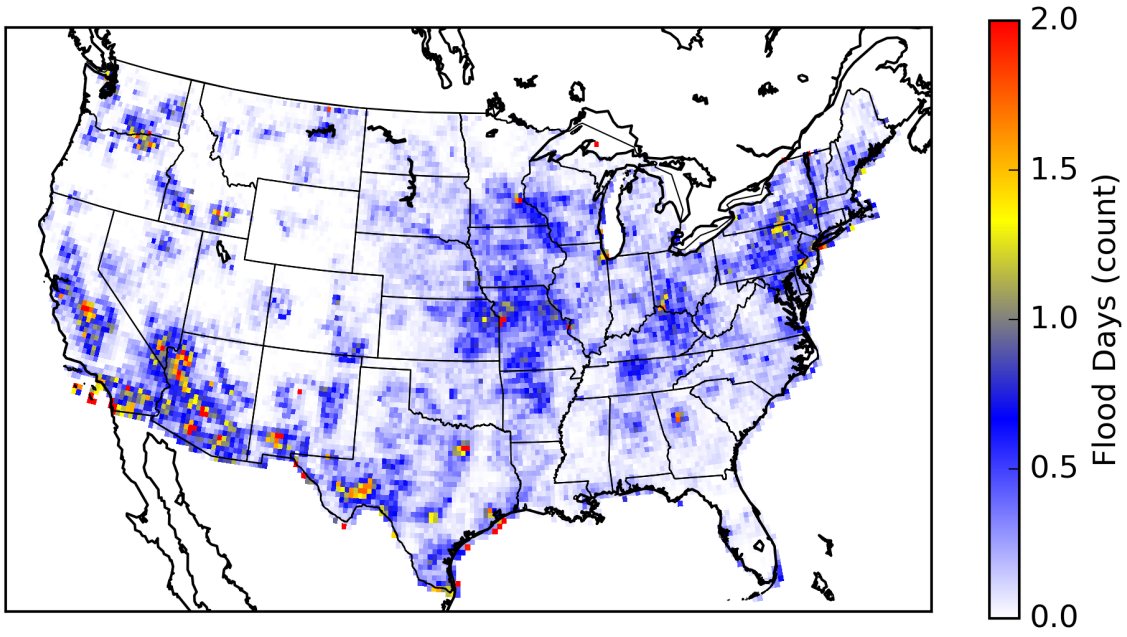

Figure 4.11: The mean annual number of flash flood days simulated by EF5/CREST from 2002-2011.

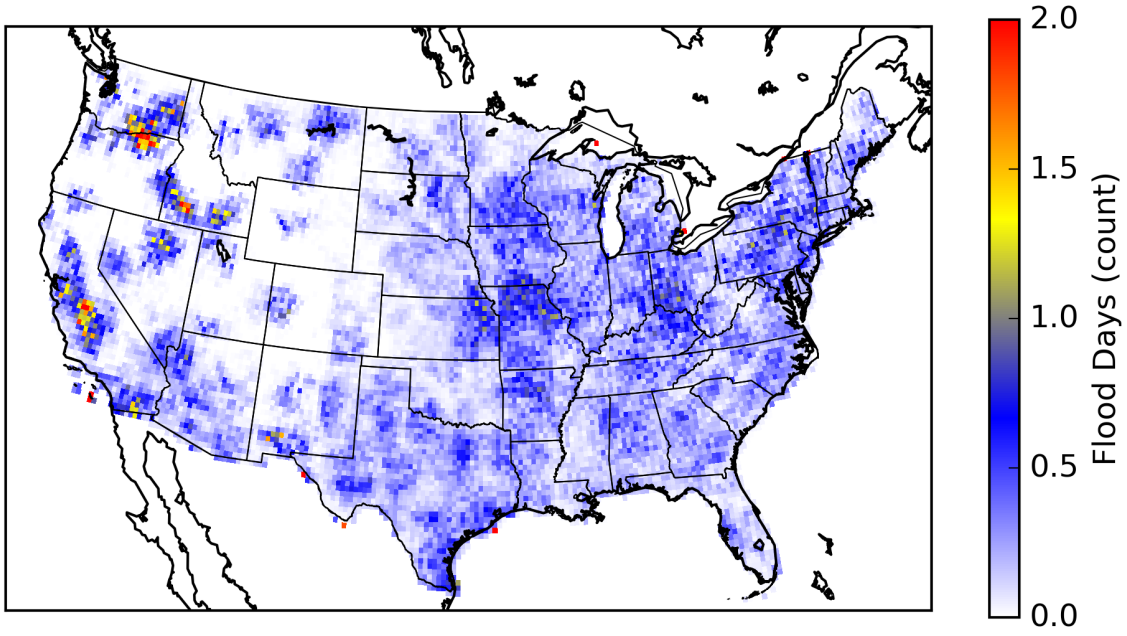

Figure 4.12: The mean annual number of flash flood days simulated by EF5/SAC-SMA from 2002-2011.

Figures 4.13 and 4.14 show the mean annual number of flash flood days simulated by EF5/CREST and EF5/SAC-SMA respectively separated by season. Starting from

the top left plot working clockwise, winter: December, January, February; spring: March, April, May; summer: June July August; and autumn: September, October, November. Both models capture well the seasonality of flash flooding with the west coast being favored in the winter. Spring flash flooding occurs in the central plains with a relatively weak signal. Summer flash flooding occurs in Arizona and the southwest associated with the summer monsoon pattern. The flash flooding hot region located in the central US is also active during the summer. In Autumn the flash flooding activity is ongoing in the southwest, and activity in the central plains has shifted eastward. This matches up well with the seasonal cycle of precipitation observed across the US.

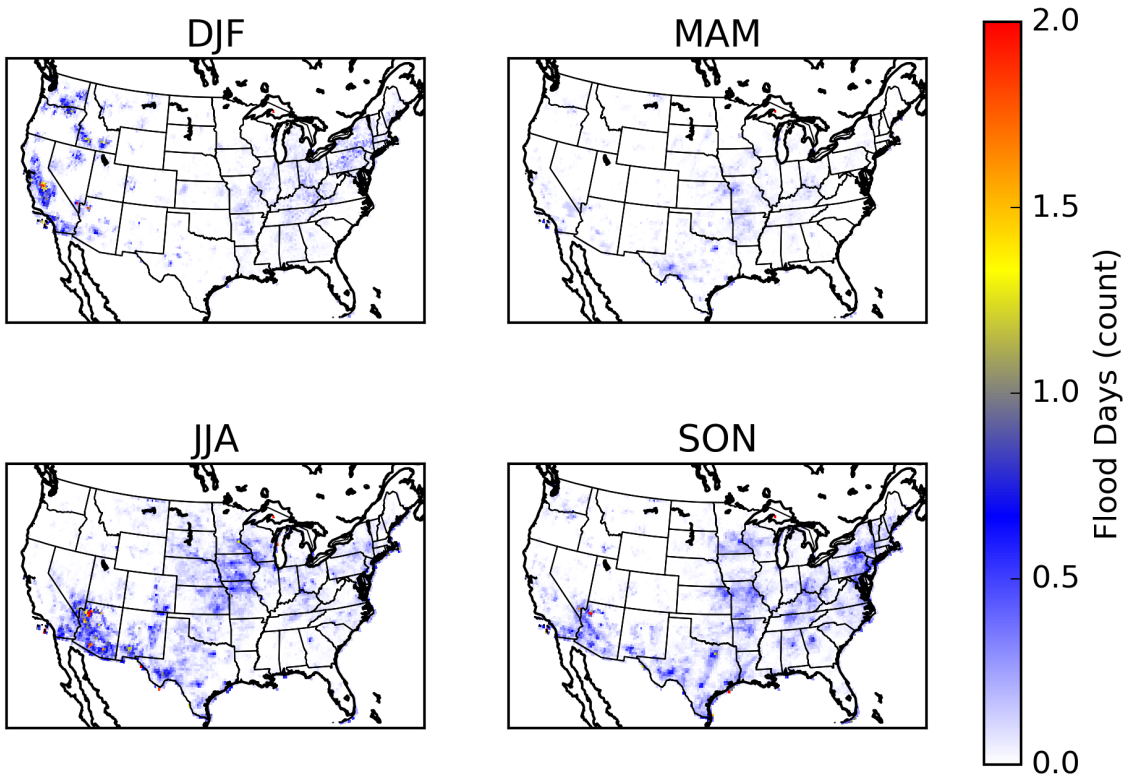

Figure 4.13: The mean annual number of flash flood days simulated by EF5/CREST from 2002-2011 plotted by season.

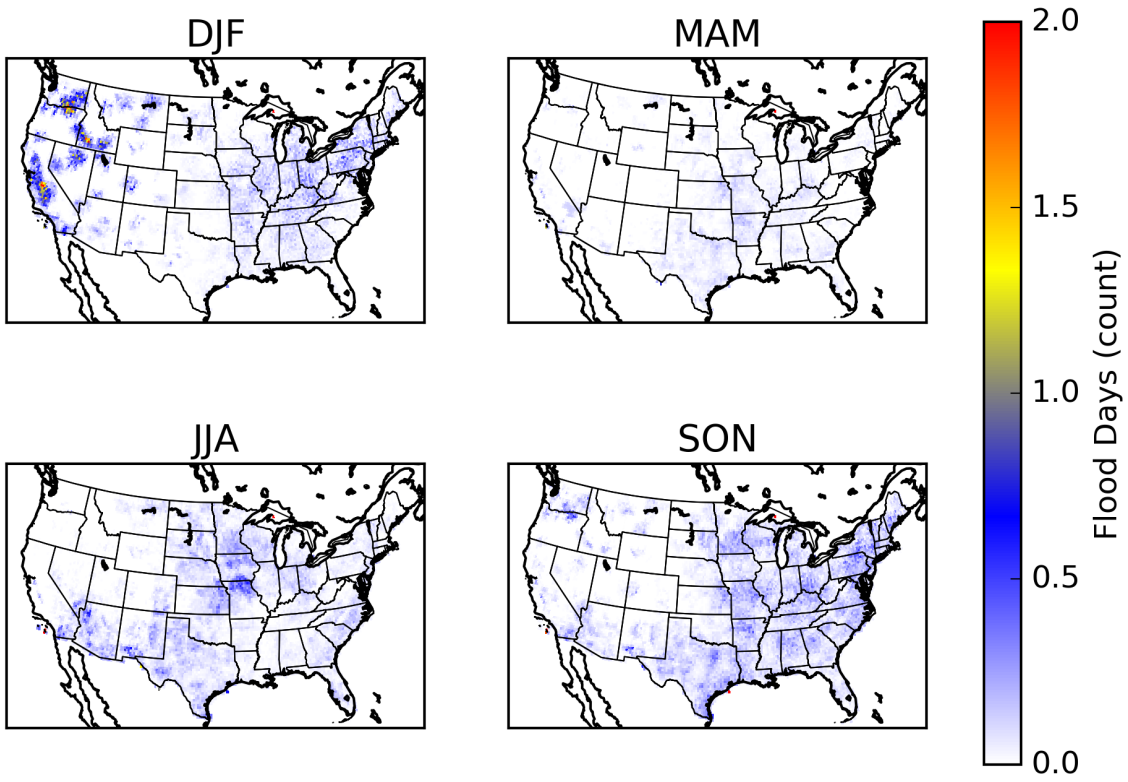

Figure 4.14: The mean annual number of flash flood days simulated by EF5/SAC-SMA from 2002-2011 plotted by season.

Figures 4.15 and 4.16 show the mean hour of the peak discharge for flash flooding days simulated by EF5/CREST and EF5/SAC-SMA respectively. Hour of the day is a circular quantity so care was taken to properly compute the mean. The average of a circular quantity can be computed by:

$$\overline{hour} = atan2(\sum_{i=1}^{N} sin(\alpha_i), \sum_{i=1}^{N} cos(\alpha_i)) \tag{4.2}$$

Where N is the number of flash flood days, and α is the hour of the peak discharge converted to a point on a unit circle. The hour of the peak flash flood discharge starts at about 00 Local Solar Time (LST) on the east side of the front range in Colorado and gradually increases going eastward from there until it reaches about 12 LST over Arkansas. Both of the hydrologic model simulations show this same result which matches well with the known overnight propagation of mesoscale convective systems

off the Rocky Mountains. Other areas of notable signal include in Arizona where the flash floods peak around 00 LST which corresponds to late evening flash floods driven by the monsoon rains. Figures 4.17 and 4.18 show the mean hour of the peak discharge for flash flooding days simulated by EF5/CREST and EF5/SAC-SMA respectively as a function of the season. Changes in the timing of the peak are visible in Arkansas where spring flash floods have peaks around 00 LST while autumn flash floods have peaks around 12 LST.

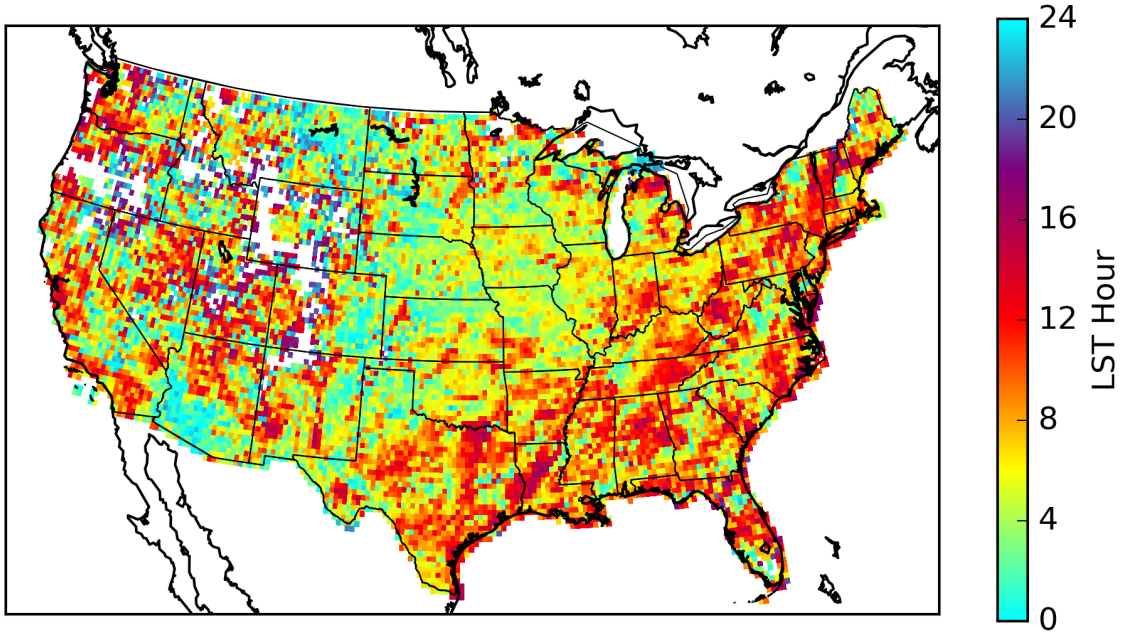

Figure 4.15: The mean hour of peak discharge during flash flooding as simulated by EF5/CREST from 2002-2011.

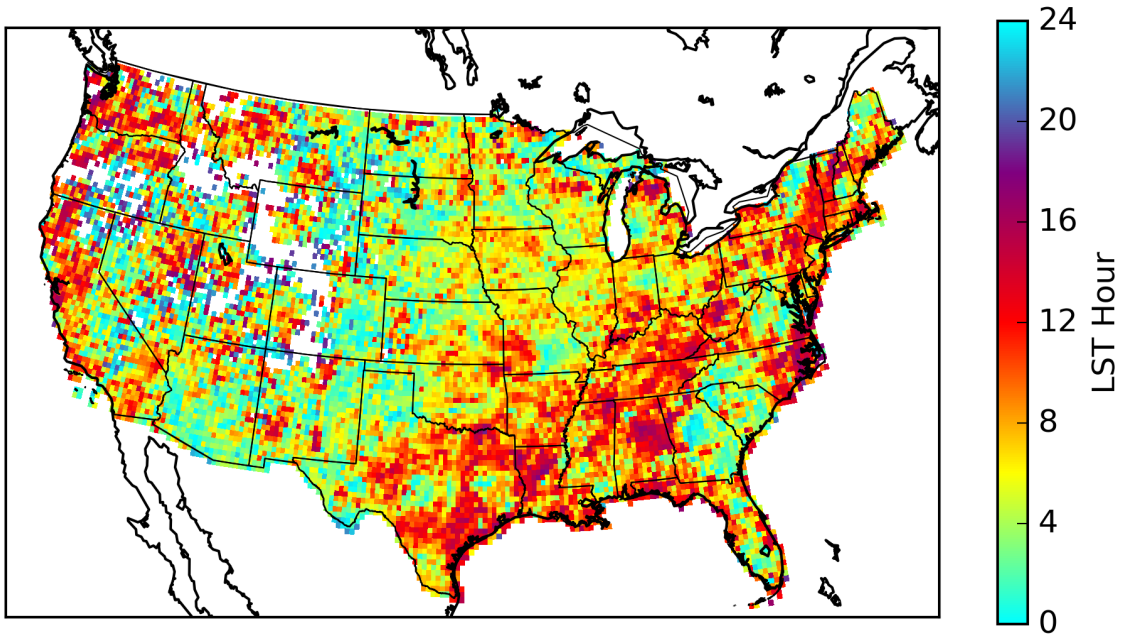

Figure 4.16: The mean hour of peak discharge during flash flooding as simulated by EF5/SAC-SMA from 2002-2011.

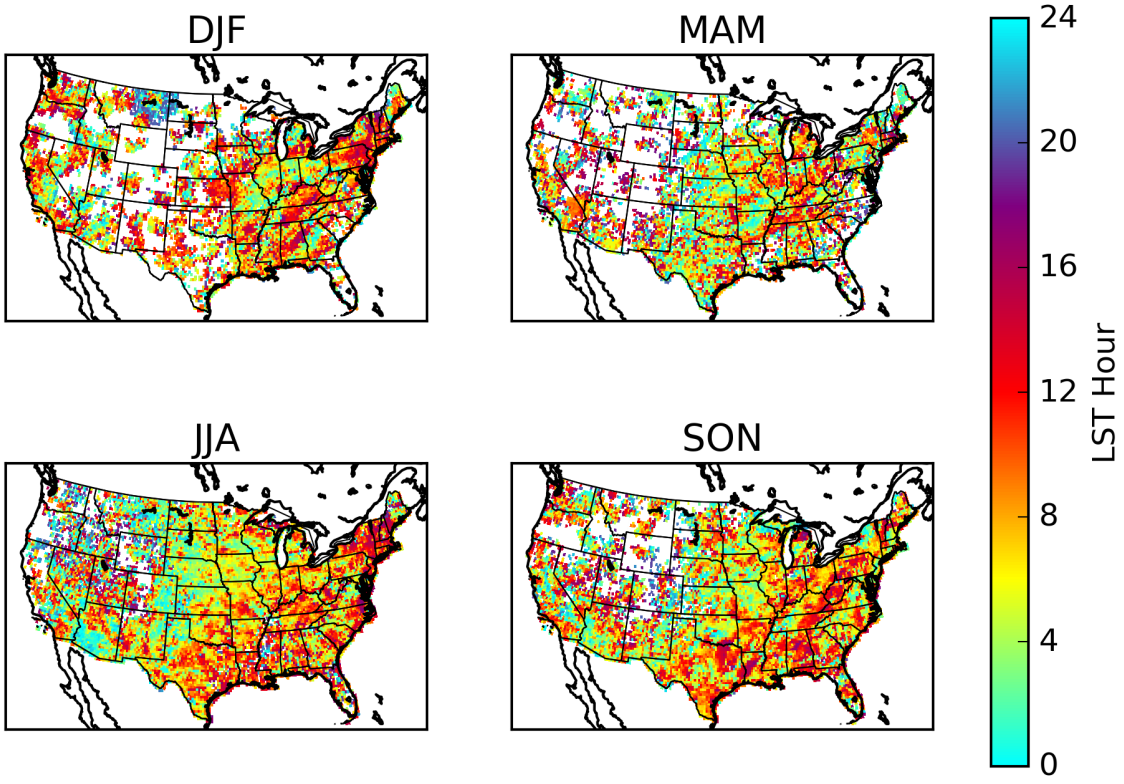

Figure 4.17: The mean hour of peak discharge during flash flooding as simulated by EF5/CREST from 2002-2011 plotted by season.

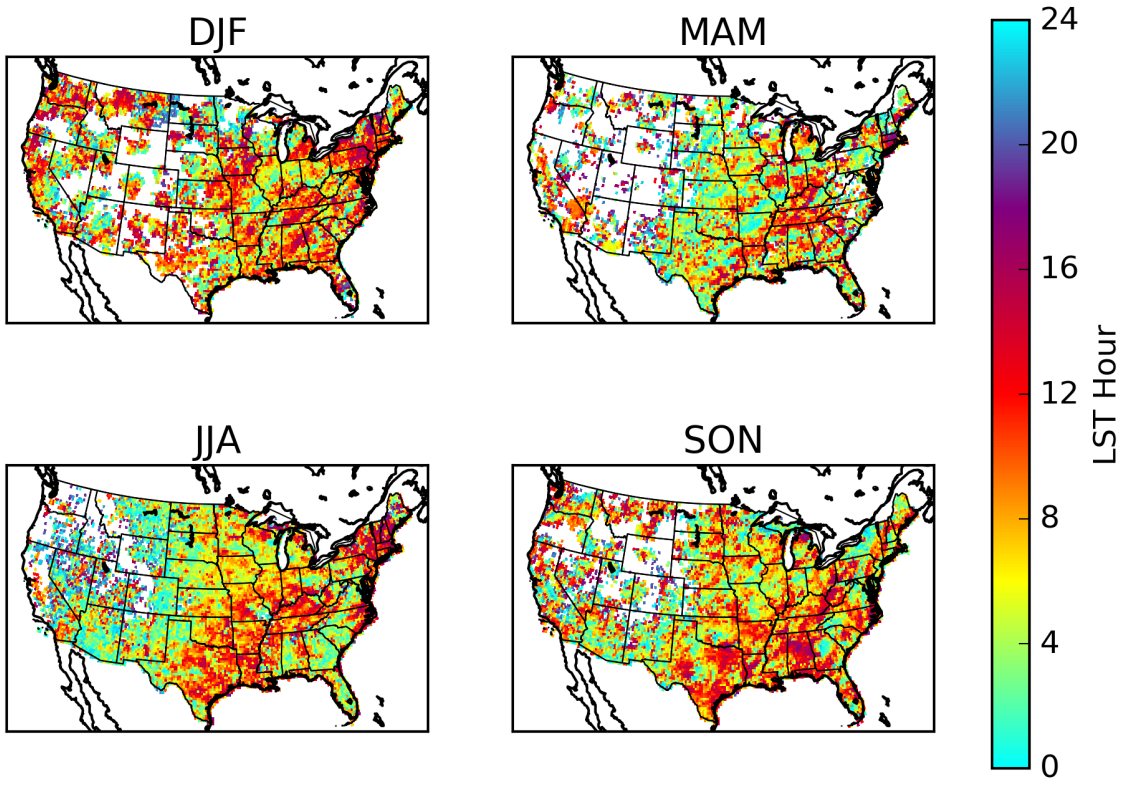

Figure 4.18: The mean hour of peak discharge during flash flooding as simulated by EF5/SAC-SMA from 2002-2011 plotted by season.

Figures 4.19 and 4.20 show the mean antecedent soil saturation for flash flood days simulated by EF5/CREST and EF5/SAC-SMA respectively. Both models simulate comparable looking spatial patterns but with an offset in relative magnitudes. The highest values across the CONUS for EF5/SAC-SMA are in the range of 70 % while EF5/CREST hits 100 % in some regions. This difference may be due to how soil saturation is defined and parameterized in the two different water balance models. Putting aside the magnitude differences, the spatial patterns are large the same. The eastern US has a more saturation mean antecedent soil saturation than the central US. California is comparable to the eastern US and has an elevated mean antecedent soil saturation for flash flood days. Surprisingly, EF5/SAC-SMA has a drier Florida than EF5/CREST even though the EF5/SAC-SMA simulations produce more flash flood days there. Figures 4.21 and 4.22 show the mean antecedent soil saturation

anomaly for flash flood days. Both models show a tendency for flash flood days to have 0–10% higher soil saturation than days without flash floods. Both models also highlight the Pacific coast of the CONUS as an area where flash flood days are preceded by significantly wetter soils.

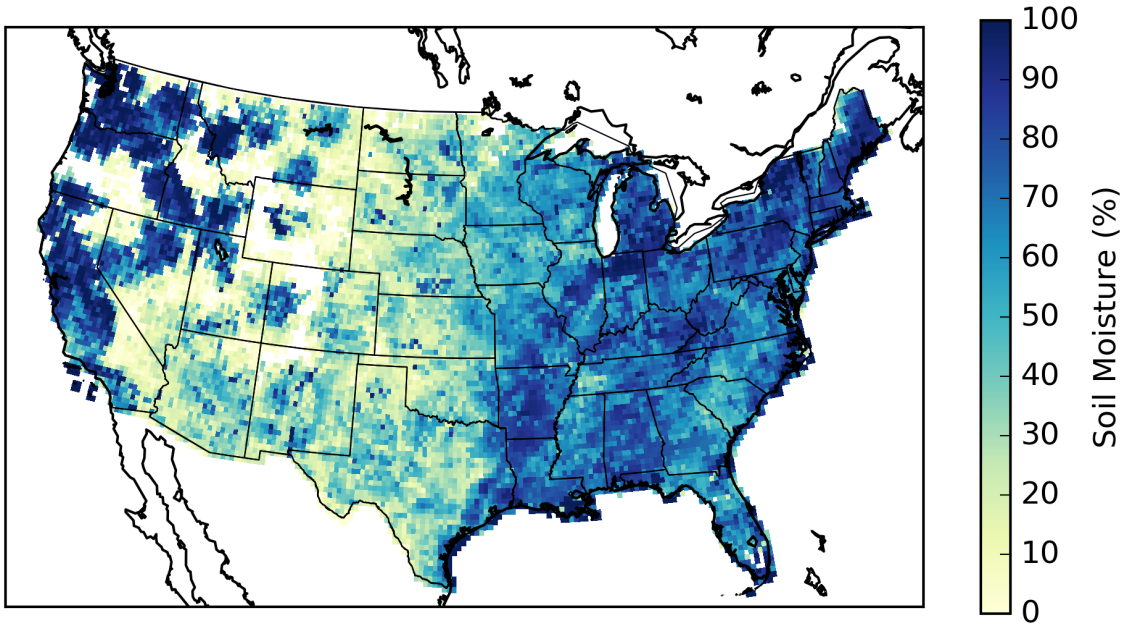

Figure 4.19: The mean antecedent soil saturation before flash flooding as simulated by EF5/CREST from 2002-2011.

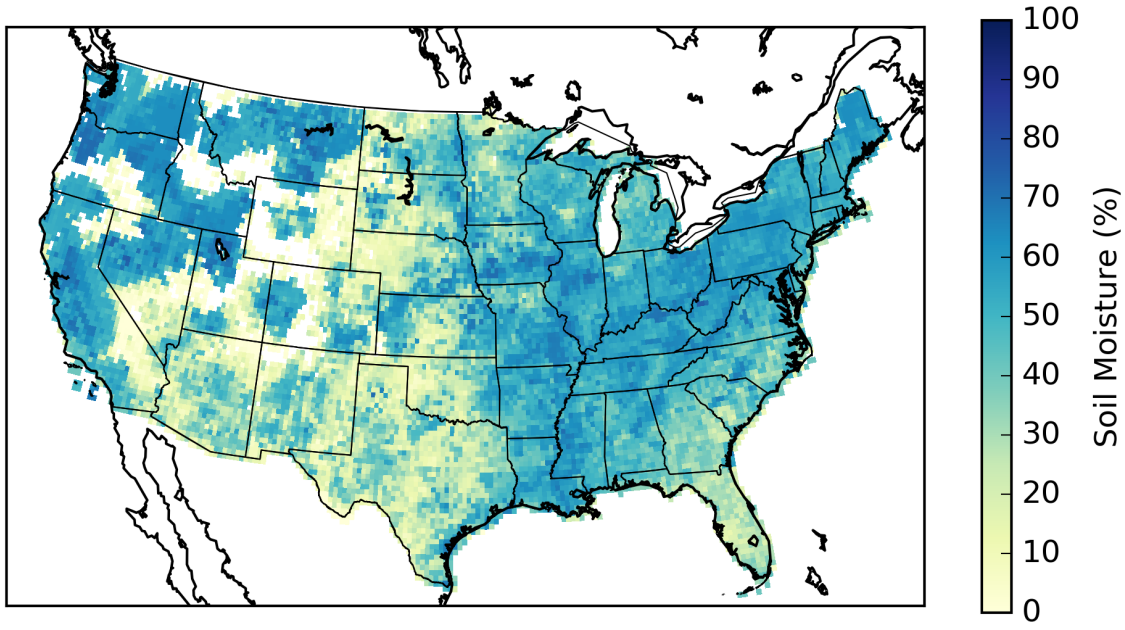

Figure 4.20: The mean antecedent soil saturation before flash flooding as simulated by EF5/SAC-SMA from 2002-2011.

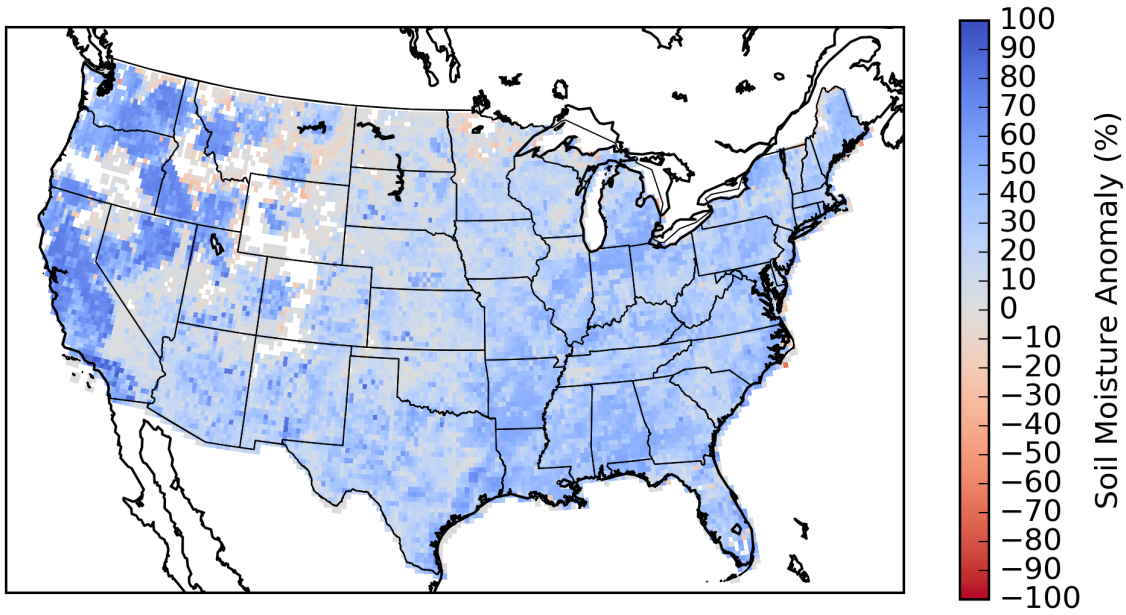

Figure 4.21: The mean difference from normal antecedent soil saturation before flash flooding as simulated by EF5/CREST from 2002-2011.

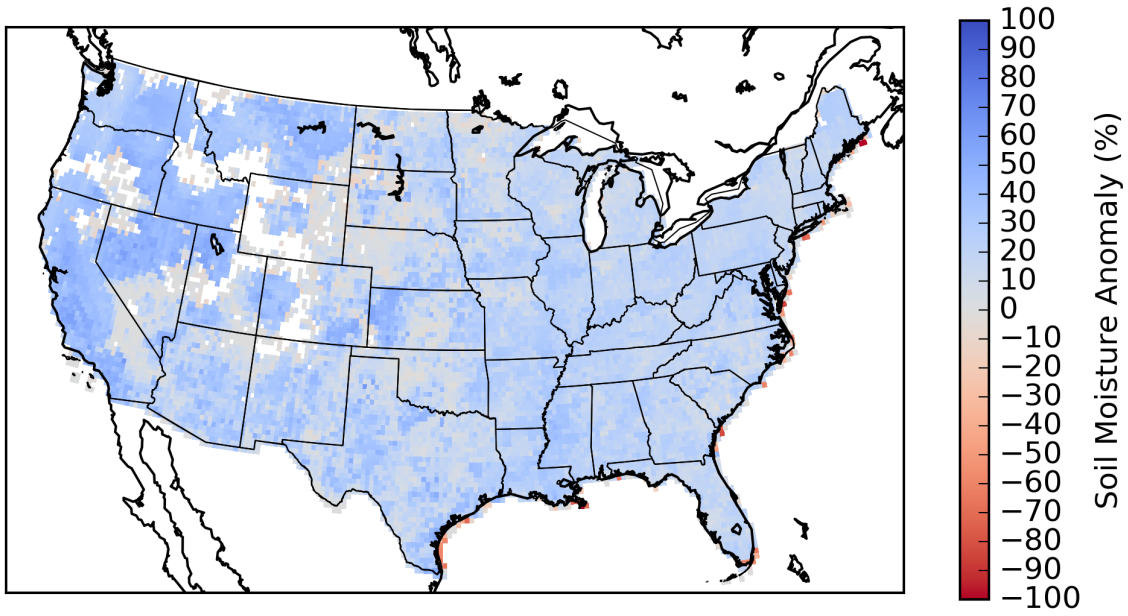

Figure 4.22: The mean difference from normal antecedent soil saturation before flash flooding as simulated by EF5/SAC-SMA from 2002-2011.

Chapter 5

Conclusions and Future Work

Flash floods are a major problem to life and property, as witnessed by 2015 which had over twice as many flood fatalities as the 30-year average in the US. Globally, flash floods are the number one killer when it comes to weather hazards. Flash floods are defined as floods that begin up to 6 hours after the preceding rainfall and occur in basins with areas less than 1,000 km^2. A new reanalysis precipitation rate dataset suitable for flash flood modeling was created using the existing MRMS system. This dataset runs from 2001 through 2011 with data every 5 minutes. A few key takeaways from this study are that MRMS precipitation rates are now available for 2001 through 2011. MRMS precipitation accumulations from 2002–2011 feature the same spatial pattern as those in other climatologies such as PRISM. The gradient of precipitation across the eastern CONUS is likely due to a decreasing number of precipitation events.

To further utilize the new precipitation dataset with high resolution distributed hydrologic models a new modeling platform, EF5, was created to facilitate this process. EF5 features flexible options for choosing which conceptual water balance models to utilize and allows coupling to two different routing schemes. The resulting software package was used for generating 5 minute simulations for 4,366 gauge locations across the CONUS with uncalibrated a priori parameters for the EF5/CREST, EF5/SAC-SMA, and EF5/HP water balance models coupled to kinematic wave routing. Furthermore, EF5 is being used for training, capacity building and operational forecasting. Key conclusions and summary items from the EF5 work are The Ensemble Framework For Flash Flood Forecasting (EF5) was created to provide a better multi-model distributed hydrologic modeling platform. EF5 is scalable from flash

flood scale up to global river scale. EF5/CREST and EF5/SAC-SMA run with uncalibrated a priori parameters over the CONUS and MRMS precipitation forcing produce skillful simulations except for in mountainous regions with NSE scores up to 0.76. EF5/HP produces useful estimates for worst case scenarios if all rainfall is converted into runoff. Differences between EF5/HP and those of the EF5/CREST & EF5/SAC-SMA model runs illustrate the inherent uncertainties with hydrologic model parameter estimation and the non-linear conversion from rainfall into runoff.

After reasonable skill was established over the CONUS on flash flood scale basins the distributed hydrologic models were used to generate simulations for all grid cells in the CONUS including ungauged basins. These simulations saved for every day the maximum discharge, unit discharge, time of maximum discharge, and minimum soil saturation. Thresholds for minor flooding, defined as flooding that may cause loss of human life, were then developed over the CONUS using statistical extrapolations of mean average annual precipitation and basin area. From these thresholds, maps of the average number of flash flood days per year were produced. This information was then used to derive the mean time of peak flooding and the mean antecedent soil saturation for floods. Specific highlights and findings are that EF5/CREST and EF5/SAC-SMA hydrologic simulations were produced for 2002 through 2011. Thresholds to define a flood based on discharge were developed from the NWS minor flood stage. Maps of the mean annual number of flash flood days were produced for the CONUS. The spatial patterns here largely match those in *Storm Data*, validating both datasets. The mean time of peak flooding and mean antecedent soil saturation were generated for these flash flood days. The seasonality of flash flooding across the CONUS was examined and described. Flash floods propagate eastward from the Rocky Mountains in the overnight hours.

The hypotheses proposed in Chapter 1 are confirmed, the infiltration and saturation excess processes described by the EF5/CREST and EF5/SAC-SMA models

coupled with kinematic wave routing skillfully predict flash flood events across the CONUS. Furthermore, a relationship was found between minor flood thresholds, contributing basin area, and mean annual precipitation allowing for a statistical model to be developed enabling the extrapolation of thresholds across the CONUS. This relationship takes the form of a power law, and confirms the second hypothesis. The results of this are a climatology of flash flood days across the CONUS.

The future for EF5, hydrologic modeling and developing climatologies of flash floods is extremely promising. EF5 is being used to power the distributed hydrologic models in the FLASH system (Hong and Gourley 2014) where NWS forecasters are using it in a warning decision support role. Future developments for EF5 may include diffusive wave routing to better handle shallow slope basins, and a parameterization for reservoirs so that they can also be accommodated. EF5 currently has a snow module, but a priori parameter development is required before it can be deployed across the CONUS and globally. Continued improvements to EF5 are a must to ensure it remains accessible to all users in the future. A better graphical user interface on the Windows operating system may improve classroom and workshop usability. Solutions for containerizing EF5 such as Docker should be explored to see if there are significant advantages to this workflow. The capacity building work started with NASA and USAID using EF5 is expected to continue well into the future and should be supported.

The MRMS precipitation reanalysis will continue to improve as it gains users. Additional improvements from rain gauge correction may be able to be downscaled to the precipitation rates improving those estimates. New methods for quality controlling the single-polarization weather radar data may be found as the dual-polarization radar data are fully exploited. This may include training machine learning algorithms to data classified using the dual-polarization algorithms but with only the single-polarization variables available. The information from the 11 year archive of

data may be of use to generate static probabilities that any given grid cell is a non-meteorological echo thus lowering the quality control thresholds in those grid cells. Going forward, cheap well calibrated radars would be a great benefit for hydrology. The overall scan rate is not as important for hydrology as is the quality of the resulting measurements. As such, radars which can be easily networked, are affordable, and produce high quality data are desired to fill in the missing coverage locations in the mountain west.

Climatologies built with distributed hydrologic models will continue to improve as the precipitation input improves. Further, as uncalibrated hydrologic modeling matures the estimates and quantifications used for a priori parameters will naturally improve as well resulting in better simulations. The data contained within the climatology built here can be further exploited to understand the roles of the parameters in the resulting skill of the EF5/CREST and EF5/SAC-SMA models. One way to do this would be to look for relationships between basin averaged parameters and the skill of the hydrologic model. Improving the thresholds used to define when a flash flood is occurring will greatly improve simulated climatologies of flash floods. Short of a break through in data measurements and computational efficiency these thresholds will be needed well into the future.

In the future, new observational platforms will be necessary to collect the observations needed to validate distributed hydrologic models. As the result the models are run at decreases the need for observations to help validate the model increases. These new observations could come from augmentations of existing datasets such as with stream radars that can map the channel cross-section, water velocity and water height. Unmanned ariel systems have a promising role in the future as well, an automated platform that maps out flood waters in real time would be invaluable as a dataset for verifying hydrologic models.

The MRMS group has plans to release the MRMS reanalysis dataset used here to the public as soon as October, 2016. The hydrologic model variables generated during the course of this research study will also be released publicly so that they can be used for future research projects. The value of these datasets is just beginning to be realized, and the expectation is that they will be seen as treasured assets in the future.

Reference List

Adhikari, P., Y. Hong, K. R. Douglas, D. B. Kirschbaum, J. Gourley, R. Adler, and G. R. Brakenridge, 2010: A digitized global flood inventory (1998-2008): compilation and preliminary results. *Natural Hazards*, **55** (2), 405–422. doi:10.1007/s11069-010-9537-2.

AMS, 2000: Prediction and Mitigation of Flash Floods. *Bulletin of the American Meteorological Society*, **81** (6), 1338–1340. doi:10.1175/1520-0477(2000)081⟨1338:pspamo⟩2.3.co;2.

Argyle, E., J. J. Gourley, Z. L. Flamig, T. Hansen, and K. Manross, 2016: Towards a User-Centered Design of a Weather Forecasting Decision Support Tool. *Bulletin of the American Meteorological Society*. doi:10.1175/BAMS-D-16-0031.

Ashley, S. T. and W. S. Ashley, 2008: Flood Fatalities in the United States. *Journal of Applied Meteorology and Climatology*, **47** (3), 805–818. doi:10.1175/2007jamc1611.1.

Barthold, F. E., T. E. Workoff, B. A. Cosgrove, J. J. Gourley, D. R. Novak, and K. M. Mahoney, 2015: Improving Flash Flood Forecasts: The HMT-WPC Flash Flood and Intense Rainfall Experiment. *Bulletin of the American Meteorological Society*, **96** (11), 1859–1866. doi:10.1175/bams-d-14-00201.1.

Beven, K., H. Cloke, F. Pappenberger, R. Lamb, and N. Hunter, 2014: Hyperresolution information and hyperresolution ignorance in modelling the hydrology of the land surface. *Sci. China Earth Sci.*, **58** (1), 25–35. doi:10.1007/s11430-014-5003-4.

Bluestein, H. B., J. C. Snyder, and J. B. Houser, 2015: A Multiscale Overview of the El Reno, Oklahoma, Tornadic Supercell of 31 May 2013. *Weather and Forecasting*, **30** (3), 525–552. doi:10.1175/waf-d-14-00152.1.

Boursicaud, R. L., L. Pnard, A. Hauet, F. Thollet, and J. L. Coz, 2015: Gauging extreme floods on YouTube: application of LSPIV to home movies for the post-event determination of stream discharges. *Hydrological Processes*, **30** (1), 90–105. doi:10.1002/hyp.10532.

Braud, I., H. Roux, S. Anquetin, M.-M. Maubourguet, C. Manus, P. Viallet, and D. Dartus, 2010: The use of distributed hydrological models for the Gard 2002 flash flood event: Analysis of associated hydrological processes. *Journal of Hydrology*, **394** (1-2), 162–181. doi:10.1016/j.jhydrol.2010.03.033.

Bryndal, T., 2015: Local flash floods in Central Europe: A case study of Poland. *Norsk Geografisk Tidsskrift - Norwegian Journal of Geography*, **69** (5), 288–298. doi:10.1080/00291951.2015.1072242.

Burnash, R. J. C., 1995 *The NWS River Forecast System – Catchment Modeling*, revised ed., Water Resources Publications.

Channan, S., K. Collins, and W. Emanuel, 2014: Global mosaics of the standard MODIS land cover type data. *University of Maryland and the Pacific Northwest National Laboratory, College Park, Maryland, USA*, **30.**

Chen, S., and Coauthors, 2015: Intercomparison of Precipitation Estimates From WSR-88D Radar and TRMM Measurement Over Continental United States. *IEEE Transactions on Geoscience and Remote Sensing*, **53** (8), 4444–4456. doi:10.1109/tgrs.2015.2399307.

——, J. J. Gourley, Y. Hong, Q. Cao, N. Carr, P.-E. Kirstetter, J. Zhang, and Z. Flamig, 2016: Using Citizen Science Reports to Evaluate Estimates of Surface Precipitation Type. *Bulletin of the American Meteorological Society*, **97** (2), 187–193. doi:10.1175/bams-d-13-00247.1.

Chow, V. T., D. R. Maidment, and L. W. Mays, 1988: Applied hydrology.

Chrisman, J. N., 2009: Automated volume scan evaluation and termination (AVSET). 34th Conference on Radar Meteorology.

Clark, R., 2016 personal communication.

Coates, L., 1999: Flood Fatalities in Australia, 1788-1996. *Australian Geographer*, **30** (3), 391–408. doi:10.1080/00049189993657.

Cosby, B. J., G. M. Hornberger, R. B. Clapp, and T. R. Ginn, 1984: A Statistical Exploration of the Relationships of Soil Moisture Characteristics to the Physical Properties of Soils. *Water Resour. Res.*, **20** (6), 682–690. doi:10.1029/wr020i006p00682.

Costa, J. E., 1987a: A comparison of the largest rainfall-runoff floods in the United States with those of the Peoples Republic of China and the world. *Journal of Hydrology*, **96** (1-4), 101–115. doi:10.1016/0022-1694(87)90146-6.

——, 1987b: Hydraulics and basin morphometry of the largest flash floods in the conterminous United States. *Journal of Hydrology*, **93** (3-4), 313–338. doi:10.1016/0022-1694(87)90102-8.

Cnovas, J. A. B., M. Eguibar, J. M. Bodoque, A. Dez-Herrero, M. Stoffel, and I. Gutirrez-Prez, 2010: Estimating flash flood discharge in an ungauged mountain catchment with 2D hydraulic models and dendrogeomorphic palaeostage indicators. *Hydrological Processes*, **25** (6), 970–979. doi:10.1002/hyp.7888.

Daly, C., R. P. Neilson, and D. L. Phillips, 1994: A Statistical-Topographic Model for Mapping Climatological Precipitation over Mountainous Terrain. *J. Appl. Meteor.*, **33** (2), 140–158. doi:10.1175/1520-0450(1994)033⟨0140:astmfm⟩2.0.co;2.

Daniel, A. E., J. N. Chrisman, and S. D. Smith, 2014: NEW WSR-88D OPERATIONAL TECHNIQUES: RESPONDING TO RECENT WEATHER EVENTS.

Devia, G. K., B. Ganasri, and G. Dwarakish, 2015: A Review on Hydrological Models. *Aquatic Procedia*, **4**, 1001–1007. doi:10.1016/j.aqpro.2015.02.126.

Elmore, K. L., Z. L. Flamig, V. Lakshmanan, B. T. Kaney, V. Farmer, H. D. Reeves, and L. P. Rothfusz, 2014: MPING: Crowd-Sourcing Weather Reports for Research. *Bulletin of the American Meteorological Society*, **95** (9), 1335–1342. doi:10.1175/bams-d-13-00014.1.

Feldman, A. D., 2000: *Hydrologic modeling system HEC-HMS: technical reference manual*. US Army Corps of Engineers, Hydrologic Engineering Center.

Flamig, Z. L., H. Vergara, R. C. III, Y. Hong, and J. J. Gourley, 2016: EF5: Version 1.0. [Available online at http://dx.doi.org/10.5281/zenodo.59123.]

Fulton, R. A., J. P. Breidenbach, D.-J. Seo, D. A. Miller, and T. OBannon, 1998: The WSR-88D Rainfall Algorithm. *Weather and Forecasting*, **13** (2), 377–395. doi:10.1175/1520-0434(1998)013⟨0377:twra⟩2.0.co;2.

Gaume, E., and Coauthors, 2009: A compilation of data on European flash floods. *Journal of Hydrology*, **367** (1-2), 70–78. doi:10.1016/j.jhydrol.2008.12.028.

Gesch, D., G. Evans, J. Mauck, J. Hutchinson, and W. C. Jr, 2009: The National Map-Elevation: US Geological Survey Fact Sheet 2009-3053, 4 p. *Last accessible online at http://ned. usgs. gov.*

Gourley, J. J., and Coauthors, 2016: The Flooded Locations And Simulated Hydrographs (FLASH) project: improving the tools for flash flood monitoring and prediction across the United States. *Bulletin of the American Meteorological Society*. doi:10.1175/BAMS-D-15-00247.

——, and Coauthors, 2013: A Unified Flash Flood Database across the United States. *Bulletin of the American Meteorological Society*, **94** (6), 799–805. doi:10.1175/bams-d-12-00198.1.

Gourley, J., J. Erlingis, T. Smith, K. Ortega, and Y. Hong, 2010a: Remote collection and analysis of witness reports on flash floods. *Journal of Hydrology*, **394** (1-2), 53–62. doi:10.1016/j.jhydrol.2010.05.042.

Gourley, J. J., S. E. Giangrande, Y. Hong, Z. L. Flamig, T. Schuur, and J. A. Vrugt, 2010b: Impacts of Polarimetric Radar Observations on Hydrologic Simulation. *Journal of Hydrometeorology*, **11** (3), 781–796. doi:10.1175/2010jhm1218.1.

Grams, H. M., J. Zhang, and K. L. Elmore, 2014: Automated Identification of Enhanced Rainfall Rates Using the Near-Storm Environment for Radar Precipitation Estimates. *Journal of Hydrometeorology*, **15** (3), 1238–1254. doi:10.1175/jhm-d-13-042.1.

Herschy, R. W., 2002: The worlds maximum observed floods. *Flow Measurement and Instrumentation*, **13** (5-6), 231–235. doi:10.1016/s0955-5986(02)00054-7.

Hirabayashi, Y., R. Mahendran, S. Koirala, L. Konoshima, D. Yamazaki, S. Watanabe, H. Kim, and S. Kanae, 2013: Global flood risk under climate change. *Nature Climate change*, **3** (9), 816–821. doi:10.1038/nclimate1911.

Hirsch, R. M. and S. A. Archfield, 2015: Flood trends: Not higher but more often. *Nature Climate change*, **5** (3), 198–199. doi:10.1038/nclimate2551.

Hong, Y. and J. Gourley, 2014: *Radar Hydrology: Principles, Models, and Applications.* Taylor & Francis.

Houser, P. R., G. J. D. Lannoy, and J. P. Walker, 2012: Hydrologic Data Assimilation. *Approaches to Managing Disaster-Assessing Hazards, Emergencies and Disaster Impacts.*

Huber, W., 1995: EPA Storm Water Management Model-SWMM, Computer Models of Watershed Hydrology, Singh, VP eds. *Water Resources Publication*, 783–708.

Kelleher, K. E., and Coauthors, 2007: Project CRAFT: A Real-Time Delivery System for NEXRAD Level II Data Via the Internet. *Bulletin of the American Meteorological Society*, **88** (7), 1045–1057. doi:10.1175/bams-88-7-1045.

Kharin, V. V., F. W. Zwiers, X. Zhang, and G. C. Hegerl, 2007: Changes in Temperature and Precipitation Extremes in the IPCC Ensemble of Global Coupled Model Simulations. *J. Climate*, **20** (8), 1419–1444. doi:10.1175/jcli4066.1.

Kitzmiller, D., and Coauthors, 2011: Evolving Multisensor Precipitation Estimation Methods: Their Impacts on Flow Prediction Using a Distributed Hydrologic Model. *Journal of Hydrometeorology*, **12** (6), 1414–1431. doi:10.1175/jhm-d-10-05038.1.

Koren, V., J. Schaake, Q. Duan, M. Smith, and S. Cong, 1998: PET Upgrades to NWSRFS, Project Plan. *Washington, DC, unpublished report.*

——, S. Reed, M. Smith, Z. Zhang, and D.-J. Seo, 2004: Hydrology laboratory research modeling system (HL-RMS) of the US national weather service. *Journal of Hydrology*, **291** (3-4), 297–318. doi:10.1016/j.jhydrol.2003.12.039.

Koutroulis, A. G. and I. K. Tsanis, 2010: A method for estimating flash flood peak discharge in a poorly gauged basin: Case study for the 13-14 January 1994 flood, Giofiros basin, Crete, Greece. *Journal of Hydrology*, **385** (1-4), 150–164. doi:10.1016/j.jhydrol.2010.02.012.

Kuczera, G., B. Renard, M. Thyer, and D. Kavetski, 2010: There are no hydrological monsters, just models and observations with large uncertainties! *Hydrological Sciences Journal*, **55** (6), 980–991. doi:10.1080/02626667.2010.504677.

Kunkel, K. E., R. A. Pielke, and S. A. Changnon, 1999: Temporal Fluctuations in Weather and Climate Extremes That Cause Economic and Human Health Impacts: A Review. *Bulletin of the American Meteorological Society*, **80** (6), 1077–1098. doi:10.1175/1520-0477(1999)080⟨1077:tfiwac⟩2.0.co;2.

Lakshmanan, V., A. Fritz, T. Smith, K. Hondl, and G. Stumpf, 2007: An Automated Technique to Quality Control Radar Reflectivity Data. *Journal of Applied Meteorology and Climatology*, **46** (3), 288–305. doi:10.1175/jam2460.1.

——, J. Zhang, and K. Howard, 2010: A Technique to Censor Biological Echoes in Radar Reflectivity Data. *Journal of Applied Meteorology and Climatology*, **49** (3), 453–462. doi:10.1175/2009jamc2255.1.

Liang, X., D. P. Lettenmaier, and E. F. Wood, 1996: One-dimensional statistical dynamic representation of subgrid spatial variability of precipitation in the two-layer variable infiltration capacity model. *J. Geophys. Res.*, **101** (D16), 21403–21422. doi:10.1029/96jd01448.

Lin, Y. and K. E. Mitchell, 2005: THE NCEP STAGE II/IV HOURLY PRECIPITATION ANALYSES: DEVELOPMENT AND APPLICATIONS. *19th Conf. on Hydrology.*

Liu, J., X. Chen, J. Zhang, and M. Flury, 2009: Coupling the Xinanjiang model to a kinematic flow model based on digital drainage networks for flood forecasting. *Hydrological Processes*, **23** (9), 1337–1348. doi:10.1002/hyp.7255.

Llasat, M. C., and Coauthors, 2010: High-impact floods and flash floods in Mediterranean countries: the FLASH preliminary database. *Advances in Geosciences*, **23**, 47–55. doi:10.5194/adgeo-23-47-2010.

Mallakpour, I. and G. Villarini, 2015: The changing nature of flooding across the centralUnited States. *Nature Climate change*, **5** (3), 250–254. doi:10.1038/nclimate2516.

Marchi, L., M. Borga, E. Preciso, and E. Gaume, 2010: Characterisation of selected extreme flash floods in Europe and implications for flood risk management. *Journal of Hydrology*, **394** (1-2), 118–133. doi:10.1016/j.jhydrol.2010.07.017.

Marshall, J. S., W. Hitschfeld, and K. L. S. Gunn, 1955: Advances in Radar Weather. *Advances in Geophysics*, **2**, 1 pp.

Martinaitis, S. M., and Coauthors, 2016: The HMT Multi-Radar Multi-Sensor Hydro Experiment. *Bulletin of the American Meteorological Society.* doi:10.1175/bams-d-15-00283.1.

Mediero, L., and Coauthors, 2015: Identification of coherent flood regions across Europe by using the longest streamflow records. *Journal of Hydrology*, **528**, 341–360. doi:10.1016/j.jhydrol.2015.06.016.

Micovic, Z. and M. C. Quick, 2009: Investigation of the model complexity required in runoff simulation at different time scales / Etude de la complexit de modlisation requise pour la simulation dcoulement diffrentes chelles temporelles. *Hydrological Sciences Journal*, **54** (5), 872–885. doi:10.1623/hysj.54.5.872.

Miller, D. A. and R. A. White, 1998: A Conterminous United States Multilayer Soil Characteristics Dataset for Regional Climate and Hydrology Modeling. *Earth Interact.*, **2** (2), 1–26. doi:10.1175/1087-3562(1998)002⟨0001:acusms⟩2.3.co;2.

Moore, R. J., 1985: The probability-distributed principle and runoff production at point and basin scales. *Hydrological Sciences Journal*, **30** (2), 273–297. doi:10.1080/02626668509490989.

Nash, J., 1957: The form of the instantaneous unit hydrograph. *International Association of Scientific Hydrology, Publ*, **3**, 114–121.

Nash, J. E. and J. V. Sutcliffe, 1970: River flow forecasting through conceptual models part IA discussion of principles. *Journal of hydrology*, **10** (3), 282–290.

NSSL, 2016: FLASH: Flooded Locations And Simulated Hydrographs Project. [Available online at http://blog.nssl.noaa.gov/flash/.]

NWS, 2016a: National Weather Service glossary. [Available online at http://w1.weather.gov/glossary/index.php.]

——, 2007: National Weather Service Instruction 10-1605 Storm Data Preparation. [Available online at https://www.ncdc.noaa.gov/stormevents/pd01016005curr.pdf.]

——, 2012: National Weather Service Manual 10-950 Operations and Services Hydrologic Services Program, NWSPD 10-9. [Available online at http://www.nws.noaa.gov/directives/sym/pd01009050curr.pdf.]

——, 2016b: Natural Hazard Statistics. [Available online at http://www.nws.noaa.gov/om/hazstats.shtml.]

——, 2014: Service assessment: May 2013 Oklahoma tornadoes and flash flooding. [Available online at http://www.nws.noaa.gov/om/assessments/pdfs/13oklahoma_tornadoes.pdf.]

Ortega, K. L., T. M. Smith, K. L. Manross, A. G. Kolodziej, K. A. Scharfenberg, A. Witt, and J. J. Gourley, 2009: The Severe Hazards Analysis and Verification Experiment. *Bulletin of the American Meteorological Society*, **90** (10), 1519–1530. doi:10.1175/2009bams2815.1.

Ponce, V. M., 1986: Diffusion Wave Modeling of Catchment Dynamics. *J. Hydraul. Eng.*, **112** (8), 716–727. doi:10.1061/(asce)0733-9429(1986)112:8(716).

Ponce, V. M., 1991: Kinematic Wave Controversy. *J. Hydraul. Eng.*, **117** (4), 511–525. doi:10.1061/(asce)0733-9429(1991)117:4(511).

Qi, Y., J. Zhang, and P. Zhang, 2013: A real-time automated convective and stratiform precipitation segregation algorithm in native radar coordinates. *Q.J.R. Meteorol. Soc.*, **139** (677), 2233–2240. doi:10.1002/qj.2095.

Rafieeinasab, A., and Coauthors, 2015: Toward high-resolution flash flood prediction in large urban areas - Analysis of sensitivity to spatiotemporal resolution of rainfall input and hydrologic modeling. *Journal of Hydrology*, **531**, 370–388. doi:10.1016/j.jhydrol.2015.08.045.

Ren-Jun, Z., 1992: The Xinanjiang model applied in China. *Journal of Hydrology*, **135** (1-4), 371–381. doi:10.1016/0022-1694(92)90096-e.

Rodriguez-Morata, C., J. Ballesteros-Cnovas, D. Trappmann, M. Beniston, and M. Stoffel, 2016: Regional reconstruction of flash flood history in the Guadarrama range (Central System, Spain). *Science of The Total Environment*, **550**, 406–417. doi:10.1016/j.scitotenv.2016.01.074.

Rosenfeld, D., D. B. Wolff, and D. Atlas, 1993: General Probability-matched Relations between Radar Reflectivity and Rain Rate. *J. Appl. Meteor.*, **32** (1), 50–72. doi:10.1175/1520-0450(1993)032⟨0050:gpmrbr⟩2.0.co;2.

Ruin, I., J.-D. Creutin, S. Anquetin, and C. Lutoff, 2008: Human exposure to flash floods - Relation between flood parameters and human vulnerability during a storm of September 2002 in Southern France. *Journal of Hydrology*, **361** (1-2), 199–213. doi:10.1016/j.jhydrol.2008.07.044.

Ruiz-Villanueva, V., A. Dez-Herrero, J. Bodoque, J. B. Cnovas, and M. Stoffel, 2013: Characterisation of flash floods in small ungauged mountain basins of Central Spain using an integrated approach. *CATENA*, **110**, 32–43. doi:10.1016/j.catena.2013.06.015.

Smith, M., J. Carrivick, J. Hooke, and M. Kirkby, 2014: Reconstructing flash flood magnitudes using Structure-from-Motion: A rapid assessment tool. *Journal of Hydrology*, **519**, 1914–1927. doi:10.1016/j.jhydrol.2014.09.078.

Tang, L., J. Zhang, C. Langston, J. Krause, K. Howard, and V. Lakshmanan, 2014: A Physically Based Precipitation-Nonprecipitation Radar Echo Classifier Using Polarimetric and Environmental Data in a Real-Time National System. *Weather and Forecasting*, **29** (5), 1106–1119. doi:10.1175/waf-d-13-00072.1.

UCAR, 2009: Distributed Hydrologic Models for Flow Forecasts Part 1. [Available online at http://www.meted.ucar.edu/hydro/DHM/dhm2/part1/print.htm.]

Velleux, M. L., J. F. England, and P. Y. Julien, 2008: TREX: Spatially distributed model to assess watershed contaminant transport and fate. *Science of The Total Environment*, **404** (1), 113–128. doi:10.1016/j.scitotenv.2008.05.053.

Vergara, H., 2015 Characterizing Uncertainty of a Hydrologic Modeling System For Operational Flood Forecasting Over the Conterminous United States. PhD dissertation, University of Oklahoma.

——, P.-E. Kirstetter, J. J. Gourley, Z. L. Flamig, Y. Hong, A. Arthur, and R. Kolar, 2016: Estimating a-priori kinematic wave model parameters based on regionalization for flash flood forecasting in the Conterminous United States. *Journal of Hydrology.* doi:10.1016/j.jhydrol.2016.06.011.

Vrugt, J. A., W. Bouten, H. V. Gupta, and S. Sorooshian, 2002: Toward improved identifiability of hydrologic model parameters: The information content of experimental data. *Water Resour. Res.*, **38** (12), 48–1–48–13. doi:10.1029/2001wr001118.

Wang, J., and Coauthors, 2011: The coupled routing and excess storage (CREST) distributed hydrological model. *Hydrological Sciences Journal*, **56** (1), 84–98. doi:10.1080/02626667.2010.543087.

WMO, 2008: *Capacity Assessment of National Meteorological and Hydrological Services in Support of Disaster Risk Reduction.* World Meteorological Organization, 388 pp.

——, 1988: *Technical regulations / World Meteorological Organization.* World Meteorological Organization Geneva, 3 v. (loose–leaf) :.

Xian, G., C. Homer, J. Dewitz, J. Fry, N. Hossain, and J. Wickham, 2011: Change of impervious surface area between 2001 and 2006 in the conterminous United States. *Photogrammetric Engineering and Remote Sensing*, **77** (8), 758–762.

Xu, X., K. Howard, and J. Zhang, 2008: An Automated Radar Technique for the Identification of Tropical Precipitation. *Journal of Hydrometeorology*, **9** (5), 885–902. doi:10.1175/2007jhm954.1.

Yilmaz, K. K., H. V. Gupta, and T. Wagener, 2008: A process-based diagnostic approach to model evaluation: Application to the NWS distributed hydrologic model. *Water Resour. Res.*, **44** (9), n/a–n/a. doi:10.1029/2007wr006716.

Yussouf, N., J. S. Kain, and A. J. Clark, 2016: Short-Term Probabilistic Forecasts of the 31 May 2013 Oklahoma Tornado and Flash Flood Event Using a Continuous-Update-Cycle Storm-Scale Ensemble System. *Weather and Forecasting*, **31** (3), 957–983. doi:10.1175/waf-d-15-0160.1.

Zhang, J., and Coauthors, 2016: Multi-Radar Multi-Sensor (MRMS) Quantitative Precipitation Estimation: Initial Operating Capabilities. *Bulletin of the American Meteorological Society*, **97** (4), 621–638. doi:10.1175/bams-d-14-00174.1.

——, and Coauthors, 2011a: National Mosaic and Multi-Sensor QPE (NMQ) System: Description, Results, and Future Plans. *Bulletin of the American Meteorological Society*, **92** (10), 1321–1338. doi:10.1175/2011bams-d-11-00047.1.

—— and Y. Qi, 2010: A Real-Time Algorithm for the Correction of Brightband Effects in Radar-Derived QPE. *Journal of Hydrometeorology*, **11** (5), 1157–1171. doi:10.1175/2010jhm1201.1.

——, C. Langston, and K. Howard, 2008: Brightband Identification Based on Vertical Profiles of Reflectivity from the WSR-88D. *Journal of Atmospheric and Oceanic Technology*, **25** (10), 1859–1872. doi:10.1175/2008jtecha1039.1.

Zhang, Y., Z. Zhang, S. Reed, and V. Koren, 2011b: An enhanced and automated approach for deriving a priori SAC-SMA parameters from the soil survey geographic database. *Computers Geosciences*, **37** (2), 219–231. doi:10.1016/j.cageo.2010.05.016.